ELECTROOXIDATION AND LOCALIZED ATTACK OF IRONS IN SLIGHTLY ALKALINE SOLUTIONS

by

Gholamreza Vatankhah

A thesis presented to the Département de chimie in fulfillment
of the requirements for the degree of philosophiae doctor (Ph.D.)

FACULTÉ DES SCIENCES
UNIVERSITÉ DE SHERBROOKE

Sherbrooke, Québec, Canada, February 1998

Le 28 AVRIL 1998 , le jury suivant a accepté cette thèse dans sa version finale.
date

Président-rapporteur:	Mme Gessie Brisard Département de chimie
Membre:	M. Andrzej Lasia Département de chimie
Membre:	M. Hugues Ménard Département de chimie
Membre:	M. Louis Brossard IREQ
Membre externe:	M. Edward Ghali Université Laval

To My Parents

SOMMAIRE

Beaucoup d'équipements électriques au Québec en opération dans des voûtes souterraines sont en contact avec des eaux résiduelles. Ces équipements (tels que transformateurs, disjoncteurs, sectionneurs, etc.) sont protégés par des peintures qui permettent de retarder la corrosion. Cependant ces équipements, généralement en acier doux sont susceptibles de présenter une délamination de la peinture avec le temps. En plus les micro-défauts initialement présents dans la peinture, ceux qui sont induits lors de l'installation et le cas échéant, les égratignures, font que le matériau de ces équipements peut être en contact avec les eaux résiduelles.

Ce projet de recherche a été approché en simulant les conditions qui peuvent être retrouvées dans les voûtes souterraines, c'est-à-dire que ces équipements sont susceptibles d'être en contact avec des solutions contenant des bicarbonates, des phosphates, des sulfates et des chlorures. Le fer a été choisi comme le matériau à étudier son comportement étant anticipé comme reflétant celui de l'acier doux.

Afin de bien comprendre le comportement électrochimique du fer dans ces milieux, plusieurs méthodes électroanalytiques ont été utilisées, dont la voltampérométrie cyclique, chronoampérométrie, chronopotentiométrie, l'électrode tournante à disque, etc. Les techniques électrochimiques ont été complétées par des mesures de microscopie électronique à balayage, d'infrarouge à transformée de Fourrier, de spectroscopie à fluorescence de rayon X, et de plasma inductivement couplé.

L'influence de l'addition des ions sulfates sur le comportement électrochimique des électrodes en solution aqueuse contenant des ions de bicarbonate a été examinée. Les solutions qui contiennent seulement des ions sulfate en présence de fer démontrent une corrosion uniforme. L'addition d'ions sulfates en présence d'ions bicarbonate génère une corrosion par piqûration. Lors de l'attaque localisée, la formation d'un produit de corrosion passivant qui recouvre les sites d'attaques a été observée. Les différents comportements électrochimiques ont été comparés et expliqués par l'analyse des produits de formation probable et par leurs propriétés physico-chimiques pendant la polarisation électrochimique.

Le comportement électrochimique du fer dans des solutions aqueuses d'ions phosphates a aussi été étudié en présence des ions chlorures ou de sulfates. Il a été démontré que les ions

phosphates se comportent comme des ions inhibiteurs très efficaces contre une corrosion localisée. La présence d'ions sulfate induit un effet similitude à celui des ions phosphates dans le domaine de potentiel où la dissolution est active/passive.

Le comportement électrochimique de l'électrode de fer en ce qui concerne l'attaque localisée initiée par la présence des ions de chlorure et/ou de sulfates dans les solutions aqueuses de bicarbonates a été étudié en utilisant le concept factoriel et le potentiel de piqûration comme fonction d'objet. On a montré que les ions de chlorures et de sulfates en présence des ions de bicarbonates sont agressifs. Toutefois en mode interactif avec des ions de bicarbonates, les ions de chlorures sont agressifs et les ions de sulfates sont inhibiteurs à l'attaque du fer quand ces anions sont présents ensemble dans la solution. Ces comportements sont attribuées à la présence de produits particuliers de corrosion "rouille verte", de leurs propriétés et réactions à la surface de l'éctrode.

ABSTRACT

Many electric components in Québec in operation are in underground vaults in contact with free waters. These components (such as transformers, circuit breakers, disconnecting switches, etc.) are protected by paintings which make it possible to delay corrosion. However this mild steel part of these equipments is subject to delamination of painting with time. Nevertheless, the micro-defects initially present in painting, those which are induced at the time of the installation and the scratches make that the material of these equipments can be in contact with free waters.

This research project was developed by simulating the conditions which can be found in the underground vaults, i.e. in solutions containing bicarbonates, phosphates, sulfate and chlorides. Iron was selected as a material to study the effects of these ions on it. It will be useful as a reference material in a more exhaustive study carried out in the laboratory.

In order to understand the electrochemical behavior of iron in these media, several electroanalytical methods were used like the cyclic voltamperometry, the chronoamperometry, the chronopotentiometry, the rotating disk electrode disc, etc. The electrochemical techniques were supplemented by measurements of scanning electron microscopy, the Fourrier transform infra-red spectroscopy, x-ray fluorescence, and inductively coupled plasma.

The addition of the sulfate ions on the electrochemical behavior of iron electrodes in the presence of bicarbonate ions was examined. In solutions which contain only sulfate ions, iron shows a uniform corrosion. The addition of sulfate ions in the presence of bicarbonate ions cause pitting corrosion. At the time of the localized attack, there is formation of a passivating product of corrosion which covers the site. The various electrochemical behaviors were compared and explained by the analysis of the formation of the probable products and their physicochemical properties during electrochemical polarization.

The electrochemical behavior of iron in aqueous solutions of phosphate ions was examined in the presence of chloride or of sulfate ions. It was shown that the phosphate ions behave like very effective inhibiting ions against a localized corrosion. In the presence of sulfates ions, there is a similarity with the phosphate ions in the active-passive dissolution region.

The electrochemical behavior of iron electrode with respect to the localized attack induced by the presence of chloride and/or sulfate ions in aqueous bicarbonate solutions has been investigated by using full factorial design and pitting potential as an object function. It has been shown that both chloride and sulfate ions in the presence of bicarbonate ions are aggressive, but interactively with bicarbonate ions, chloride ions are aggressive and sulfate ions are inhibitive toward iron attack when these anions are present together in the solution. These observations had been linked to the presence of particular corrosion products (green rusts), and to their properties and reactions.

ACKNOWLEDGMENTS

I would like to present my great appreciation to professor Hugues Menard for his direction, guidance, and support during the course of this research. Professor Menard has been always open for discussions and ideas exchange. He is also a very kind and very supporting. This helped me a lot to feel Canada as a second home far away from my motherland home. I wish to express my special thanks to Prof. Menard.

I would also like to gratefully acknowledge Dr. Louis Brossard, my research co-director, for all the discussions, encouragement and supports throughout the research project.

I wish to thank Dr. Maria Drogowska for discussions, encouragement, and help she made during my research studies.

I am also thankful to chemistry department technicians for helping in nonelectrochemical techniques like ICP measurements and FTIR spectroscopy and P. Magny for SEM analysis.

I would like to thank all my friends and colleagues in our research group and chemistry department for their friendship and help during my presence in the chemistry department.

I would like to gratefully acknowledge the Ministry of Culture and Higher Education (MCHE) of Iran for my graduate scholarship (May 1993 to May 1997).

I would also like to acknowledge the financial support of Hydro-Québec (IREQ), Natural Sciences and Engineering Research Council of Canada (NSERCC).

Above all, I would like to show my special respects and thanks to my parents for their love, encouragement, support and patience during my studies in the chemistry department. They have been always with me even so far away from home.

TABLE OF CONTENTS

List of Figures

List of Tables

List of Symbols

i_l	limiting Current
n	number of electrons exchanged in redox reaction
F	Faraday's constant ; charge on one mole of electrons
D_z	diffusivity
ω	angular velocity in radians/time
v	kinematics viscosity
C_B	bulk solution concentration
N	number of combination in factorial design
n	number of levels in factorial design
k	number of factors in factorial design
z_j	factors in factorial design (j=1 to k)
x_j	coded (dimentionless) factor (j=1 to k)
y	object function
Δz_j	unit or interval of variation on the z_j-axis
B	coefficients matrix
b_j	elements of matrix B (j=1 to k)
S_e	pooled standard deviation
S_{res}	residual standard deviation
t	Student's t-distribution
F	variance ratio in F-test
r	rotation speed in rpm

INTRODUCTION

Corrosion can be defined as the reaction of a metallic material with its environment. The products of this reaction may be solid, liquid or gaseous. Both the physical and chemical properties of the products are important since they may both influence the subsequent rate of reaction.

The loss of metal and the cost of the consequences of corrosion are very high in any industrial country and any improvement that can be brought about is to be welcomed. In developed countries, the cost of corrosion has been estimated to be around 3% of the Gross National Product, if all the costs of protection, etc., are included. It causes a terrible waste of natural resources and may cause all types of unacceptable ecological damage.

In urban areas, the transformers in the electricity power systems may be operating in underground vaults. The transformer tanks are made of iron base alloys coated with liquid paint systems and may be in contact with residual waters (with slightly alkaline pH) containing bicarbonate, chloride and possibly sulfate ions (1). When the coating is damaged, the metallic part may therefore be in contact with the solution and corrosion damages are possible. In this work, the electrochemical behavior of iron in aqueous solutions of bicarbonate, chloride, sulfate, and phosphate ions has been investigated for better understanding of the corrosion of iron base alloys in such environments.

1 Literature review

Corrosion is the electrochemical reaction of a material with its environment, which may occur in many forms, depending on the material, construction and environment. Pitting corrosion is very dangerous in industrial systems because of its localized attack on materials. Investigation of electrochemical behavior of iron for better understanding of its corrosion has been the

subject of many works. The available literature on the pitting corrosion of iron and its alloys is mainly focused on the effect of chloride ions (2-9). By contrast, the literature for pitting by sulfate ions is scarce (10-17). Although it has been considered that Cl^- ions are more aggressive than other anions, the effect of $SO_4^=$ ions is probably seen most frequently. It has been reported that pitting induced by sulfate ions on iron occurs within the active-passive region and sulfate ions may counteract the effect of chloride ions (13,14).

The film breakdown potential of iron in the presence of chloride or sulfate ions obeys the logarithmic behavior with the difference that with sulfate ions the mechanism of pitting changes over time (10). Ellipsometric measurements of film grown on iron in a borate buffer solution containing sulfate ions, revealed a different structure of the surface film in the potential range with and without pitting (15). MacDougall and Bardwell (16) have shown that in sulfate solutions of pH 3.0 and/or 8.4, the passivation is highly inefficient with a very large anodic charge prior to a substantial decrease in current. They concluded that passivation (in these solutions) appears to be associated with the precipitation of a salt film and/or changes in the solution pH near the surface, thus allowing a passive oxide to form.

Recently, the considerable influence of pH on the passive film formed on iron in a Na_2SO_4 solution was shown (17) through the use of surface enhanced Raman spectroscopy (SERS). At pH 10, the passive film consists of microcrystalline/amorphous $Fe(OH)_2 + Fe_3O_4$ and /or γ-Fe_2O_3, with the sulfate anions being adsorbed on the film surface. Sulfate ions are incorporated into the film and bind covalently with the iron cations at pH 5.

Acosta *et al.*(18) have investigated the effect of sulfate ions on the pitting corrosion of mild steel in phosphate-borate solutions in a potential region from -1.0 to 0.0 V (SCE). A linear relationship between the logarithm of the sulfate ion concentration and the breakdown potential E_b is reported, with the pitting process being limited to a narrow potential range in the passive region due to the existence of an inhibition process.

To our knowledge, the only available data for the electrochemical behavior of iron in a mixture of sulfate and bicarbonate ions is from Pound *et al.* (19). They have reported one voltammogram (Fig. 1) only for iron in a solution of 1M sodium sulfate + 0.003M sodium bicarbonate and a scan rate of 50 mV/s from -1 to 0.8 V (SHE). A broad anodic peak located at -0.15 V with a maximum peak current density of 60 mA cm^{-2} along with a small conjugated cathodic peak at -0.90 V were observed. The large anodic peak is linked to a dissolution reaction.

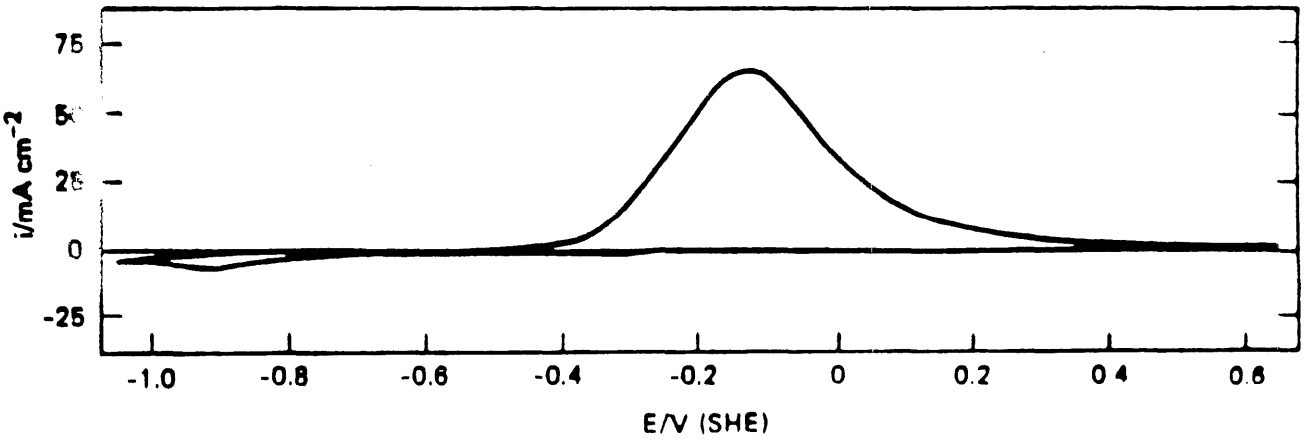

Figure 1. Cyclic voltammogram of iron in 1 M Na_2SO_4 + 0.003 M $NaHCO_3$ (After B.G. POUND, G.A. WRIGHT and R.M. SHARP, Corrosion (NACE) 45, 386 (1989)).

Génin *et al.*(20-27) published a series of articles on E-pH diagrams of iron in different solutions of sulfate, chloride, carbonate/bicarbonate, and their mixtures. They considered both thermodynamically (thermodynamic stability) and experimentally (kinetics) the existence of green rusts, which are very important corrosion transient products in such media. The green rusts are transients compounds which participate in corrosion reactions. They show different ion selectivity toward different ions and considering these properties, they are very useful for interpreting data obtained for the study of pitting corrosion by chloride and sulfate ions in the presence of bicarbonate ions.

Phosphate ions are known as corrosion inhibitors for iron and its alloys (28-33). Phosphate compounds are also used to generate conversion coatings on mild steel (34) to improve the corrosion protection performance of paints; the low solubility of phosphate compounds induces the precipitations of such compounds on the metal surface. The effect of sulfate ions on the electrochemical processes of iron electrodes in the presence of bicarbonate ions was investigated (35); it was determined that the formation of green rusts played a key role in the passivation and pitting initiation processes.

Burstein and Davies (36) have studied the behavior of scratched iron electrodes (bare metal surface) in solutions containing chloride, phosphate and bicarbonate ions. It has been deduced that bicarbonate ions do not react directly with the bare metal surface while chloride and phosphate ions react directly with the bare metal surface to form FeCl and FeH_2PO_4. For metal surfaces covered with an oxide film, there is no direct contact between metal surface and electrolyte solution, and anodic oxidation occurs across the metal/film interface.

Armstrong *et al.* (31) have reported that the addition of sodium phosphate up to 10 mM in aqueous solutions of carbonate and acetate buffers does not have any effect on the electrochemical behavior of iron in such solutions, whether aerated or deaerated. They have discussed the inhibitive effect of phosphate ions based on buffered and unbuffered solutions

and concluded that phosphate ions have an inhibitive effect in unbuffered solutions. However, their unbuffered solution contained perchlorate ions, which are usually used as accelerators in phosphating baths and have an oxidizing effect to help phosphate ions protect the iron surface.

Oxide films formed on iron in phosphate solutions are characterized by the incorporation of phosphate ions into the film (37-41); phosphate ions can block the film defects with a beneficial influence on the protection against further dissolution (41).

Benzakour and Derja (30) have established that the passivation process of iron in aqueous phosphate solutions is due to the formation of a precipitate layer instead of direct phosphate formation (solid state process). The electrodissolution in the passivity range is limited by the diffusion of phosphate ions towards the interface which is caused by the precipitation of the oxidized iron species.

Potentiodynamic trace of iron in sulfate aqueous solutions shows an active-passive dissolution behavior with a very large dissolution rate prior to quasi-passivation (34). In sulfate solutions with bicarbonate ions, potentiodynamic curves display two anodic dissolution regions, the effect of bicarbonate ions being dominant in the first region, the effect of the sulfate ions being dominant in the second peak region. The second anodic peak region is characterized by the occurrence of pitting which is followed by a passivation region at more positive potentials. In aqueous chloride solutions (without any buffer), the iron electrode does not passivate and passes from an active dissolution state to the polishing-state dissolution due to the formation of iron chloride hydrates at the anodic iron interface (10). Potentiodynamic curves for an iron electrode in chloride solutions containing buffer anions display an active-passive dissolution region before passivation at more positive potentials. The passivation range is small because the presence of chloride ions induces the film breakdown.

It is a common procedure to change one parameter at a time for investigating the effect of that particular parameter on the characteristics of the system under study. This method gives information about the behavior of the system with this particular parameter into account, keeping others constant. However, some interactions between different parameters may exist. Methods for which it is possible to change parameters simultaneously may be attractive to establish the both direct and interactive effects of parameters on the system. One of these methods is the Full Factorial Design (42) which one run experiments based on an experimental design constructed for factors involved in a particular system.

Some authors have applied factorial design in the past for investigation of major parameters in their researches about corrosion. Cragnolino and Sridhar (43) have studied the effect of anions like chloride, sulfate , nitrate and fluoride on localized corrosion of alloy 825. They have used a combination of visual observation and electrochemical parameters into an index called localized corrosion index (LCI). They have found that chloride ion is a promoter of localized corrosion and nitrate an inhibitor. Fluoride was found to be an inhibitor of localized corrosion, its effect being evident mainly in the low-chloride environment. Sulfate ion was found to be a weak promoter of localized corrosion.

Mansfeld *et al.* have published two papers (44,45) on the application of factorial design for optimization of the alternating voltage passivation of stainless steel. They have considered DC bias potential, pulse length (P) and amplitude (A), and ratio of the duration of the anodic portion to the cathodic portion of the pulse as effective parameters on the passive properties of stainless steel. They have obtained significant improvements of passivation for higher A and wider P of the potential square wave. Their result suggested that the optimum process parameters should have created conditions in which the anodic potential was located near, but not in, the transpassive region.

Peng and Park (46) have investigated principal factors and interactions affecting microbiologically influenced corrosion. They considered chemical oxygen demand (COD), sulfate ion concentration, calcium precipitation, and bacteria inoculation as factors in their investigation. They found that $CaCO_3$ precipitation has a significant effect on biocorrosion of steel. In the supersaturated conditions, sulfate ion concentration and bacterial inoculation had no appreciable effects on corrosion, but was affected by them in the conditions below saturation.

Jordan *et al.* (47) have studied the effect of pH, oxygen, and red rust on the cathodic half-cell reaction on corroding electrogalvanized steel. They have found that the predominant cathodic reaction involves the reduction of atmospheric red rust (γ-FeOOH).

2 Outline of the thesis

The body of the electric components operating underground in Hydro-Québec is made of iron base alloys. More understanding of corrosion phenomena is necessary to protect these components against the corrosive anions in their environment. The aim of this thesis is to study the electrodissolution behavior of iron in slightly alkaline solutions containing bicarbonate, phosphate, sulfate, and chloride ions. In this study, the relation between pitting corrosion and the above mentioned ions in the solution has been considered with major attention. In chapter 3, the electrochemical behavior of the iron electrodes in the solutions of bicarbonate and sulfate ions is given and discussed. In chapter 4, the behavior is shown for the iron electrode in the solutions of phosphate, sulfate, and chloride ions. Application of factorial design toward relation between pitting potential on concentration level of aggressive and inhibitive ions is given in chapter 5. Based on the obtained equations, correlations between the breakdown potential and the aggressive and inhibitive ions and their interactive relations has been explained.

CHAPTER 1
THEORY

1.1 Introduction

The electrochemical behavior of iron base alloys in aqueous solutions shows characteristic features which are linked to solution compositions (Fig. 2). Scanning potential from hydrogen evolution toward more noble potentials (anodic scan), electrodissolution reaction starts which through an active-passive transition, it transfers to a passive region. Sweeping potential more in positive direction, there is a range of potential called transpassive region which is accompanied with oxygen evolution. In passive region if there are aggressive anions in the solution, it is possible that passivation breaks down and causes localized attacks like pitting on the electrode surface. In further sections, the different regions are considered separately.

1.2 The active-passive transition and passivity

The state in which a metal exhibits a very low corrosion rate is known as 'Passivity'. A convenient way to understand the passivity of metals is by considering the potential-current density diagram, generally known as a polarization curve. Increasing the applied potential in the noble direction from E_{corr} and recording the resulting current, ultimately yields a somewhat unexpected potential-current density variation, as shown in Fig. 2. First the measured current ceases to increase with applied potential, and at a potential usually called E_{pp} (the primary passivation potential) it begins to decrease. The beginning of this decrease is known as the 'active-passive transition.' Above this potential, the current drops to a very low value, i_{pass} (the passive current density), and remains at a low value (although in practice not necessarily constant) over a wide range of potentials. The potential range over which the current remains at a low value is termed the 'passive potential range,' and it is the range that defines passivity for a given metal-environment combination. Corrosion rates in this passive range are very low.

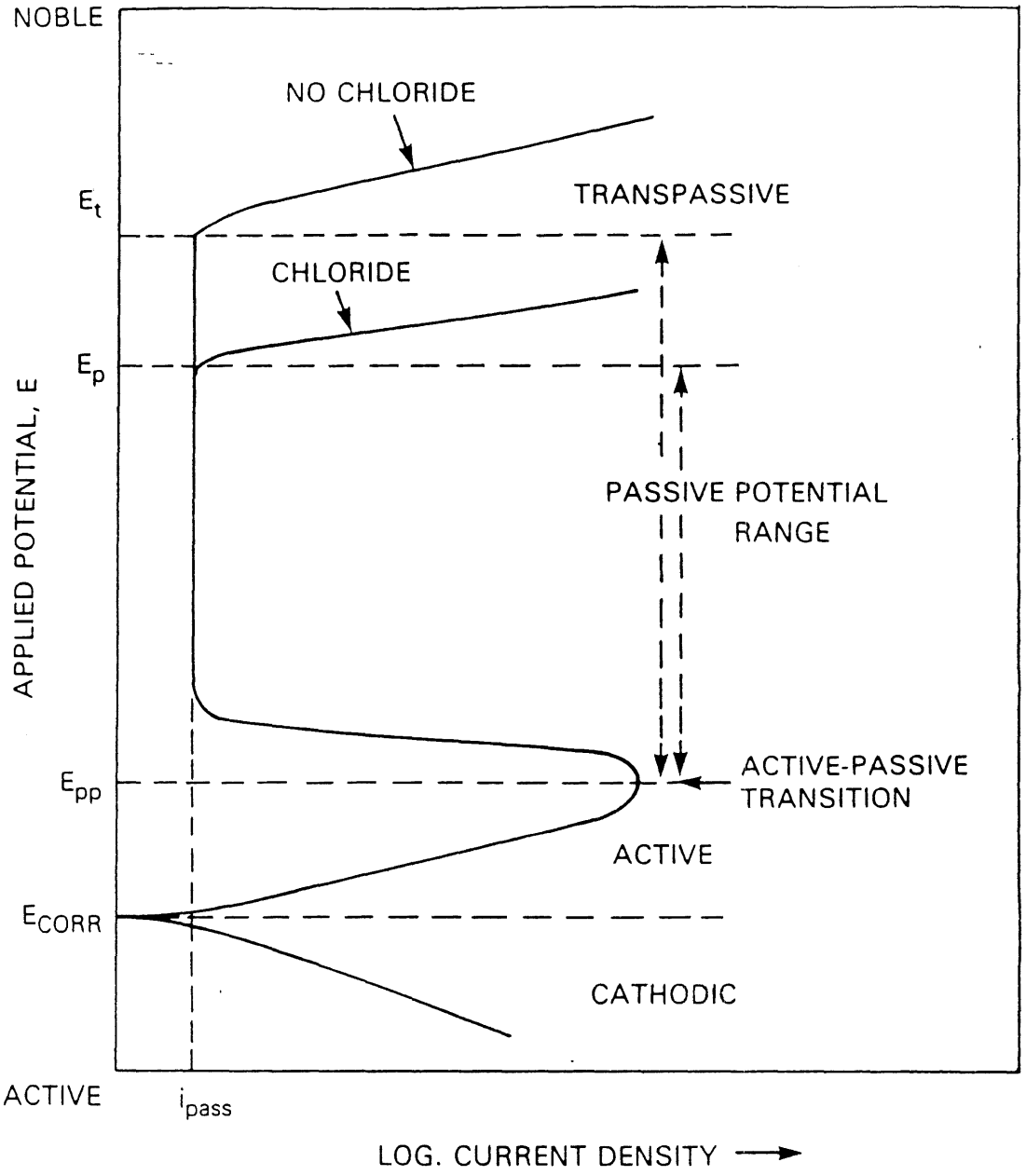

Figure 2. A schematic polarization curve for iron base metals in aqueous media (After A.J. Sedriks, Corrosion of Stainless Steels 2nd ed., John Wiley & Sons, New York, 1996).

On continuing to increase the applied potential in the noble direction, another potential will be reached at which the measured current will again begin to increase. The potential at which this current increase takes place is critically dependent on the corrodent. For example, in a chloride-free aqueous sulfuric acid solution, this represents the onset of the evolution of gaseous oxygen by the electrolysis of water, and is known as E_t, the potential representing the onset of transpassive behavior. However, in chloride-containing solutions, the current 'breaks' at somewhat lower (more active) potentials, as shown in Figs. 2 and 3. This 'breakthrough' is accompanied by the formation of corrosion pits on the test specimen surface and is usually known as the 'pitting potential', E_p or the 'breakdown potential,' E_b. Since pitting can perforate and destroy industrial equipment, the potential E_p represents a limiting potential that should not be exceeded. The passive potential range can be practically defined as the range between E_{pp} and E_p, when pitting is present or E_t in the absence of pitting.

1.3 Localized corrosion

From the point of view of reaction kinetics, the corrosion of metals in aqueous media is evidently an electrochemical phenomenon, the corrosion process occurring as electrode reactions. Localized corrosion can be described as corrosion occurring at one part of a metal surface at a much higher rate than over the rest of the surface. Generally, localized corrosion includes various types of corrosion phenamena such as pitting, crevice corrosion, and intergranular attack as well as stress corrosion cracking and corrosion fatigue. Pitting corrosion (a frequent form of localized corrosion) is associated with the breakdown of a film and it occurs frequently on a completely flat surface. It occurs where the protective oxide film on a metal suffers only local attack and is otherwise stable in the solution to which the metal is exposed. The Pourbaix diagrams indicate the likely pH range, which is usually in the neutral/slightly alkaline range. On passive surfaces or metals covered with highly resistant film, pitting occurs only in the presence of certain anions, which are usually described as

aggressive, like chloride ions. Pits are nucleated wherever the oxide film is likely to be discontinuous and where the local environmental conditions are most suitable. A pit will often become covered with a membrane of corrosion product and if some of this falls down the face of a vertical specimen it may help initiate further pits, particularly if it becomes loosely attached to the surface.

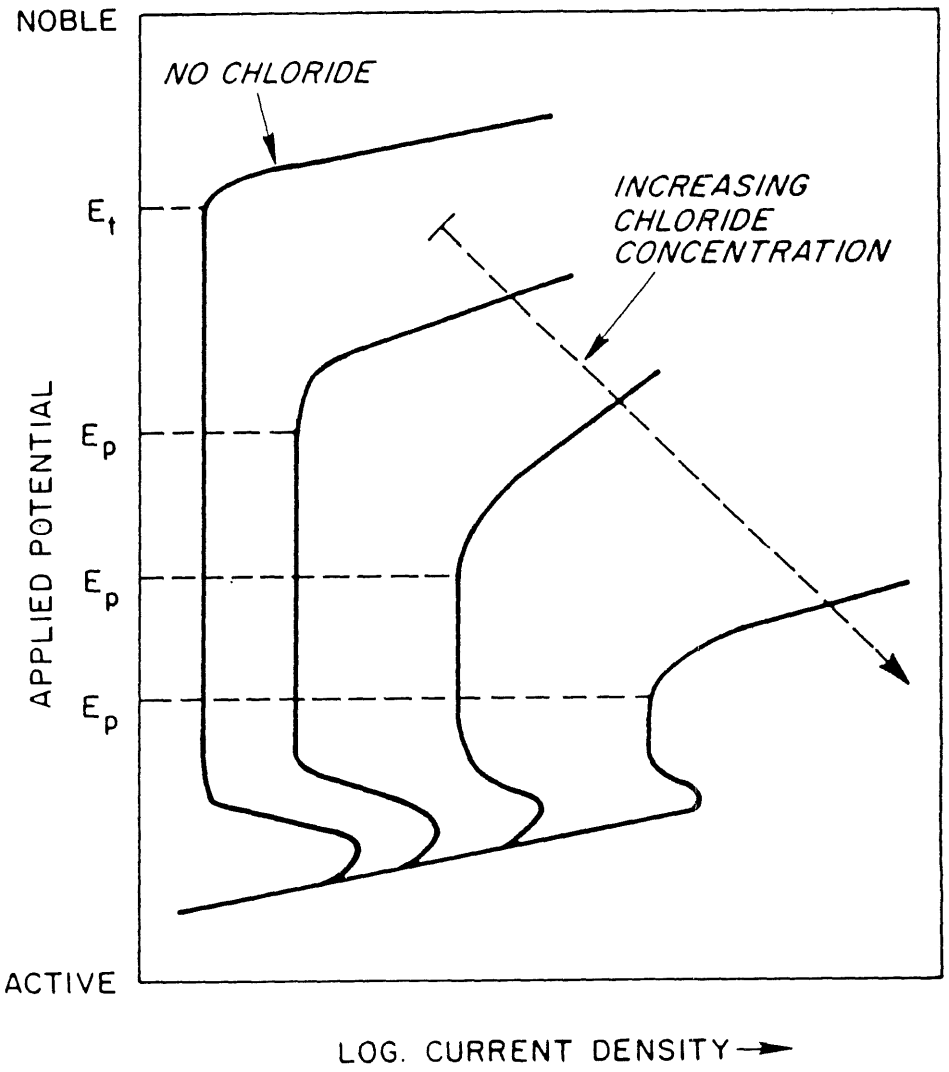

Figure 3. Typical polarization curves for an iron base metal in aqueous solutions containing increasing amount of chloride ions (After A.J. Sedriks, Corrosion of Stainless Steels 2nd ed., John Wiley & Sons, New York, 1996).

Crevice corrosion, another important form of localized corrosion, occurs in narrow spaces where an electrolyte can creep, usually by capillary forces, between two piece of metal or between a metal and an insulator. This type of corrosion is usually found where two metals have been riveted together, under the head of a bolt, or under an insulating O-ring. Crevice corrosion often can be prevented at the design stage by avoiding crevices, or during construction by filling them with a durable jointing compound that will exclude moisture and remain resilient.

Due to main concern of this work to pitting corrosion, next part is mainly devoted to this subject.

1.4 Pitting Corrosion Mechanisms

Pitting, as the name suggests, is a form of localized corrosive attack that produces pits. It can be a destructive form of corrosion in engineering structures if it causes perforation of equipment. However minor pitting that does not cause perforation is often tolerated and accepted in engineering equipment for economic reasons. It is not surprising, therefore, that there has been a considerable research effort to develop techniques, mostly ones employing electrochemical methods, capable of defining conditions under which a given metal-environmental system is likely to exhibit pitting. (10).

Once pits develop, they may continue to grow by a self-sustaining mechanism (48). Accordingly, much attention has been paid to obtaining an understanding of the factors controlling their initiation. A number of mechanisms have been proposed that attempt to explain the initiation of pits in perfect surfaces (i.e., surfaces containing no physical defects, such as inclusions or compositional heterogeneities) that consider pit initiation to result from certain interactions between discrete species in the environment (e.g., chloride ions) and the passive surface. Among these mechanisms are: the penetration mechanism, the film breaking

mechanism, and the adsorption mechanism. The penetration mechanism, first discussed by Hoar *et al.* (49), involves the transfer of anions through the oxide film to the metal surface, where they start their specific action. The film breaking mechanism, proposed by Vetter and Strehblow (50) and Sato *et al.* (51), requires breaks within the film which give direct access of anions to the unprotected metal surface. The adsorption mechanism, discussed by Kolotyrkin (52) and Hoar and Jacob (53), starts with the adsorption of aggressive anions at the oxide surface, which enhances catalytically the transfer of metal cations from the oxide to the electrolyte. This effect leads to thinning of the passive layer with possible final total removal and the start of intense localized dissolution. Strict separation of these mechanisms might not always be appropriate, as penetration of a passive layer via some very small defect is not necessarily very different from the occurrence of fissures in the film which permit easy access of the aggressive anions to the metal surface as in the film breaking mechanisms.

Although there are many common features of the different systems, one should also take into account the specific chemistry of a system. In this case the tendency of halides to complex with metal cations is very important and seems to be the key for an understanding of the stabilization of a corrosion pit by prevention of the repassivation of a defect site within the passive layer. Enhancement of the transfer of metal cations from the oxide to the electrolyte by halides holds for many metals.

The propagation of pits is thought to involve the dissolution of metal and the maintenance of a high degree of acidity at the bottom of the pit by hydrolysis of the dissolved metal ions (48). There is relatively wide acceptance of this propagation mechanism, although all its facets are not fully understood. The pit propagation process is illustrated schematically in Figure 4 for an iron base metal pitting in neutral sodium chloride solution.

The anodic metal dissolution reaction (equation [1.1]) at the bottom of the pit, is balanced by the cathodic reaction on the adjacent surface (equation [1.2]). The increased concentration of

M^+ within the pit results in the migration of chloride ions (Cl^-) to maintain neutrality. The metal chloride formed, M^+Cl^-, is hydrolyzed by water to the hydroxide and free acid (equation [1.3])

$$M \rightarrow M^+ + e^- \qquad [1.1]$$

$$2H_2O + 4e \rightarrow 4OH^- \qquad [1.2]$$

$$M^+Cl^- + H_2O \rightarrow MOH + H^+Cl^- \qquad [1.3]$$

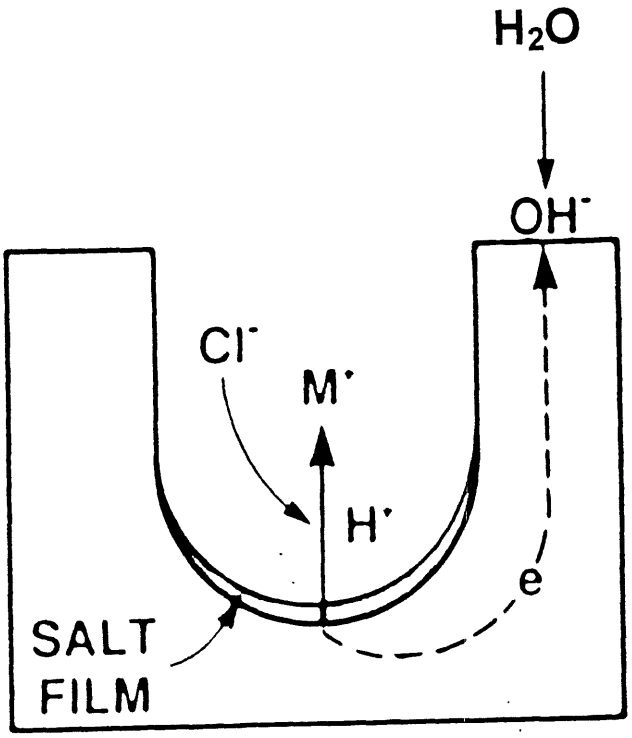

Figure 4. Schematic illustration of the pit growth mechanism (After A.J. Sedriks, Corrosion of Stainless Steels 2nd ed., John Wiley & Sons, New York, 1996).

The generation of this acid can reduce the pH values at the bottom of the pit to below zero, and the concentration of chloride ions can rise to 6M or more (54,55). It should be noted that pH values as low as zero or below cannot be obtained from the hydrolysis of metal ions alone (e.g., see Table 1). To explain these very low pH values, it is necessary to postulate that the chloride ion buildup in the solution at the pit bottom increases the activity of the H^+ ions, resulting in a lowering of pH to the observed values (54-56).

Table 1. Expressions for limiting pH of hydrolysis reactions of iron (56).

Reaction	Equilibrium pH	pH of 1N Solution
$Fe^{2+} + H_2O \rightarrow FeOH^+ + H^+$	$pH = 4.75 - 1/2 \log [Fe^{2+}]$	4.75
$Fe^{2+} + 2H_2O \rightarrow Fe(OH)_2 + 2H^+$	$pH = 6.64 - 1/2 \log [Fe^{2+}]$	6.64
$Fe^{3+} + 3H_2O \rightarrow Fe(OH)_3 + 3H^+$	$pH = 1.61 - 1/3 \log [Fe^{3+}]$	1.61
$Fe^{3+} + 2H_2O \rightarrow Fe(OH)_2^+ + 2H^+$	$pH = 2.00 - 1/3 \log [Fe^{3+}]$	2.00
$Fe^{3+} + 2H_2O \rightarrow Fe(OH)_2^{4+} + 2H^+$	$pH = 0.71 - 1/3 \log [Fe^{3+}]$	0.71
$Fe^{3+} + H_2O \rightarrow Fe(OH)^{2+} + H^+$	$pH = 1.52 - 1/2 \log [Fe^{3+}]$	1.52

1.5 Electrochemical Techniques for Measuring the Tendency for Pitting

Electrochemical techniques aimed at establishing whether a given metal-environment combination will give rise to pitting rely on comparing the corrosion potential, E_{corr}, with pitting potential, E_p, as illustrated in Fig. 4. Many investigations in the past have measured E_p from the anodic polarization curve (57-59).

Sometimes the anodic polarization curve does not resolve as clearly an identifiable current breakout at E_P as the one shown in Fig. 5. In such cases, it can be helpful to refine the estimate of E_p by holding the specimen at various applied potentials E, near E_p, and to monitor the current decay characteristics, as shown in Fig. 6. When $E = E_p$, the current decays to a value that becomes constant with time.

Electrochemical impedance techniques are also capable of detecting pitting. The charge transfer resistance, R_t, which is inversely proportional to the corrosion rate, decreases with the occurrence of pitting, as illustrated schematically in Fig. 7. In the Nyquist diagram shown in Fig. 7, the occurrence of pitting decreases the charge transfer resistance from R_{t1} to R_{t2}.

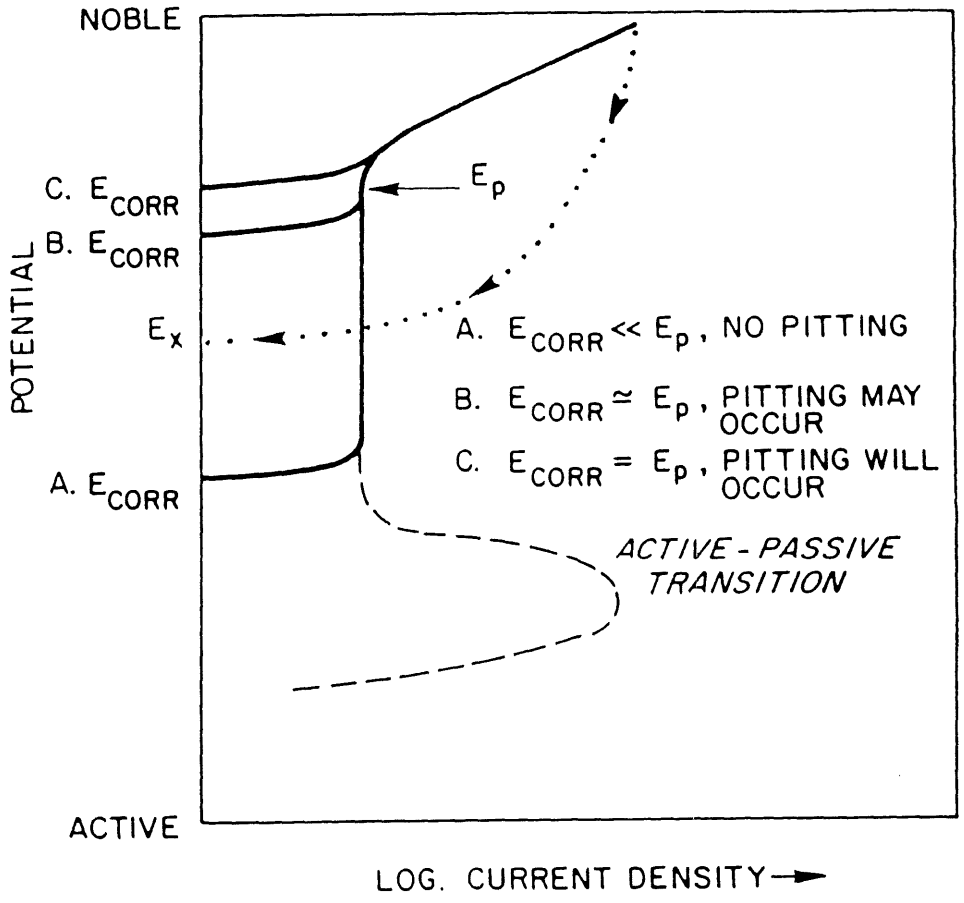

Figure 5. Schematic polarization curve illustrating conditions under which pitting may or may not occur (After A.J. Sedriks, Corrosion of Stainless Steels 2nd ed., John Wiley & Sons, New York, 1996).

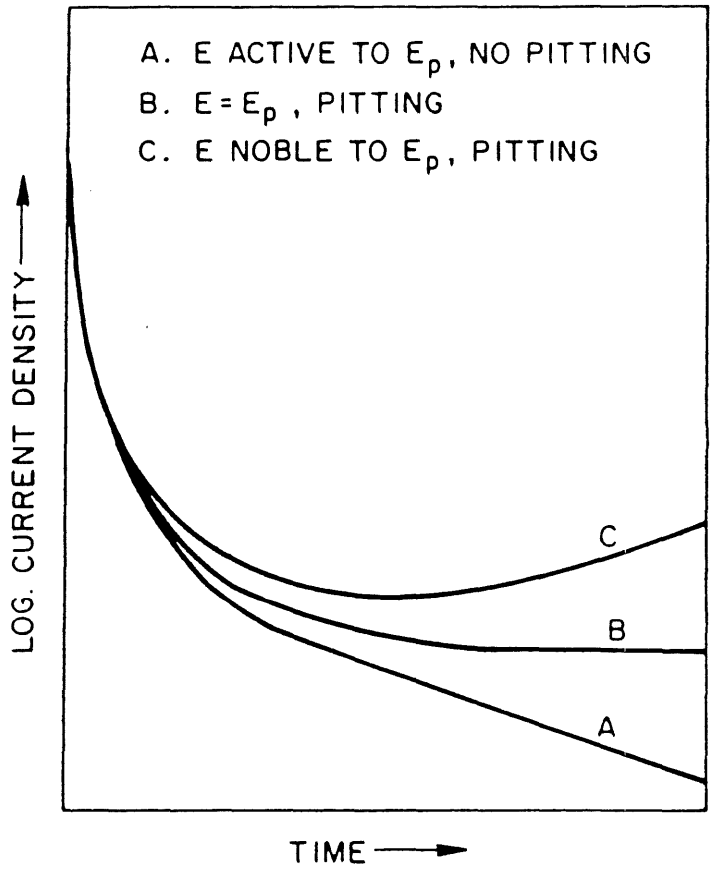

Figure 6. Current decay characteristics at various applied potentials (E) (After A.J. Sedriks, Corrosion of Stainless Steels 2nd ed., John Wiley & Sons, New York, 1996).

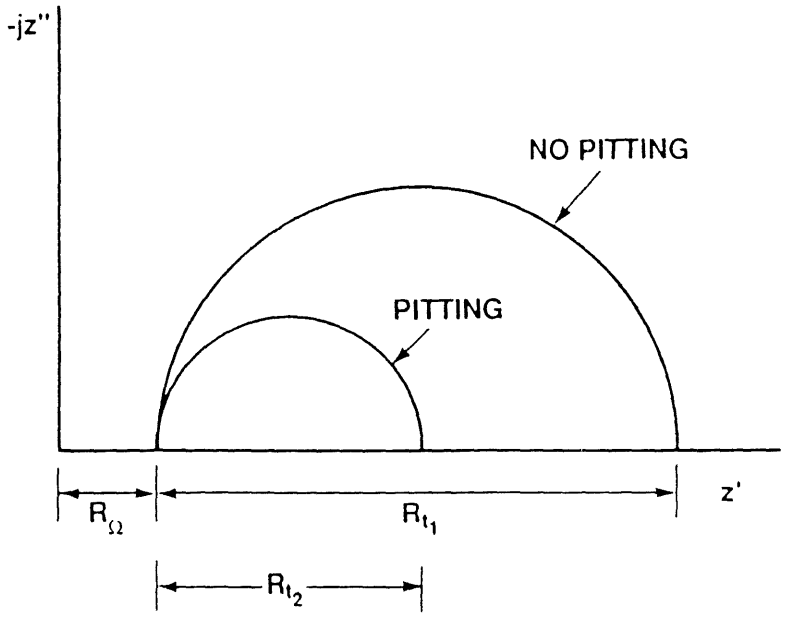

Figure 7. Nyquist diagram showing that pitting decreases the charge transfer resistance from R_{t1} to R_{t2} (After A.J. Sedriks, Corrosion of Stainless Steels 2nd ed., John Wiley & Sons, New York, 1996).

1.6 Rotating Disk Electrode

One of the few convective electrode systems for which the hydrodynamic equations and the convective-diffusion equation have been solved rigorously for the steady state is the rotating disk electrode (RDE). This electrode is rather simple to construct and consists of the electrode material imbedded in a rod of insulating material. More frequently the metal is imbedded into Teflon, epoxy resin, or another plastic. It is important that there is no leakage of the solution between the electrode material and the insulator. The rod is attached to a motor directly by a chunk or by a flexible rotating shaft and at a certain frequency. The electrical connection is made to the electrode by means of a brush contact or a mercury pool; the noise level observed in the current at the RDE depends on this contact.

Mass transport is improved and concentration polarization is reduced at a corroding electrode by increased mixing (convection). Reproducible control of convection is achieved under laminar flow, which is most easily produced experimentally by electrode rotation. Rotating disk electrode is mainly used in corrosion investigations which yield substantial decreases in concentration polarization and increases in limiting current, i_L. The rotating disk electrode has been well characterized mathematically with confirmation by experiment (60). The limiting current at RDE is

$$i_L = 0.620\, nFD_z^{2/3}\omega^{1/2}v^{-1/6}C_B \qquad [1.4]$$

where n is the number of electrons exchanged, F the Faraday's constant (96500 coulombs/equivalent), ω is the angular velocity in radians/time, v is kinematic viscosity, and C_B and D_z are the bulk solution concentration and diffusivity, respectively, of the reacting species. Mass transport (current density) is uniform over the surface of the RDE in the usual conditions where the solution is highly conductive and the reduction/oxidation rate is at i_L.

1.7 Factorial Designs

Factorial designs (61) are an enormously popular class of experimental designs that are often used to investigate multifactor response surfaces. The word factorial does not have its usual mathematical meaning of an integer multiplied by all integers smaller than itself (e.g.,3!=3*2*1), but instead indicates that many factors are varied simultaneously in a systematic way. One of the major advantages of factorial designs is that they can be used to reveal the existence of factor interaction when it is present in a system.

1.7.1 Full Factorial Design (61)

A full factorial design is one in which all of the possible combinations of the factors at all of the levels involved in the experiment are used. The number, N, of all possible combinations to be performed during the experiment is given by,

$$N=n^k \qquad [1.5]$$

where n is the number of levels and k is the number of factors. For a two-level factorial experiment in which every factor is fixed at two levels and all combinations of k factors are used, we deal with a 2^k full-factorial design. The term level of the factor refers to the boundary of the region to be searched for a given variable. For example one may be interested in the effect of three factors on product yield (y,%), namely temperature (z_1) in the range 100-200 °C, pressure (z_2) in the range $2x10^5$ to $6x10^5$ Pa, and reaction time in the range 10 to 20 min. If the upper temperature level z_1^{max} is 200°C and the lower level z_1^{min} is 100°C, then

$$z_1^{\circ} = (z_1^{max} + z_1^{min})/2 = 150^{\circ}C \qquad [1.6]$$

$$\Delta z_1 = (z_1^{max} - z_1^{min})/2 = 50^{\circ}C \qquad [1.7]$$

Generally, for any factor z_j, we have

$$z_j^{o} = (z_j^{max} + z_j^{min})/2 \; ; j=1,2,...,k \qquad [1.8]$$

$$\Delta z_j = (z_j^{max} - z_j^{min})/2 \qquad [1.9]$$

The point with coordinates (z_1^{o}, z_2^{o}, ..., z_k^{o}) is called the center point of the design or the basic level, and Δz_j is the unit or interval of variation on the z_j-axis. It is usual to pass from the z_1 ,z_2, ... z_k coordinates to a new dimensionless system of coordinates x_1, x_2, ..., x_k by a coding equation,

$$x_j = (z_j - z_j^{o})/\Delta z_j \; ; j=1,2,...,k \qquad [1.10]$$

In the dimensionless coordinate system, the upper and lower levels are at +1 and -1, respectively. The coordinates of the center point of the design are zero and coincides with the origin of the coordinates. In the above example k=3. The number of all possible combinations, N, for the three factors each fixed at two levels is $N=2^k=2^3=8$. The design matrix may be shown in the following table.

Table 2. 2^3 full factorial design

	Factors on natural scale			Coded Factors			
Obs. No.	z_1	z_2	z_3	x_1	x_2	x_3	Exper. Yield
1	100	20	10	−1	−1	−1	2
2	200	20	10	+1	−1	−1	6
3	100	60	10	−1	+1	−1	4
4	200	60	10	+1	+1	−1	8
5	100	20	30	−1	−1	+1	10
6	200	20	30	+1	−1	+1	18
7	100	60	30	−1	+1	+1	8
8	200	60	30	+1	+1	+1	12

The coded design of Table 2 can be shown geometrically as a cube (Figure 8), in which eight corners represent the experimental points. If we augment the design matrix for the 2^3 full factorial design with a column of 1's for a dummy variable (x_0=1), we have the experimental matrix shown in Table 3.

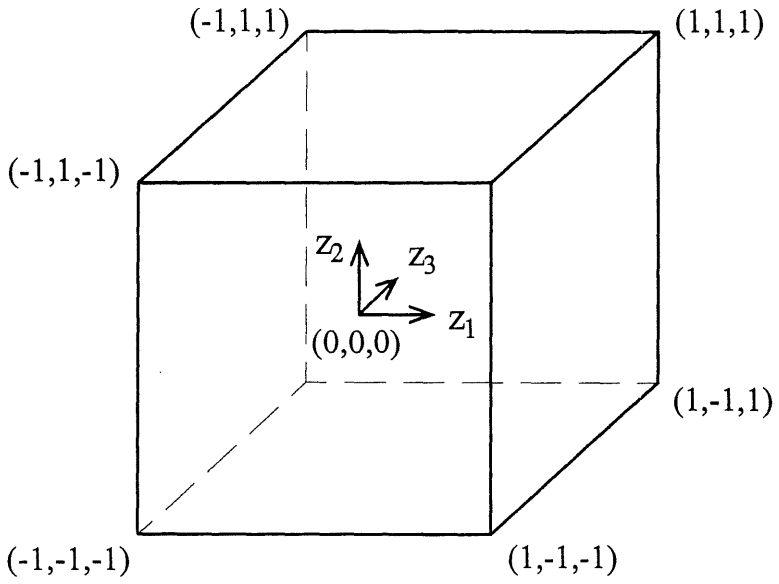

Figure 8. 2^3 Full factorial design.

Table 3. Experimental Matrix

N	x_0	x_1	x_2	x_3	y
1	+1	−1	−1	−1	y_1
2	+1	+1	−1	−1	y_2
3	+1	−1	+1	−1	y_3
4	+1	+1	+1	−1	y_4
5	+1	−1	−1	+1	y_5
6	+1	+1	−1	+1	y_6
7	+1	−1	+1	+1	y_7
8	+1	+1	+1	+1	y_8

The experimental matrix of Table 3 has the following properties:

$$\sum_{i=1}^{N} x_{ui}x_{ji} = 0\,,\ u \neq j\,,\ u,j = 0,1,\ldots,k \qquad [1.11a]$$

$$\sum_{i=1}^{N} x_{ji} = 0\,,\ j = 1,2,\ldots,k\,,\ j \neq 0 \qquad [1.11b]$$

$$\sum_{i=1}^{N} x_{ji}^2 = N\,,\ j = 0,1,\ldots,k \qquad [1.11c]$$

where k is the number of factors and N is the number of experiments. The first property expressed by equation [1.11a] is called the property of orthogonality, that is, the quantity of the scalar products of all column vectors are equal to zero. This property materially reduces the difficulties in the estimation of coefficients for the regression equation, because the coefficient matrix (X^TX) of normal equations becomes diagonal, and its diagonal elements are equal to the number of experiments, N, in the design matrix.

Using the least-squares method, we can determine coefficients of the regression equation ($Y = X^TXB$) by using matrix calculus.

$$B = \begin{bmatrix} b_0 \\ b_1 \\ b_2 \\ b_3 \end{bmatrix} = (X^TX)^{-1}X^TY \qquad [1.12]$$

The moment matrix (X^TX) corresponding to Table 3 takes the form ($\Sigma = \sum_{i=1}^{8}$):

$$\begin{bmatrix} \sum x_{0i}^2 & \sum x_{0i}x_{1i} & \sum x_{0i}x_{2i} & \sum x_{0i}x_{3i} \\ \sum x_{1i}x_{0i} & \sum x_{1i}^2 & \sum x_{1i}x_{2i} & \sum x_{1i}x_{3i} \\ \sum x_{2i}x_{0i} & \sum x_{2i}x_{1i} & \sum x_{2i}^2 & \sum x_{2i}x_{3i} \\ \sum x_{3i}x_{0i} & \sum x_{3i}x_{1i} & \sum x_{3i}x_{2i} & \sum x_{3i}^2 \end{bmatrix}$$

In agreement with the properties described by equations [1.11], a diagonal moment matrix results,

$$X^TX = \begin{bmatrix} 8 & 0 & 0 & 0 \\ 0 & 8 & 0 & 0 \\ 0 & 0 & 8 & 0 \\ 0 & 0 & 0 & 8 \end{bmatrix} \qquad [1.13]$$

The inverse of the matrix product X^TX (the variance matrix) is

$$(X^TX)^{-1} = \begin{bmatrix} 1/8 & 0 & 0 & 0 \\ 0 & 1/8 & 0 & 0 \\ 0 & 0 & 1/8 & 0 \\ 0 & 0 & 0 & 1/8 \end{bmatrix} \qquad [1.14]$$

The last term in equation [1.12] for B is

$$X^TY = \begin{bmatrix} \sum x_{0i}y_i \\ \sum x_{1i}y_i \\ \sum x_{2i}y_i \\ \sum x_{3i}y_i \end{bmatrix} \qquad [1.15]$$

Thus we have,

$$B = \begin{bmatrix} b_0 \\ b_1 \\ b_2 \\ b_3 \end{bmatrix} = \begin{bmatrix} 1/8 & 0 & 0 & 0 \\ 0 & 1/8 & 0 & 0 \\ 0 & 0 & 1/8 & 0 \\ 0 & 0 & 0 & 1/8 \end{bmatrix} \begin{bmatrix} \sum x_{0i}y_i \\ \sum x_{1i}y_i \\ \sum x_{2i}y_i \\ \sum x_{3i}y_i \end{bmatrix} \qquad [1.16]$$

As a consequence, any coefficient, b_j, of the estimated regression equation is defined by the scalar product of a y column by the respective x_j column divided by the number of experiments, N, in the design matrix.

$$b_j = \frac{1}{N} \sum_{i=1}^{N} x_{ji}y_i \qquad [1.17]$$

Using the design presented in Table 2, first we find the coefficients of the estimated linear regression equation

$$y = b_0 + b_1x_1 + b_2x_2 + b_3x_3 \qquad [1.18]$$

For example, b_1, can be determined by multiplying the x_1 by y columns and summing the products,

$$\begin{matrix} x_1 & y \end{matrix}$$

$$\begin{bmatrix} -1 \\ +1 \\ -1 \\ +1 \\ -1 \\ +1 \\ -1 \\ +1 \end{bmatrix} \begin{bmatrix} 2 \\ 6 \\ 4 \\ 8 \\ 10 \\ 18 \\ 8 \\ 12 \end{bmatrix} = \begin{bmatrix} -2 \\ 6 \\ -4 \\ 8 \\ -10 \\ 18 \\ -8 \\ 12 \end{bmatrix}$$

$$\sum_{i=1}^{8} x_{1i}y_i = 20$$

$$b_1 = \sum_{i=1}^{8} x_{1i} y_i / 8 = +2.5$$

Similarly,

$$b_0 = +8.5 \; , \; b_2 = -0.5 \; , \; b_3 = +3.5$$

In the case of a complete regression equation such as :

$$y = b_0 + b_1x_1 + b_2x_2 + b_3x_3 + b_{12}x_1x_2 + b_{13}x_1x_3 + b_{23}x_2x_3 + b_{123}x_1x_2x_3 \qquad [1.19]$$

which contains two and three factors, the interaction coefficients i.e. b_{12},b_{13}, and b_{23} (the second order interaction terms) and b_{123} (the third order interaction term) must also be determined.
The experimental matrix of Table 3 has an augmented form shown in Table 4.

Table 4. Experimental matrix for 2^3 full factorial design

N	x_0	x_1	x_2	x_3	x_1x_2	x_1x_3	x_1x_3	$x_1x_2x_3$	y
1	+1	−1	−1	−1	+1	+1	+1	−1	2
2	+1	+1	−1	−1	−1	−1	+1	+1	6
3	+1	−1	+1	−1	−1	+1	−1	+1	4
4	+1	+1	+1	−1	+1	−1	−1	−1	8
5	+1	−1	−1	+1	+1	−1	−1	+1	10
6	+1	+1	−1	+1	−1	+1	−1	−1	18
7	+1	−1	+1	+1	−1	−1	+1	−1	8
8	+1	+1	+1	+1	+1	+1	+1	+1	12

The interaction terms are determined in the same manner as the linear terms. For example to find b_{12}:

$$
\begin{matrix} & x_1x_2 & y \end{matrix}
$$

$$
\begin{bmatrix} +1 \\ -1 \\ -1 \\ +1 \\ +1 \\ -1 \\ -1 \\ +1 \end{bmatrix} \cdot \begin{bmatrix} 2 \\ 6 \\ 4 \\ 8 \\ 10 \\ 18 \\ 8 \\ 12 \end{bmatrix} = \begin{bmatrix} +2 \\ -6 \\ -4 \\ +8 \\ +10 \\ -18 \\ -8 \\ +12 \end{bmatrix}
$$

$$
\sum_{i=1}^{8} (x_1x_2)_i y_i = -4
$$

$$
b_{12} = \frac{1}{N} \sum_{i=1}^{8} (x_1x_2)_i y_i = \frac{-4}{8} = -0..5
$$

The remaining coefficients are found in a similar manner,

$$
b_{13} = +0.5 \, , \, b_{23} = -1.5 \, , \, b_{123} = +0.11
$$

By making replicate observations, it is possible to determine S_e^2 (pooled standard deviation), in order to test the significance of the regression coefficients. In addition, so with respect to degrees of freedom, the adequacy of the equation may be evaluated. Since the variance (covariance) matrix $(X^TX)^{-1}$ for a designed experiment is a diagonal matrix, then

$$
(X^TX)^{-1} = \begin{bmatrix} 1/N & & & 0 \\ & 1/N & & \\ & & . & \\ & & & . \\ 0 & & & 1/N \end{bmatrix} \qquad [1.20]
$$

The coefficients of the regression equation are uncorrelated. The significance of each coefficient can be tested on the basis of the student's t-test. Deletion of an insignificant coefficient from the regression equation, (equation [1.19]) will have no effect on the remaining coefficients.
The diagonal elements of the variance matrix are equal to one another, therefore all of the coefficients in equations [1.19] and [1.20] can be determined with the same accuracy.

$$S_{b_j} = \frac{S_e}{\sqrt{N}} \qquad [1.21]$$

where S_e is the standard deviation of the observation at center point. For example, if three replicate observations have been made at the center point of the design to yield following values : $y_1 = 8$, $y_2 = 9$, and $y_3 = 8.8$, then,

$$\bar{y} = \frac{1}{3}\sum_{u=1}^{3} y_u = 8.6 \qquad [1.22]$$

$$S_e^2 = \frac{1}{2}\sum_{u=1}^{3} (y_u - \bar{y})^2 = 0.28 \qquad [1.23]$$

$$S_e = 0.55$$

$$S_{b_j} = \frac{0.55}{\sqrt{8}} = 0.2$$

The significance of the coefficients can be tested using the Student's t-test.

$$t_0 = \frac{|b_0|}{S_{b_0}} = \frac{8.5}{0.2} = 42.5 \qquad t_1 = \frac{|b_1|}{S_{b_1}} = \frac{2.6}{0.2} = 12.5$$

$$t_2 = \frac{|b_2|}{S_{b_2}} = 2.5 \qquad t_3 = \frac{|b_3|}{S_{b_3}} = 17.5$$

$$t_{12} = \frac{|b_{12}|}{S_{b_{12}}} = 2.5 \qquad t_{13} = \frac{|b_{13}|}{S_{b_{13}}} = 2.5$$

$$t_{23} = \frac{|b_{23}|}{S_{b_{23}}} = 7.5 \qquad t_{123} = \frac{|b_{123}|}{S_{b_{123}}} = 1.25$$

For a significant level of $\alpha = 0.05$ and degrees of freedom, $\nu=2$, the tabulated value of the Student's t-distribution is $t_\alpha(\nu) = 4.3$. Thus, the coefficients b_2, b_{12}, b_{13} and b_{123} are insignificant, and they must be rejected from the equation. After the rejection of the insignificant coefficients the regression equation takes the form,

$$\hat{y} = 8.5 + 2.5x_1 + 3.5x_3 - 1.5x_2x_3 \qquad [1.24]$$

Now the estimated regression equation is tested to see how it fits the observations, using F test (61). The variance ratio, $F = S^2_{res} / S^2_e$, in which

$$S^2_{res} = \frac{\sum_{i=1}^{8}(y_i - \hat{y}_i)^2}{N - L} = \frac{6}{8} = 1.5 \qquad [1.25]$$

$$S^2_e = 0.28$$

and L = 4 is the number of significant coefficients in the regression equation. Then,

$$F = 1.5 \div 0.28 = 5.3$$

The tabulated value of F for $\alpha = 0.05$ and $\nu_1 = 4$ and $\nu_2 = 2$ is

$$F_{1-\alpha}(\nu_1,\nu_2) = 19.3$$

Thus, $F < F_{1-\alpha}(\nu_1,\nu_2)$, and the above estimated regression equation fits the experimental data adequately.

In the example above, as it is seen from equation[1.24] temperature has a positive direct effect (x_1 coefficient) on experimental yield and reaction time has also a positive direct effect (x_3 coefficient). The interactive effect is related to pressure and reaction time together and it is a negative one (x_2x_3 coefficient). Pressure does not show any direct effect on experimental yield. This method as shown above is useful for studying both direct and interactive effect of parameters on the system under investigation. It is also useful for optimizing the parameters to obtain the best results from the system.

CHAPTER 2

EXPERIMENTAL

2.1 Electrodes and electrochemical cell

Working electrodes were made of iron (Materials research Corporation, 99.99%) mounted in a Kel-F holder used as a rotating-disk electrode. The exposed area was 0.13 cm^2. The electrodes were mechanically polished with alumina paste (0.1 and 0.05μ) to a mirror-like finish and rinsed with distilled water. The electrode surface was examined before and after the experiments using a Bausch and Lomb optical microscope (CAT. NO. 31-35-40) with maximum magnification of 70x. For each experiment, the electrode was kept at a constant applied potential of -1.0 V(SCE) for one minute in order to reduce any air-formed surface oxides. Special care was taken to get reproducible results in terms of surface roughness and homogeneity. The auxiliary electrode was a platinum grid, separated from the main compartment by a Nafion membrane. The reference electrode was a saturated calomel electrode (SCE) with a Luggin capillary bridge connected to the main cell. A scheme of the electrochemical cell used in the studies is shown in Fig.9.

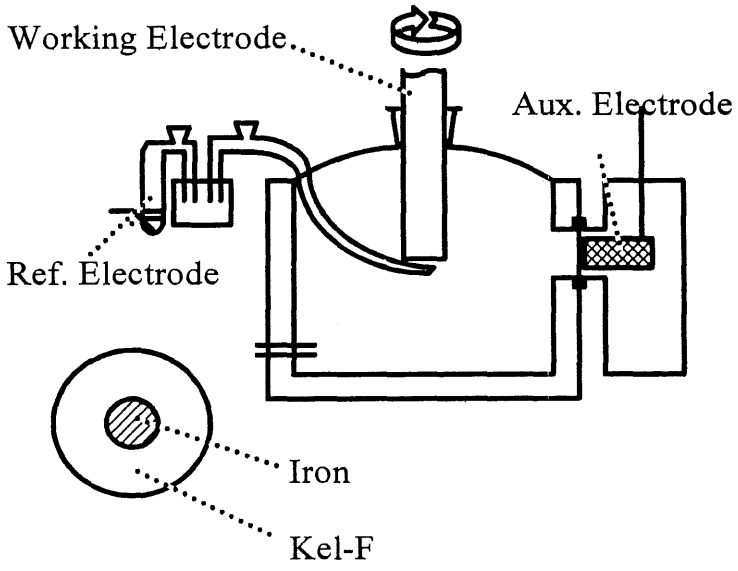

Figure. 9. scheme of the electrochemical cell used in the measurements.

The volume of the cell was ~600 mL to minimize the enrichment of the solution in dissolved ions during the experiments.

2.2 Solutions

Aqueous solutions of 0.3-1 M Na_2SO_4 and 0.1-0.3 M $NaHCO_3$ were prepared from analytical grade materials (BDH) and deionized water. The pH was ~8 for all solutions and no pH adjustment was done. All solutions were deaerated by high-purity nitrogen bubbling before each experiment and were purged continuously during the measurements. All of the experiments were conducted at room temperature.

Aqueous solutions of 0.1-0.5 M Na_2SO_4 and 0.01-0.1 M Na_2HPO_4 plus 0.01-0.02 M NaCl were prepared from analytical grade materials (BDH) and deionized water. Solutions of $NaHCO_3$ (0.1-0.5 M), NaCl (0.05-0.15 M) and Na_2SO_4 (0.05-0.5 M) were prepared from analytical grade materials (BDH) and deionized water.

2.3 Equipments

The instrument used for all the experiments was a Potentiostat/Galvanostat model 273 from Princeton Applied Research (PAR) controlled by a PC using M270 PAR electrochemical software (M270) version 4.10. Electrode rotation was done using an electrode rotator from Pine instrument company (Analytical Rotator model AFASR). Electrical contact to the rotating working electrode was made trough a mercury pool for lowering the noise level of the signal.

Fourier transform infrared (FTIR) spectroscopy was done using a BOMEM FTIR spectrometer model MB-102. This technique was used for qualitative analysis of the precipitate on the electrode surface formed in solution containing sulfate and phosphate ions.

Inductively coupled plasma (ICP) analytical measurements was carried on by an Applied Research Laboratories (ARL) model 3560 AES spectrometer. The ICP measurement was used for quantitative analysis of the ratio between iron and phosphate ions in the precipitate formed on the surface electrode in solution of sulfate and phosphate ions.

Scanning electron microscopy (SEM) pictures were taken a scanning electron microscope from JEOL model JSM 840-A. SEM microscopy was used for the examination of the electrode surface after electrochemical experiments in solutions containing sulfate ions. It gives information about the localized attack on the electrode surface, the morphology inside the pits and distribution of the precipitates on the surface and pit sites.

2.4 Chemicals

Sodium bicarbonate, sodium chloride, sodium sulfate, and sodium phosphate were of analytical grade supplied by BDH Chemical Co. All these salts has been used as received from company and no further treatment has been done.

2.5 Samples preparation and procedures

Aqueous solutions of 0.1-0.5 M Na_2SO_4, 0.01-0.1 M Na_2HPO_4 plus 0.01-0.02 M NaCl , $NaHCO_3$ (0.1-0.5 M), NaCl (0.05-0.15 M) and Na_2SO_4 (0.05-0.5 M) were prepared by dissolving their salts in deionized water. These solutions were transferred to the electrochemical cell shown in Fig. 9 for studying the effect of anions on electrochemical behavior of iron electrode. The pH was ~8 for all solutions without adjustment and the pH was not adjusted during the course of the measurements. All solutions were deaerated by high-purity nitrogen bubbling before each experiment and were purged continuously during the measurements. All of the experiments were carried out at room temperature.

For surface analysis experiments, iron electrode with removable tip was used. The electrode tip was removed from the body of the electrode system and then used in surface analysis techniques like scanning electron microscopy (SEM), x-ray fluorescence spectroscopy and x-ray photoelectron spectroscopy (XPS). XPS measurements were done at Institut national de la recherche scientifique INRS-Énergie in Varennes, Québec.

In solutions of phosphate and sulfate together bulky precipitate on electrode surface was removed gently and rinsed very well with deionized water. The precipitate then was used in transmission Fourier transform infrared spectroscopy (FTIR) using the mull technique for sample preparation. For sample preparation, the precipitate was grounded and mixed with KBr in a mortar and then pressed in a hydraulic press at pressure of 10000 lb/in^2 to obtain a transparent solid pellet. The pellet after putting it in sample holder was used in FTIR spectrometer. A KBr pellet was prepared as a standard sample for correcting the spectra.

CHAPTER 3

Electrodissolution of Iron in Sodium Sulfate and Sodium Bicarbonate Solutions

3.1 Results

3.1.1 Sulfate solutions

A voltammogram of an iron electrode rotated at 1000 rpm with a potential scan rate of 0.005 Vs^{-1} from -0.85 to 1.5 V in 1 M Na_2SO_4 (pH ~8) solution is shown in Fig. 10. The anodic current starts to increase at -0.85 V to reach a maximum of 480 mA cm^{-2} at 0.11 V. The large anodic charge is related to the iron dissolution as Fe(II) (63). After the peak current, there is a sharp decrease of three orders of magnitude in anodic current to 480 μAcm^{-2} at 0.25 V and a large quasi-passive region extending over 1 V with a current as low as 50 μAcm^{-2}. In the transpassive region for potentials more anodic than 1.25 V, the oxidation current increases with the potential and oxygen evolution is observed. For the potential scan in the negative direction, the passivation remains up to -0.3 V with a minimum current of 2-3 $\mu A\ cm^{-2}$. There is a small broad anodic current peak maximum of 65 $\mu A\ cm^{-2}$ at -0.3 V, which indicates an activation (dissolution) of the electrode surface. The height and location of the activation peak for the potential sweep in the negative direction are dependent on the anodic potential scan limits (Fig. 11), i.e. 0 V, 0.2 V, and 0.4 V. The activation current peak maximum is lowered by increasing the anodic potential limit E_a; for $E_a \geq 0.5$ V, the anodic reactivation peak current disappears and cathodic current is observed. Fig. 10 also illustrates the effect of a negative potential scan direction ranging from 1.5 V to -0.85 V; the potentiodynamic trace overlaps the one with a starting potential of -0.85 V in a positive potential scan direction. At the end of each experiment, it was observed that the electrode surface is etched strongly and looks very rough.

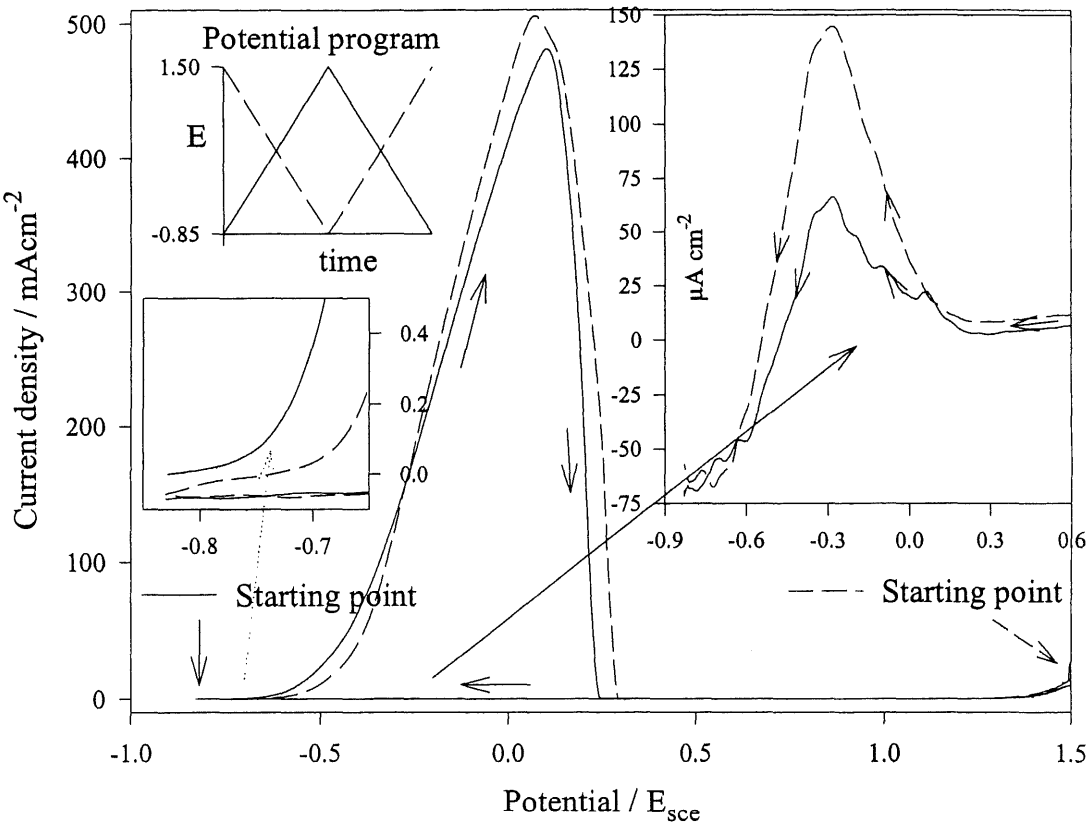

Figure. 10. Potentiodynamic trace for a rotating iron disk electrode, in 1M sodium sulfate solution, dE/dt=5 mVs^{-1}; rotation speed =1000 rpm; compensated for the IR drop. Starting potential: -0.85 V (continuous line); +1.5 V (dashed line).

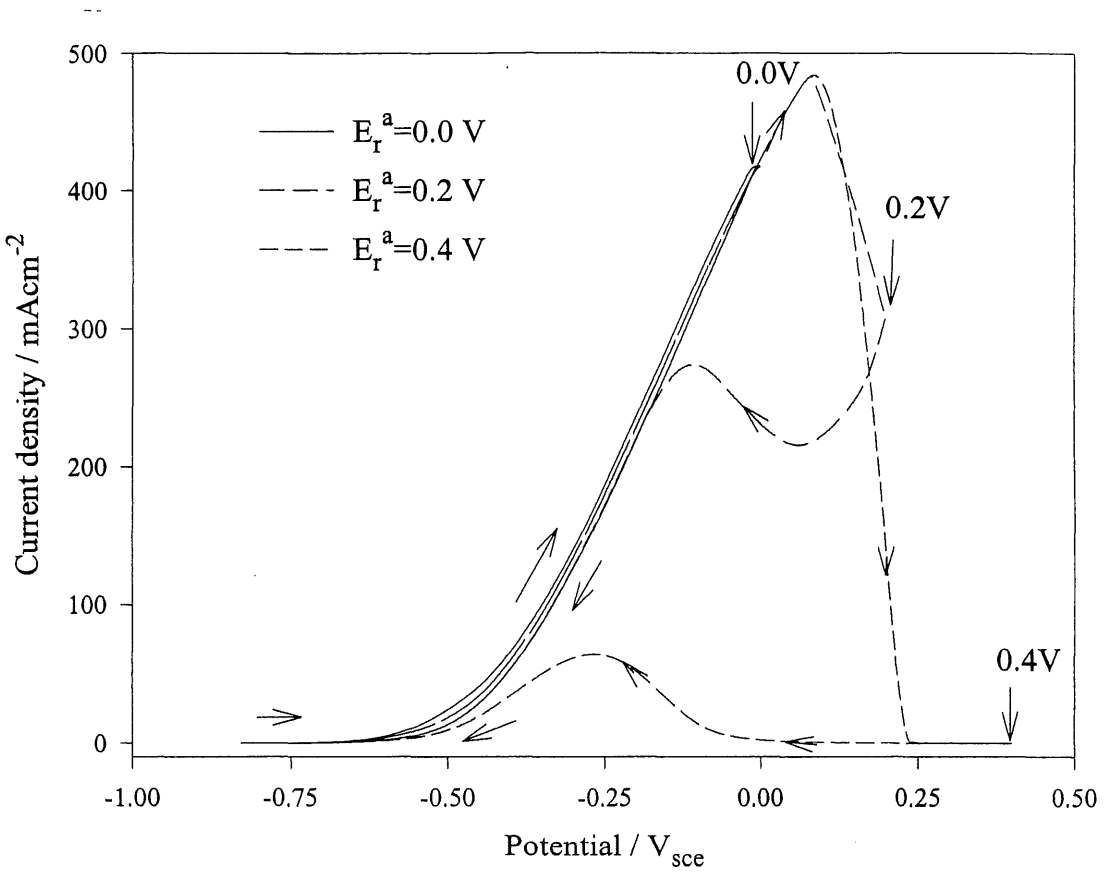

Figure. 11. Effect of the anodic potential limit (0-0.4 V) on the voltamogram during the return sweep. Starting potential: -0.85 V. The other experimental conditions are those of Fig. 10.

The oxidation current in the passive region is dependent on the sulfate ion concentration i.e. it is equal to 60 $\mu A\ cm^{-2}$ for 1 M Na_2SO_4 (Fig. 10) and 110 $\mu A\ cm^{-2}$ for 0.3 M Na_2SO_4 at E=0.8 V. For the scan in the negative potential direction, the current from 1 V to 0.2 V is independent of the sulfate concentration.

The chronoamperograms for the iron electrode in 0.3M Na_2SO_4 for two different constant applied potentials, i.e. 0.2 V and 0.4 V, are illustrated in Fig. 12, the potential being stepped from -1 V to 0.2 or 0.4 V. The current is anodic with peaks and spikes related to pitting. For E=0.2 V, the curve displays an anodic current maximum for Fe(II) dissolution after ~600 s of polarization; for a longer time, the anodic current decreases over time to reach a quasi-steady value of 140 $\mu A\ cm^{-2}$ for t=3200s. For E=0.4 V, a passivation current of 100 $\mu A\ cm^{-2}$ is attained quickly to reach 16 $\mu A\ cm^{-2}$ after 2000 s.

SEM pictures of the electrode surface after 8000 s of polarization under the experimental conditions of Fig. 12 are shown in Figs. 13 and 14. The sample maintained at 0.2 V (Fig. 13) shows a large number of pits without any precipitate on the electrode surface. For E=0.4 V (Figs. 14), few pits are noticed with a precipitate inside and outside the pits. A further increase of the anodic potential up to 1 V results in a passive current of 20 $\mu A\ cm^{-2}$ and a shiny golden colored surface after 2000 s is obtained.

3.1.2 Bicarbonate solutions

The potentiodynamic behavior of an iron electrode in 0.1 M $NaHCO_3$ solution (pH ~8) has been investigated (Fig. 15) in the same conditions as in Fig.10. The potentiodynamic trace in the anodic direction displays an anodic active dissolution peak (region A) with a peak current of 190 $\mu A\ cm^{-2}$ at -0.64 V, which is followed by a large passive region from -0.4 V to 0.9 V (region B). For potentials more positive than 0.9 V, i.e. the transpassive region (region C), the anodic current increases with the potential and a plateau current from 1.1 V to 1.3 V is

observed before the onset of oxygen evolution. The current plateau in the transpassive region is related to oxidation of Fe(III) to Fe(VI) species (54-66). The anodic peak current in region A and the anodic plateau current in region C are higher as the bicarbonate concentration is increased. For the scan in the negative potential direction, the potentiodynamic trace is unchanged in the plateau region and a single cathodic peak is noticed at -0.72 V. The oxidation charge related to the oxidation peak in region A is much larger than its conjugated cathodic peak current.

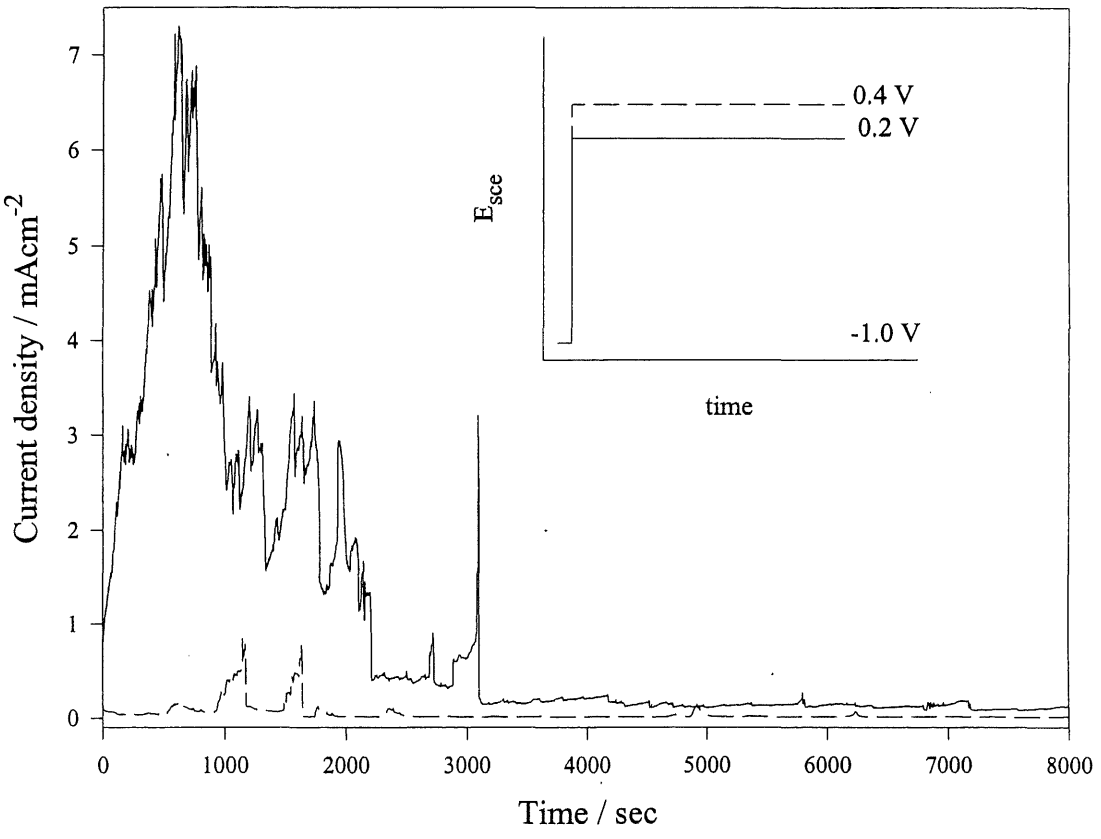

Figure. 12. Current-time curve for an iron electrode in 0.3 M sodium sulfate solution for applied potentials of 0.2 and 0.4 V; ω=1000 rpm.

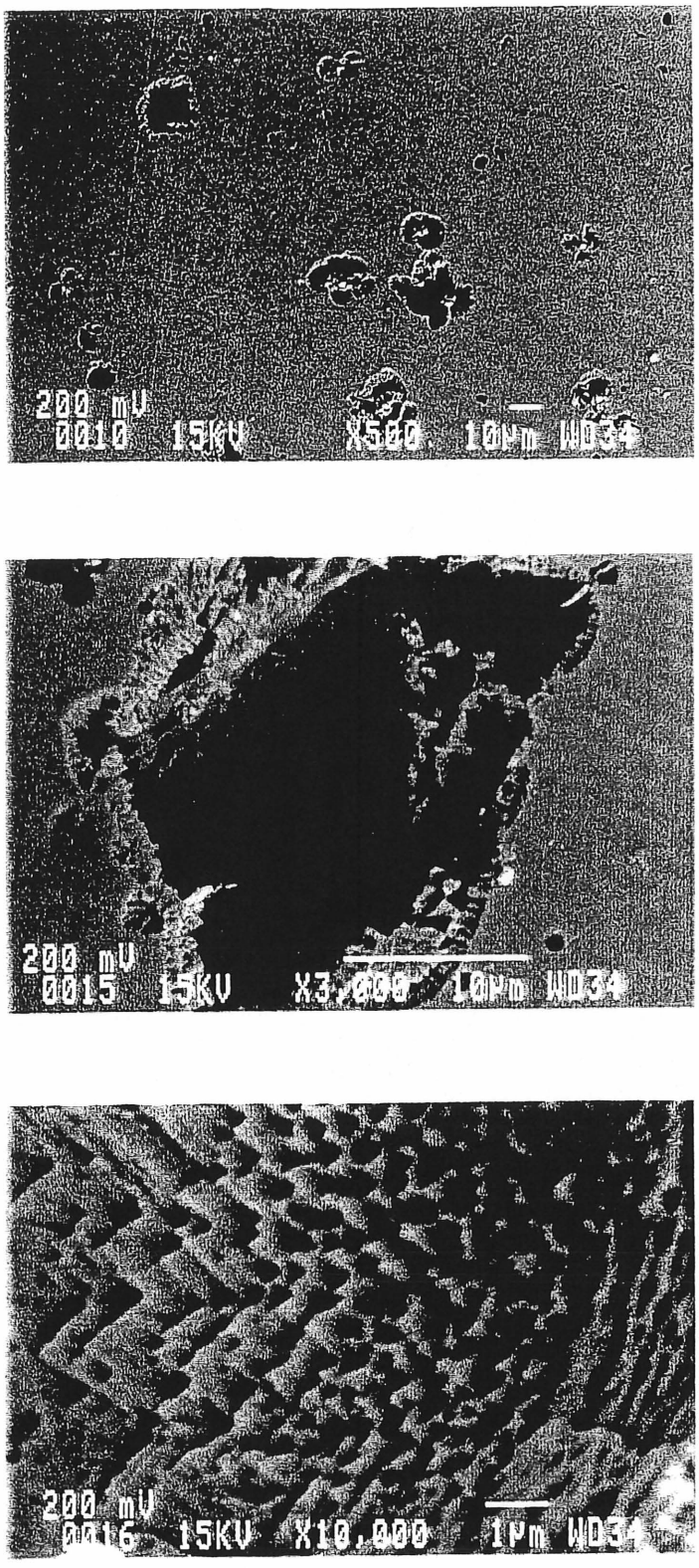

Figure. 13. SEM pictures after iron electrode oxidation at 0.2V for 8000 s in 0.3M sodium sulfate solution; rotation speed =1000 rpm.

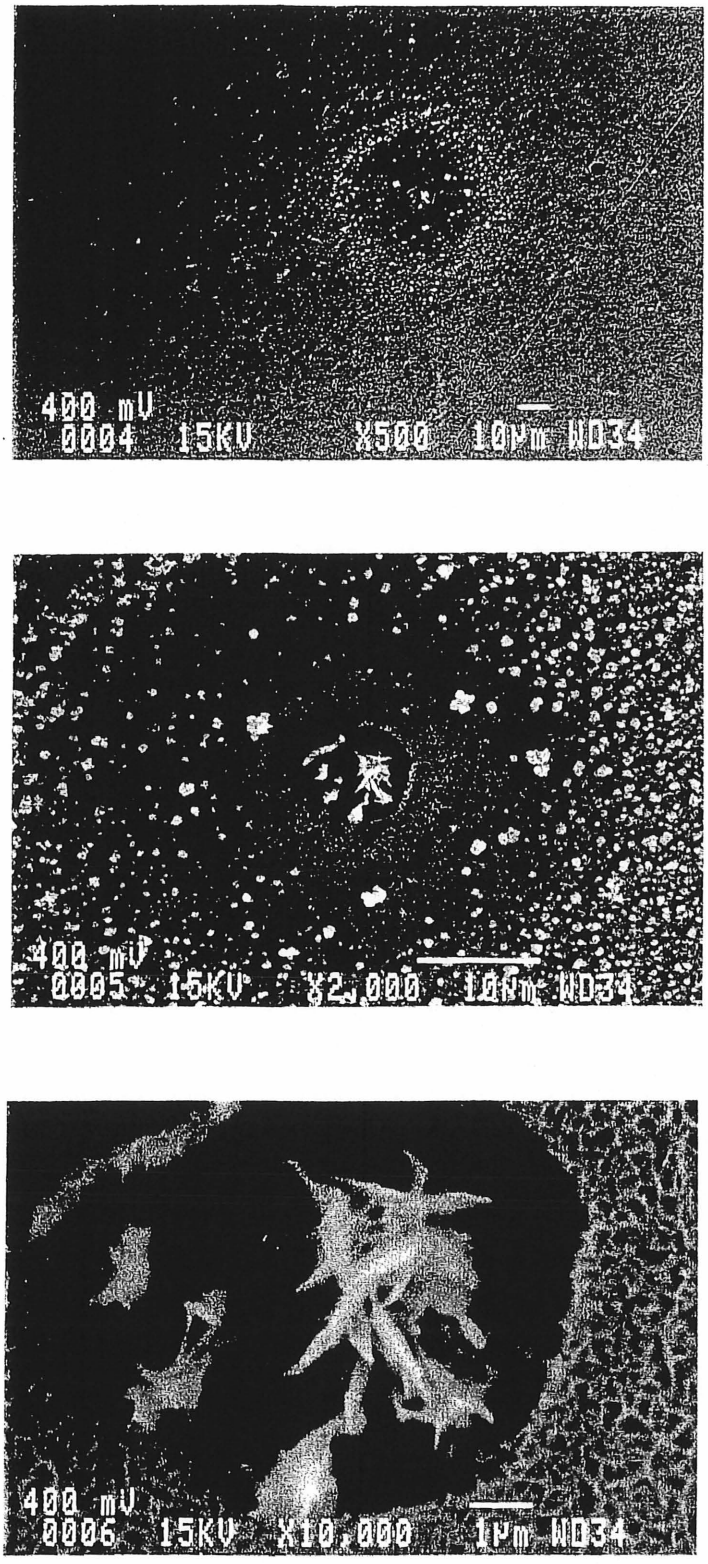

Figure. 14. SEM pictures after electrode oxidation at 0.4V for 8000 s in 0.3M sodium sulfate solution; rotation speed =1000 rpm.

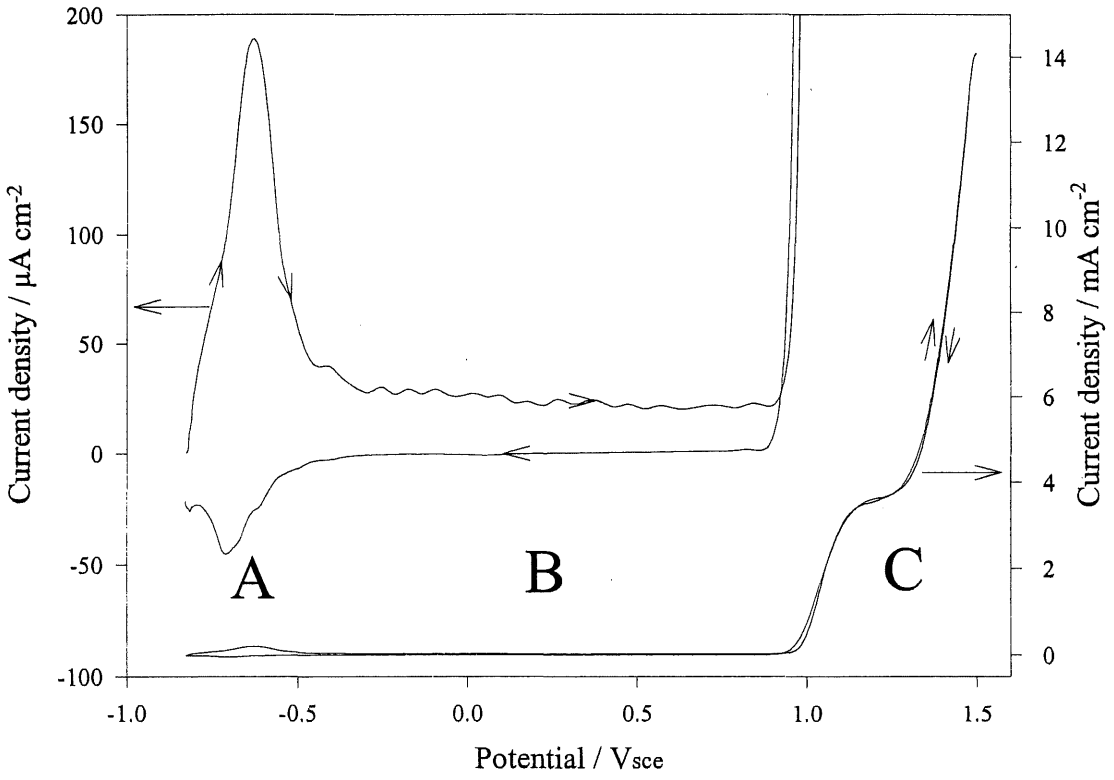

Figure. 15. Potentiodynamic trace for an iron electrode in 0.1M sodium bicarbonate solution and a scan rate of 5 mVs^{-1}. Potential scan limits: -0.85 V and 1.5 V; rotation speed =1000 rpm. A. active-passive dissolution region, B. passivation region and C. transpassive region.

3.1.3 Solutions with bicarbonate and sulfate ions

The voltammogram of a rotating iron disk electrode in 0.3M Na_2SO_4 + 0.01M $NaHCO_3$ solution with the conditions of Fig. 10 is shown in Fig. 16. For the scan in the anodic potential direction, the following features have been noticed: (i) a small anodic peak current (peak I) located at -0.6 V, (ii) a second, dominant anodic peak current (peak II) with its maximum close to 0 V, (iii) a passive region extending from 0.4 V to 0.9 V, which is followed by a transpassive region prior to the onset of the oxygen evolution at potentials higher than 1.0 V.

The electrode surface remains passive for the potential scan reversal and a broad cathodic peak current at -0.75 V is observed. The presence of peak I and the plateau current in the transpassive region is associated with the effect of dissolved $NaHCO_3$ (Fig. 15). The anodic current peak II and the pit formation, which is manifested by small anodic current oscillations close to the peak potential, are induced by the presence of sulfate ions. In Fig. 17 the voltammograms with increasing positive potential limits, i.e. -0.35 V, -0.325 V, and -0.3 V, illustrate the growth of initial pits by an increase in current for the scan reversal, with the protection potential being close to -0.52 V.

With an increase in the bicarbonate concentration, the sulfate ions concentration being constant, the height of peak current I increases, peak current II decreases and there is an increase in the plateau current in the transpassive region (Fig. 18). With an increase in the sulfate concentration, the concentration in sodium bicarbonate being constant, the anodic current peaks I and II and the current in the passive region increase but the plateau current in the transpassive region decreases. Peak II is accompanied with pitting corrosion in all cases (Figs. 16, 17, and 18). From Figs. 18 and 19, it is observed for the reverse potential scan in the region of peak I, that there is more anodic reactivation with an increase in the ratio of sulfate to bicarbonate ions.

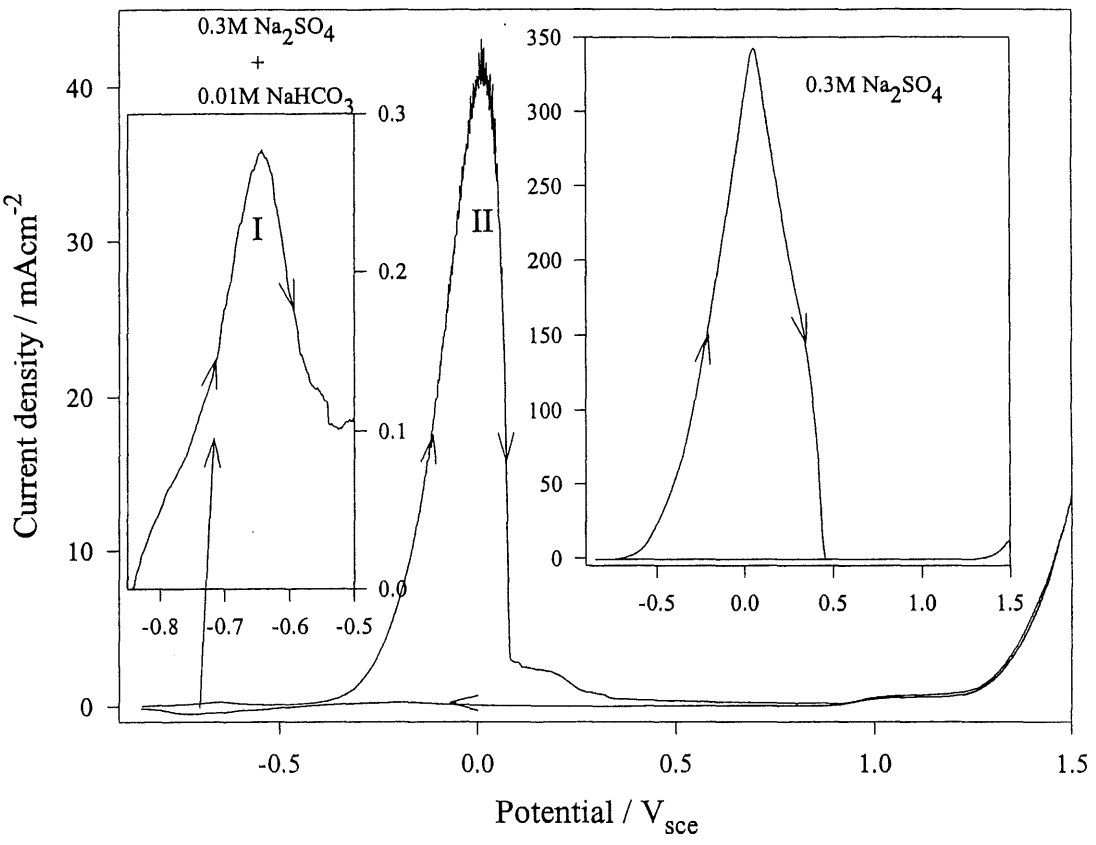

Figure. 16. Potentiodynamic trace for an iron electrode in a solution containing 0.3M sulfate + 0.01M bicarbonate, IR drop compensated. Insert: 0.3M sodium sulfate solution only. dE/dt=5 mVs^{-1}; rotation speed =1000 rpm. Potential scan limits: -0.85 V and 1.5 V.

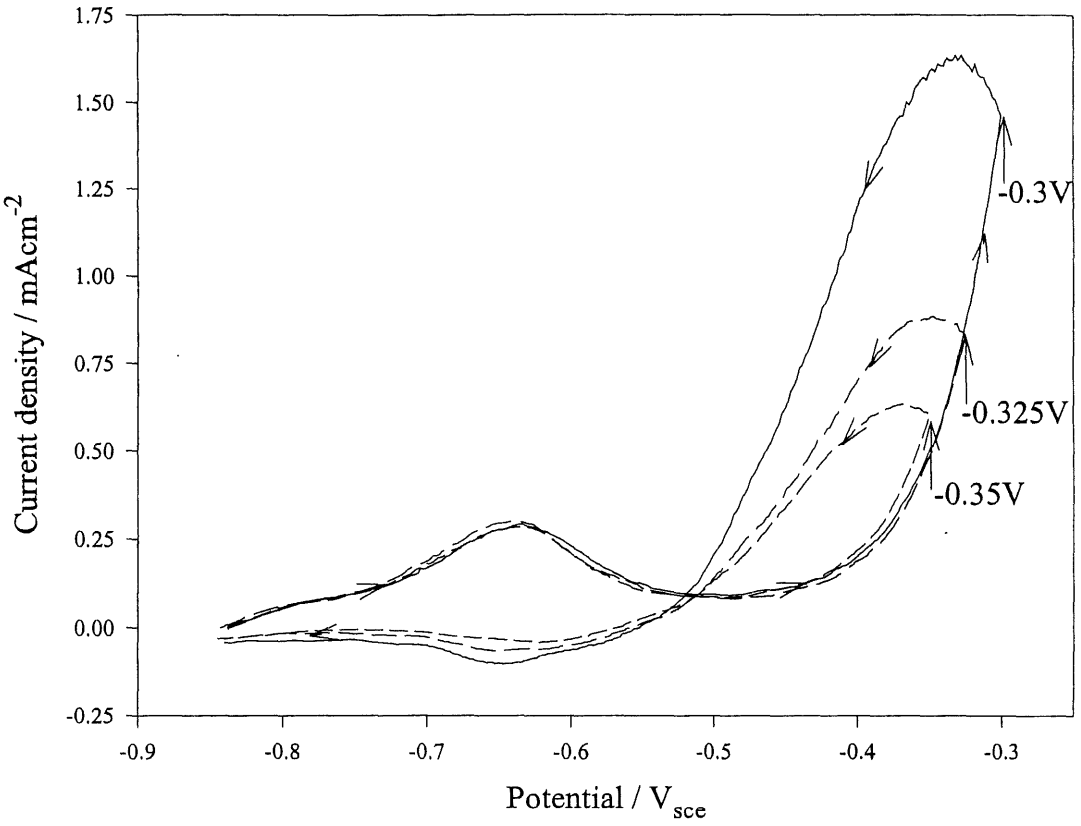

Figure. 17. Effect of switching potentials on the potentiodynamic trace during the return sweep for a solution containing 0.3M sulfate + 0.01M bicarbonate. The other experimental conditions are those of Fig. 16.

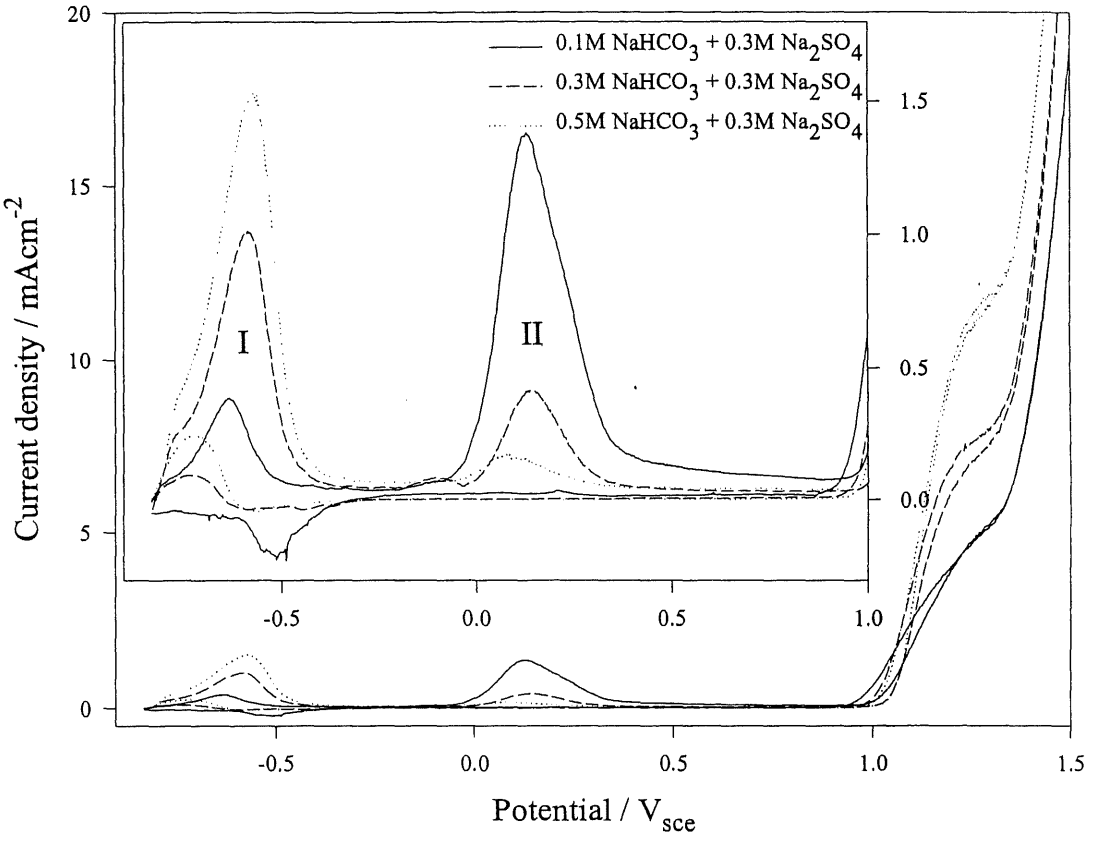

Figure. 18. Voltammograms for an iron electrode in 0.3M sulfate + x M bicarbonate, x= 0.1, 0.3, and 0.5M; dE/dt=5 mVs^{-1}; rotation speed =1000 rpm; starting potential: -0.85 V.

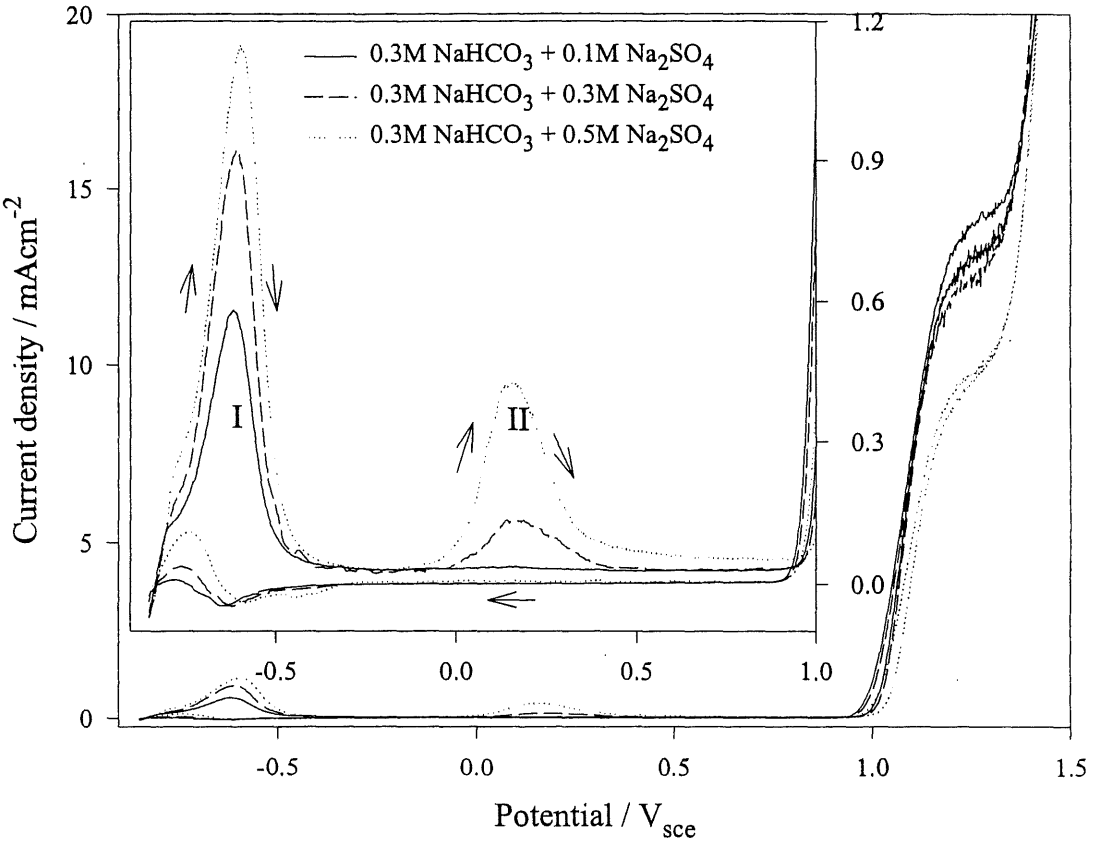

Figure. 19. Voltammograms for an iron electrode in 0.3M bicarbonate + x M sulfate, x= 0.1, 0.3, and 0.5M; dE/dt=5 mVs^{-1}; rotation speed =1000 rpm; starting potential: -0.85 V.

The current versus time curve for an iron electrode at 0.0 V in 0.1M $NaHCO_3$ + 0.1M Na_2SO_4 solution is shown in Fig. 20. The current increases over time to reach a quasi steady-state value for iron oxidation after ~150 s. The appearance of the iron surface in the region of the steady-state current remains unchanged over time (Fig. 21). The pictures in Fig. 21 show the formation of a precipitate on the surface during the electrodissolution process.

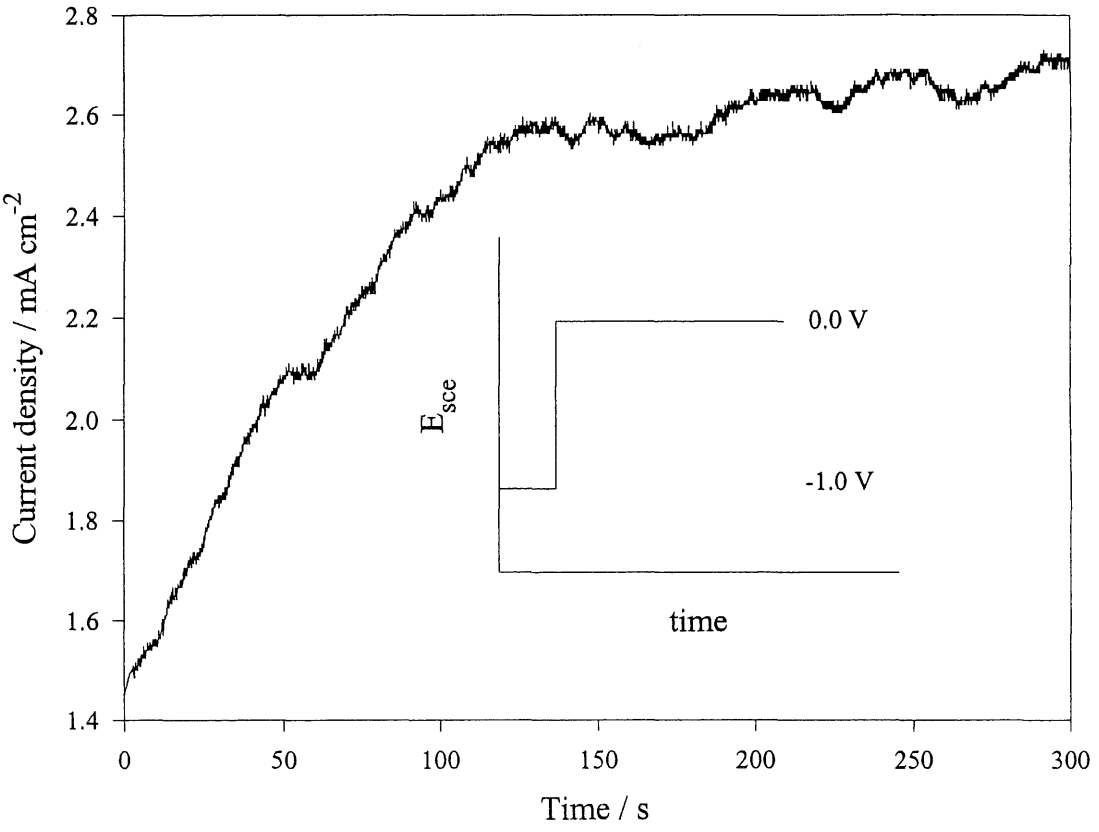

Figure 20. Chronoamperogram for an iron electrode in a 0.1M sulfate + 0.1M bicarbonate solution. rotation speed =1000 rpm. Insert: Applied potential versus time.

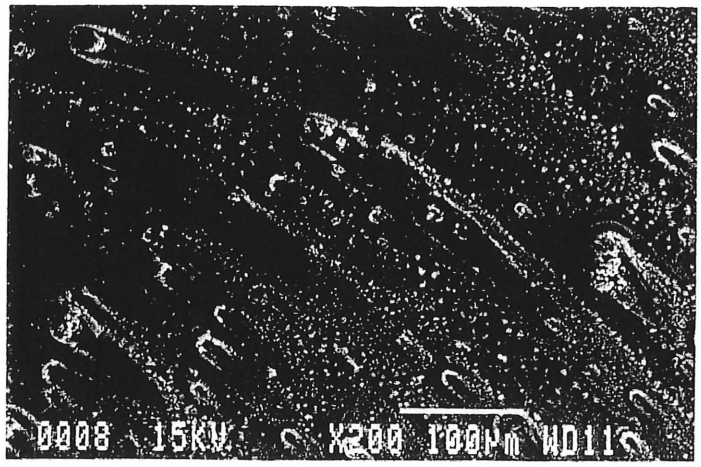

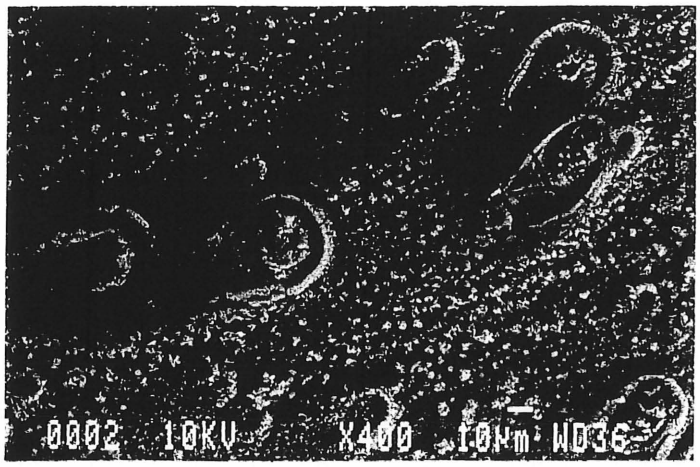

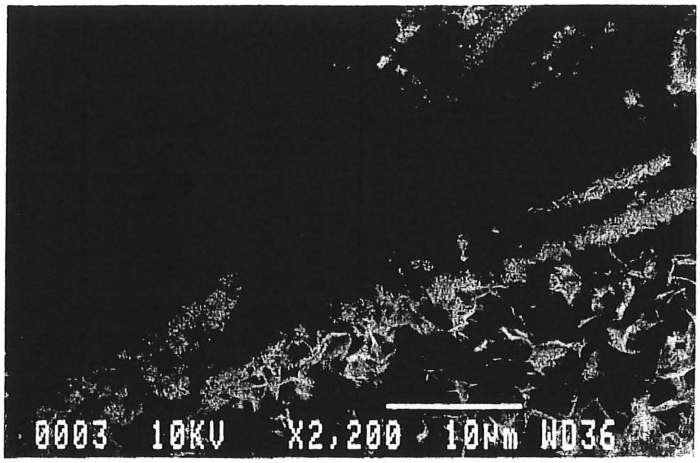

Figure 21. SEM pictures for an iron electrode after 300 s of oxidation in a 0.1M sulfate + 0.1M bicarbonate solution.

In another set of experiments (Figs. 22a-d), the effect of different preoxidation treatments of an iron electrode prior to potentiodynamic characterization in solutions containing bicarbonate ions, sulfate ions, and mixture of both ions was established. For bicarbonate solutions, the iron electrodes have been preoxidized at 0.9V in 0.1 M $NaHCO_3$ solution to reach an oxidation charge of 500 μC (4 mC cm^{-2}) prior to the potential sweep in the cathodic direction at a scan rate of 0.005 V s^{-1}; the potentiodynamic trace is illustrated in Fig. 22a. In a second set of experiments, the potentiodynamic traces were obtained under the experimental conditions of Fig. 22a (including the preoxidation treatment) except that 0.3M Na_2SO_4 was added just prior to the potentiodynamic scan in the cathodic direction (Fig. 22b). For a third set of experiments, the electrode has been preoxidized at 0.9 V, to reach an oxidation charge of 500 μC in the presence of 0.1 M $NaHCO_3$ + 0.3 M Na_2SO_4 and then the potentiodynamic trace has been recorded (Fig. 22c). For a fourth set of experiments, potentiodynamic traces in the solution containing 0.1 M $NaHCO_3$ + 0.3 M Na_2SO_4 without any preoxidation treatment have been recorded (Fig. 22d).

In bicarbonate solution only, the potentiodynamic trace (Fig. 22a) displays a passivation region up to +0.4V, a cathodic peak current with its maximum at -0.6 V and an anodic peak current at ~-0.7 V. The picture is different with the addition of sulfate ions to the bicarbonate solution (Fig. 22b): (i) the oxidation current is bigger at potential values anodic enough, (ii) the current becomes cathodic below ~0.3 V and a plateau current between 0.1 and -0.3 V is noticed, (iii) two consecutive cathodic peaks located at -0.45 and -0.55 V, respectively, are noted. For 0.1 M $NaHCO_3$ + 0.3 M Na_2SO_4 solutions, the potentiodynamic trace (Fig. 22c) displays a significant oxidation current up to -0.2 V with two cathodic current peaks, being located at ~-0.3 V and -0.55 V. Further, the potentiodynamic trace for an iron electrode without any preoxidation treatment in 0.1 M $NaHCO_3$ + 0.3 M Na_2SO_4 (Fig. 22d) has approximately the same characteristics as the trace with a preoxidation treatment (Fig. 22c), except that the height of the cathodic current peaks at low potentials tends to be lower without preoxidation. In both cases (Figs. 22c and 22d), the two cathodic peaks are associated with the

reduction of the pitting products and other reducible oxide compounds present on the iron electrode surface.

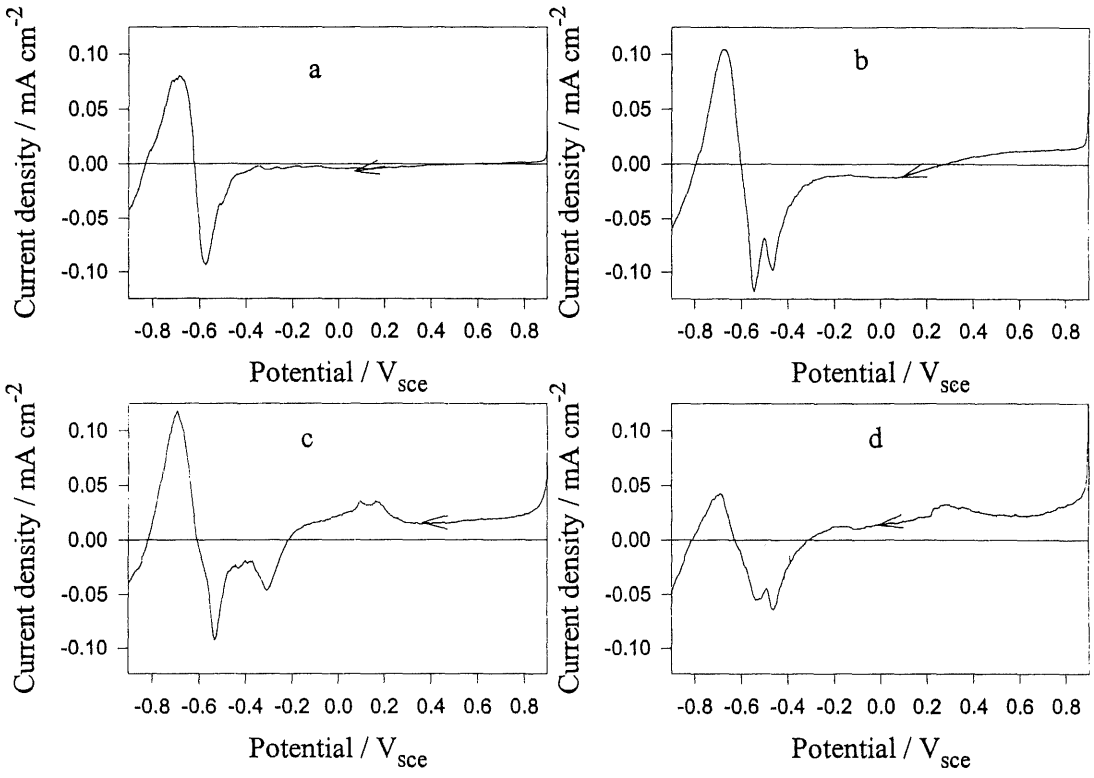

Figure 22. Voltammograms for an iron electrode: a) after preoxidation* in 0.1M bicarbonate solution. starting potential: 0.9 V, the potential is swept** in the negative direction; b) after preoxidation* in 0.1M bicarbonate and the addition of 0.3M sulfate prior to the potential sweep** in the cathodic direction, starting potential: 0.9 V, c) after preoxidation* in 0.1M bicarbonate + 0.3M sulfate; starting potential: 0.9V, the potential is swept** in the negative direction, d) without preoxidation; starting potential: 0.9 V; the potential is swept** in the negative direction, solution: 0.1M bicarbonate + 0.3M sulfate.
*Preoxidation conditions: E=0.9V to reach an oxidation charge of 500 μC (4 mC cm^{-2}).
**dE/dt=5 mV/s.

In order to determine the critical molar ratio of bicarbonate to sulfate required to avoid any localized attack, experiments have been carried out in the presence of 0.03 and 0.06 M of sulfate plus 0.3 M bicarbonate solutions. The current versus time curve for E=0 V is characterized by pitting corrosion for 0.06 M sulfate and the absence of localized attack for 0.03 M sulfate solutions. The absence of any localized attack for 0.03 M sulfate + 0.3 M bicarbonate has also been noticed for 5 consecutive potentiodynamic cycles with a scan rate of 0.005 Vs^{-1} and ω=1000 rpm, with the potential limits of -0.85 V and 1.5 V. Compared to cyclic voltammograms obtained in the presence of bicarbonate solutions only (5 consecutive cycles), the electrode surface has the same appearance and no localized attack is found. Consequently, it may be deduced that a molar ratio of 10:1 of bicarbonate to sulfate results in the complete suppression of any localized attacks induced by the presence of sulfate

3.2 Discussion and conclusions

In the part of the potentiodynamic curve for which the oxidation current increases with the potential for low potentials, the corrosion process is uniform in the presence of SO_4^{2-} ions only and the formation of Fe(II) species is postulated (Fig. 10). The SO_4^{2-} ions participate in the formation of an $FeSO_4$ ion pair complex (67) and the anodic current increases up to a very large value. At more anodic potentials, the large passivation region is explained by a dissolution-precipitation reaction and solid-state oxidation of iron to Fe(II)/Fe(III) oxide/hydroxide (11). The dark-green precipitate observed on the electrode surface is most likely related to a ferrous hydroxy sulfate according to Gibbs and Cohen (68). Génin *et al.* (22,27) proposed, as a transient compound, the green rust 2 (GR2) with the following formula: $4Fe(OH)_2.2FeOOH.FeSO_4.nH_2O$ where n is probably 4. The latter compound corresponds to an oxidation number of 2.29 i.e. $5Fe^{2+}$ and $2Fe^{3+}$ ions. At more anodic potentials, the formation of a passive film may be considered according to ref. 26:

$$4Fe(OH)_2.2FeOOH.FeSO_4 + 2H_2O = 7\gamma FeOOH + SO_4^{2-} + 7H^+ + 5e^- \qquad [3.1]$$

When the anodic potential increases from 0.25 V to 1.25 V, it is postulated that the hydroxides change to oxides and the Fe(III) oxides may form the passive film. At potentials more anodic than ~1.25 V, a transpassive region is noticed with the oxygen evolution at the potentials that are sufficiently anodic.

The potentiodynamic trace for the potential scan in the negative direction has a passive region as large as 1.55 V (Fig. 10), which is in agreement with the fact that Fe_2O_3 is very stable (69). The minimum passive current in forward (positive) scan (50 $\mu A\ cm^{-2}$) is large compared to the one of the backward (negative) scan (2.5 $\mu A\ cm^{-2}$); it is due to the effect of the oxidation potential and time. The passive film is resistant against the sulfate ion attack and the passivation region extends to more negative potentials. At -0.85 V, the cathodic current (80 $\mu A\ cm^{-2}$) is linked to reduction of an oxides film and hydrogen evolution.

The precipitation of the green rust GR2 is potential and time-dependent, as shown by the potential scan in the negative direction (Fig. 11). The surface oxidation at positive potentials in the presence of sulfate ions induces the formation of a passive film but the precipitation of a sulfate product alone can not protect the electrode against localized attack or uniform electrodissolution.

The effect of the applied potential on the passive film formation as shown by chronoamperometric transients at 0.2 V and 0.4 V (Fig. 11) for iron electrodes in 0.3M sulfate solution illustrates that pit formation is more difficult and precipitate products are formed at higher potentials. When the potential was stepped from -1 V to 1 V and maintained for 1 h at 1 V, the electrode experienced no localized attack and appeared golden and shiny, indicating the surface film growth. It shows the optical phenomenon of multiple thin layer light beam interference (70) and can be related to the existence of a hydrous iron oxide layer which is yellow-green at positive potentials (71).

The voltammogram for the iron electrode in bicarbonate solution only shows an oxidation current peak at ~-0.6 V (Fig. 15), which is ascribed to the onset of the formation of solid oxides species on the electrode surface. The dissolution current is of three orders of magnitude lower with the passivation region being 400 mV wider than that of the iron electrode in a sulfate solution with the same concentration. The electrochemical behavior of iron in bicarbonate solution is similar to the one for borate solution but the current is larger (72). In the active dissolution region, iron dissolves as an unstable $FeHCO_3^+$ complex (73) and at the anodic current peak (-0.6 V), $FeCO_3$ ($FeCO_3$ $K_{sp} = 3.07x10^{-11}$) (73) starts to precipitate (74). As the positive potential increases, $FeCO_3$ may be transformed into an oxide, and the oxidation state of the iron species in the passive layer changes. The surface enhanced Raman spectrum (74) of the film formed at -400 mV and at 0 V is different from each other. The spectrum at -400 mV indicate the presence of $Fe(OH)_2$ as well as $FeCO_3$, but when the potential is subsequently stepped to 0 V, the peaks associated with $FeCO_3$ are absent. In the passive film, the oxidation of Fe^{2+} to Fe^{3+} passes by a green rust transient ($[Fe_4^{(II)}Fe_2^{(III)}(OH)_{12}][CO_3.2H_2O]$) between ferrous hydroxides and ferric oxyhydroxides (21). The composition of transient compounds changes with the ratio of Fe^{2+}/OH^-.

The bicarbonate ions participate in the kinetics of oxidation in the transpassive region and it is possible to separate the processes corresponding to the formation of Fe(VI) species and the oxygen evolution reaction. It was discussed in the literature (64-66) that the OH^- concentration markedly influences the production of FeO_4^{2-} and that the free ferrate in solution decomposes at a higher rate than the surface Fe(VI) complex. The anodic plateau current (Fig. 15) illustrates that the presence of bicarbonate/carbonate ions in the solution stabilizes ferrate in the surface film. In the study of mild steel (75) and stainless steel 304 (76) in bicarbonate solutions, a current plateau in the transpassive region was also reported and attributed to the generation of ferrate species. In the case of iron in borate and sulfate solutions at the same pH, the anodic current increased with the onset of oxygen evolution and no ferrate formation was observed.

Voltammograms of iron in solutions containing both sulfate and bicarbonate ions are characterized by the presence of two anodic peak currents in two separate potential regions (Fig. 16). The addition of more $NaHCO_3$ to Na_2SO_4 solutions resulted in a substantial increase of peak current I, a decrease of peak current II and potential range increase for the passive region (Figs. 18 and 19). The anodic peak currents I and II are most likely related to the formation of soluble $FeHCO_3^+$ complex and green rust 2 (GR2), respectively. SERS studies show that the films formed on iron in mildly alkaline solutions of nitrate, carbonate/bicarbonate, sulfate and borate are similar (74). The rate of iron oxidation in sulfate and nitrate is greater than that in carbonate/bicarbonate which is, in turn, greater than that in a borate buffer. The major constituents of all solutions are similar and it is suggested that the effect of the anions on the rate of oxidation of iron in mildly alkaline solutions results from their abilities to form soluble complexes with either Fe^{2+} or Fe^{3+} (74).

A different electrochemical behavior of iron in sulfate solutions and chloride solutions containing inhibitive ions has been reported in the literature (10,11). The main difference is that for iron in a chloride solution after pit initiation, the current increases markedly and does not show any inhibition potential, indicating that the pitting corrosion products are not protective because of their high solubility. For sulfates, the increasing concentration of dissolution products in the pits during pitting corrosion results in the precipitation of corrosion products which further hinder the pitting growth process. With an ionic radius ratio of 8:1 for sulfate to chloride (73), it is deduced that sulfate ions have less mobility than chloride ions to leave the pit sites. In the presence of aggressive ions when an appropriate pH is attained at the surface, sulfate ions can adsorb and react with the passive layer and later with metallic iron. Since sulfate ions adsorb better than carbonate ions (76), sulfate ions compete with carbonate species and cause pitting. When pitting products cover the pits, these reactions slow down and local passivation starts. When pitting manifests, it causes a potential drop inside the pits shifting the potential inside the pits to the active dissolution region and accelerate the dissolution rate (77). In accordance with the existence of green rusts, depending

on the ratio of Fe^{2+}/OH^- during the dissolution reactions and changes in the surface pH, different transient compounds can be formed. However, in such a case, there is competition between sulfate and carbonate species. It has been found that these transient compounds have a different selectivity towards sulfate and carbonate ions and their tendency is more toward carbonate than sulfate ions (78,79). Hence, as transient compounds form on the surface with an accumulation of carbonate species on the electrode surface, the current starts to decrease and passivation begins.

CHAPTER 4

Electrochemical Behavior of Iron in Aqueous Phosphate Solutions Containing Sulfate and Chloride ions

4.1 Introduction

In the previous chapter, the behavior of iron electrode in solutions containing sulfate and bicarbonate ions has been shown. It has been shown that iron has passivating behavior in bicarbonate ion solutions but tremendous electrodissolution in sulfate ion solutions. In the mixture of both bicarbonate and sulfate ions, iron shows both behavior of iron in aggressive and passivative media, i.e. there is a region in passivation region which shows pitting corrosion and then repassivation again attained. In this chapter main attention is on the electrochemical behavior of iron in phosphate solutions in the presence of sulfate and chloride ions.

4.2 Results

Figure 23 shows a potentiodynamic curve of an iron electrode rotated at 1000 rpm in 0.01M Na_2HPO_4 (pH ~8) solution with a potential scan rate of 0.005 Vs^{-1} and potential limits of -0.84 and 2.0 V. The curve displays a dominant anodic peak current located at -0.6 V, its maximum current being ~90 μAcm^{-2}. The peak current is ascribed to a dissolution-passivation process, which is common for buffer inhibitors (81). The peak current is followed by a large passive region extending from -0.4 V to +0.85 V. For E > +0.85 V, the transpassive region, the more anodic the applied potential, the larger the current density due to the onset of oxygen evolution; no waves associated to ferrate species are noted as reported for bicarbonate aqueous solutions (35). The potentiodynamic trace of the negative potential scan is characterized by a small cathodic peak at -0.6 V.

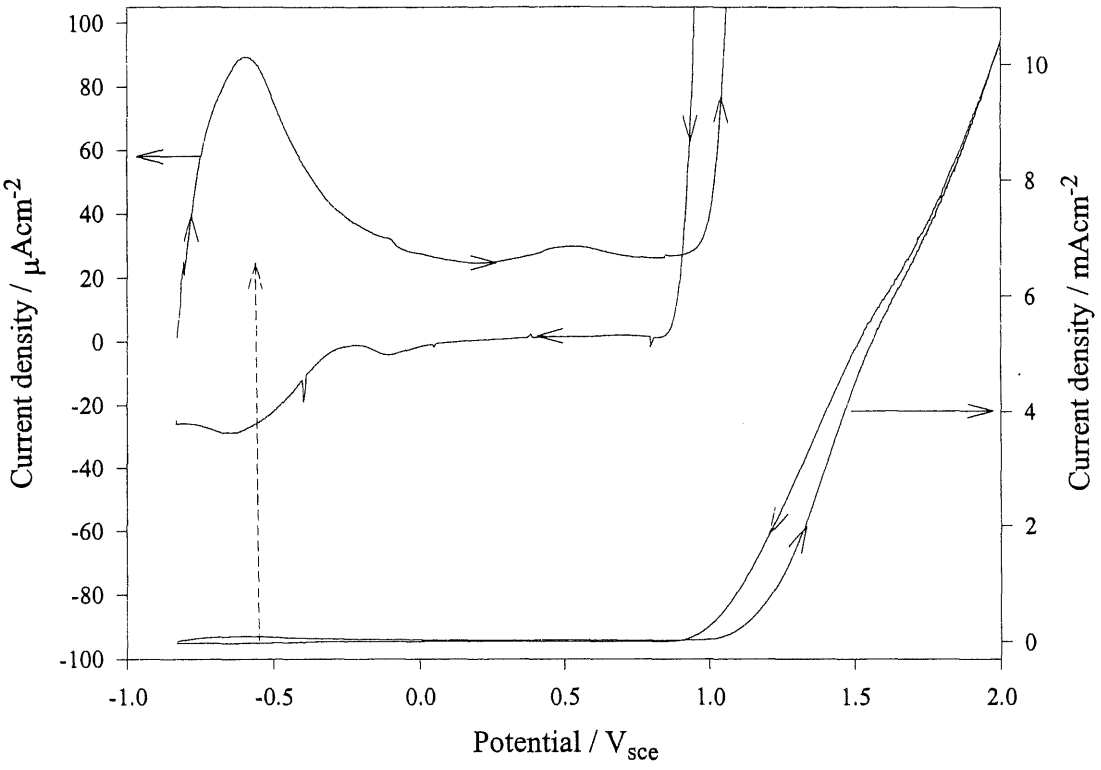

Figure 23. Potentiodynamic trace for a rotating iron disk electrode, in 0.01M sodium phosphate solution, dE/dt=5 mVs^{-1}; rotation speed =1000 rpm. Starting potential: -0.84 V.

The picture of the potentiodynamic behavior of a rotating iron disk electrode is different in the presence of 0.01M Na_2HPO_4 + 0.1M Na_2SO_4 solution (Fig. 24), as the potential scan rate and the potential scan limits are those of Fig. 23: (i) the height and the location of the first anodic peak (peak I) is practically the same for both solutions; (ii) a second anodic peak current (peak II) close to 0.22 V is noted with some current oscillations in the presence of sulfate ions; (iii) a repassivation region extending from 0.5 V to 0.9 V with some current oscillations is observed in the presence of sulfate ions; (iv) at potentials higher than 1.0 V, a transpassive region with a small plateau current prior to the onset of the oxygen evolution reaction appears in the presence of sulfate ions. The small plateau current is absent on the potentiodynamic curve of iron when recorded in separate solutions of phosphate and sulfate ions and a synergetic effect of phosphate and sulfate ions together is deduced (in a solution containing both sulfate and phosphate ions); the electro-oxidation current remains non-negligible during the return sweep from 0.9 V to -0.2 V with a broad cathodic wave current at -0.6 V. The small anodic current oscillations in the region of anodic peak current II are ascribed to the metastable pitting induced by the presence of sulfate ions in the phosphate solution.

For a constant phosphate ion concentration, the greater the sulfate ion concentration, the greater the height of both peak current I and II and the lower the plateau current in the transpassive region (Fig. 25). The location of the two oxidation peaks is practically the same in 0.01 M Na_2HPO_4 + 0.1 to 0.5 M Na_2SO_4. the greater the phosphate ion concentration, the concentration in sulfate ions being constant, the lower the anodic current peaks I and II (Fig. 25). Peak II is accompanied by pitting corrosion in the presence of sulfate ions. The formation of a white precipitate as a corrosion product is observed at the pit sites.

The solution containing 0.01M Na_2HPO_4 + 0.1M Na_2SO_4 (Fig. 24) has been further considered to establish the effect of the anodic potential reversal on the potentiodynamic curves during the return sweep (Fig. 27). When the potential reversal is located in the region of pit initiation, i.e. the first part of peak II, the current is larger during the return sweep due to pit

growth. For the descending part of peak current II, the electrode surface is completely covered with corrosion products and the current during the return sweep is lower. As the anodic potential reversal becomes more anodic than ~0.5 V, the passivation range for the potential scan reversal is larger and the height of the cathodic peak current at -0.6 V increases.

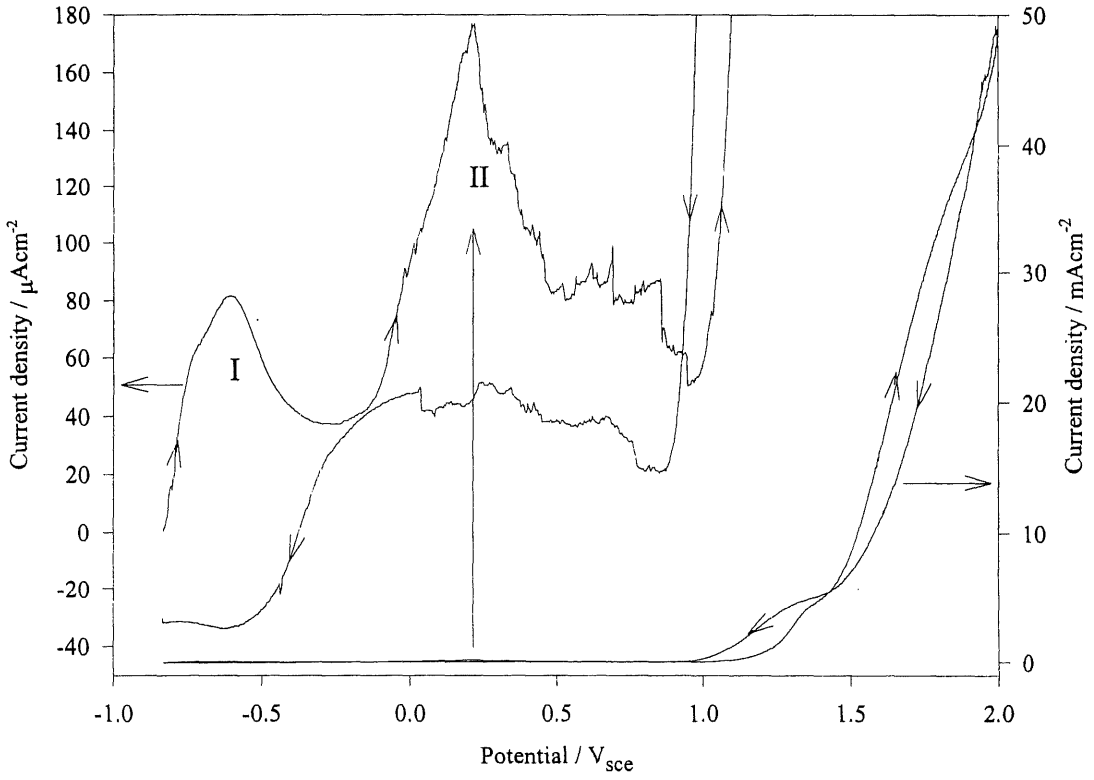

Figure 24. Potentiodynamic trace for a rotating iron disk electrode, in 0.01M sodium phosphate + 0.1M sodium sulfate solution, dE/dt=5 mVs^{-1}; rotation speed =1000 rpm. Starting potential: -0.84 V.

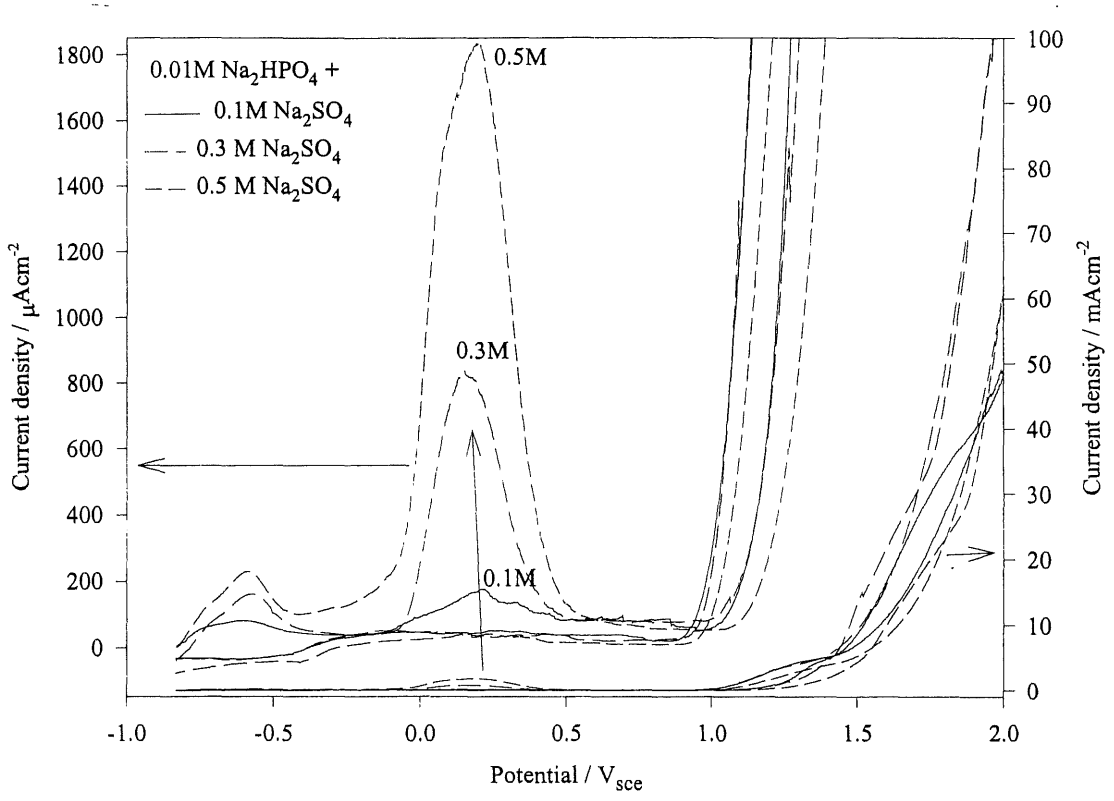

Figure 25. Voltammograms for an iron electrode in 0.01M phosphate + x M sulfate, x= 0.1, 0.3, and 0.5M; dE/dt=5 mVs^{-1}; rotation speed =1000 rpm; starting potential: -0.84 V.

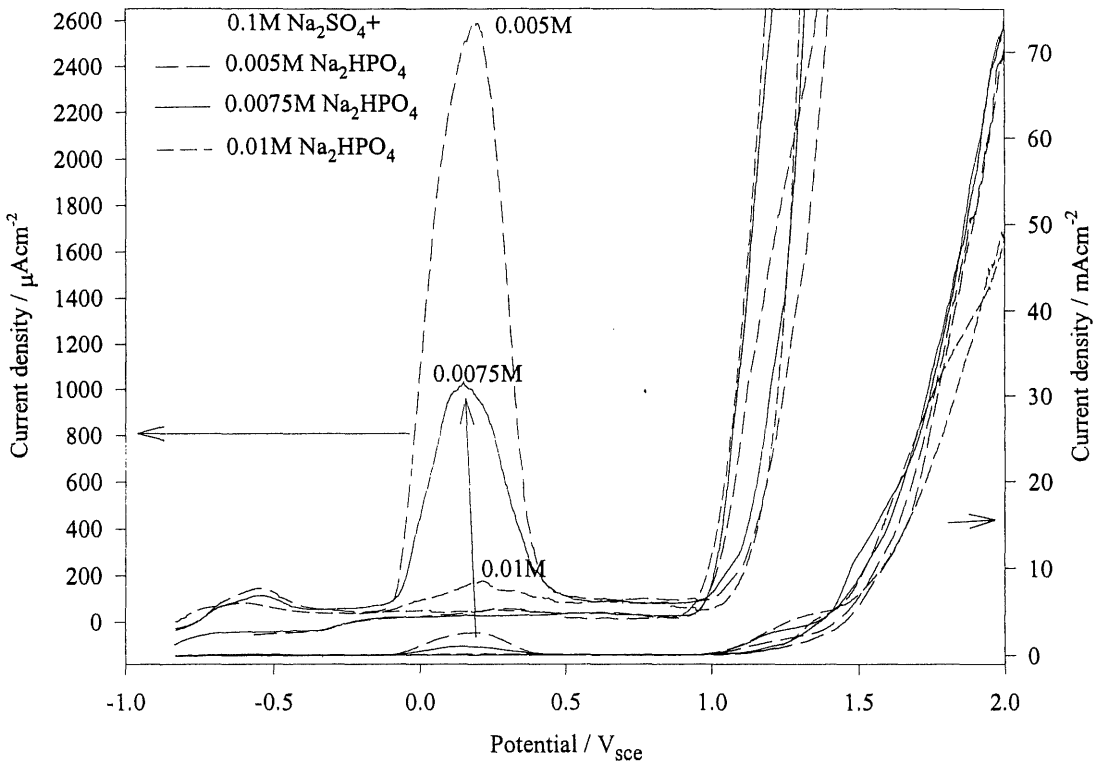

Figure 26. Voltammograms for an iron electrode in 0.1M sulfate + x M phosphate, x= 0.005, 0.0075, and 0.01M; dE/dt=5 mVs^{-1}; rotation speed =1000 rpm; starting potential: -0.84 V.

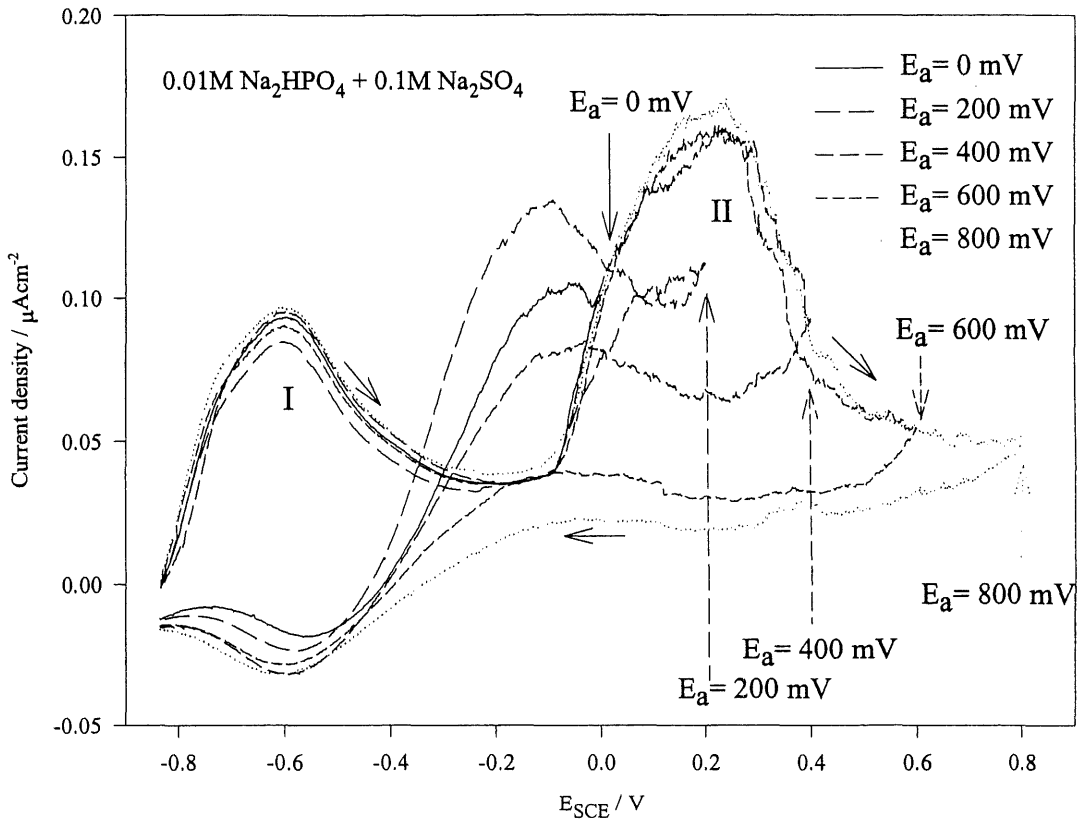

Figure 27. Effect of switching potentials on the potentiodynamic trace during the return sweep for a solution containing 0.1M sulfate + 0.01M phosphate. The other experimental conditions are those of Fig. 24.

The effect of ω on the steady-state electrodissolution current at -0.6 V (i.e. the maximum of current peak I) for rotation speed ranging from 500 to 4000 rpm is illustrated in Fig. 28. The steady-state current has been attained after 20 min. of polarization. A linear relationship is observed for the steady-state current density expressed against $\omega^{1/2}$ with $i \neq 0$ for $\omega \rightarrow 0$, ω being below 4000 rpm. It is deduced that the rate-determining-step of iron dissolution is mainly the diffusion of ionic species into the solution in the vicinity of the electrode surface. The effect of the potential scan rate (dE/dt) on the location of peak I and its height is illustrated in Fig. 29 for a stationary electrode in a quiescent solution. Again, it is deduced that diffusion of ionic species into the solution in the vicinity of the electrode surface plays a key role in limiting of the electrodissolution process involved in the region of peak I. As a first approximation, both peak current density and potential increase linearly with the square root of the scan rate, with a dissolution-precipitation mechanism being deduced (30).

The current versus time curves recorded at constant applied potentials located in the region of peak II are characterized by a high oxidation charge before surface passivation as shown in Fig. 30 for an applied potential of 0.0 V (SCE) (Q_{ox}=250 C cm^{-2} after 8000 s). Chronoamperograms for constant applied potentials located in the ascending part of peak current II on the potentiodynamic curve have the following features: (i) for short enough times, the electrooxidation current increases with time to reach a maximum value which is very high (ii); current oscillations are noted close to the current maximum and in the region where the current decreases with time. The current oscillations are ascribed to a local film breakdown followed by a repair process. As the steady-state current was attained after several thousand seconds, the electrode surface was completely covered with a white precipitate which is poorly protective and adheres to the electrode surface. The precipitate was easily removed after each experiment and rinsed carefully with deionized water for further investigation. The ICP analysis, X-ray fluorescence analysis and FTIR spectroscopy were done for the precipitate obtained under different constant applied potentials located in the peak II region. The precipitate formed on the electrode surface in the solution is white but becomes green in

contact with air. In spite of the 10:1 molar ratio of sulfate to phosphate ions in the solution, the precipitate contains mainly phosphate and a negligible amount of sulfate. FTIR spectra of the precipitate are in good agreement with the formation of iron phosphate. From ICP measurements, a molar ratio Fe/P of 1.6 has been obtained for different constant applied potentials located in the peak II region; which is consistent with the formation of iron (II) phosphate. The same result was obtained with the X-ray fluorescence analysis (Fig. 31), i.e. Fe/P = 3/2.

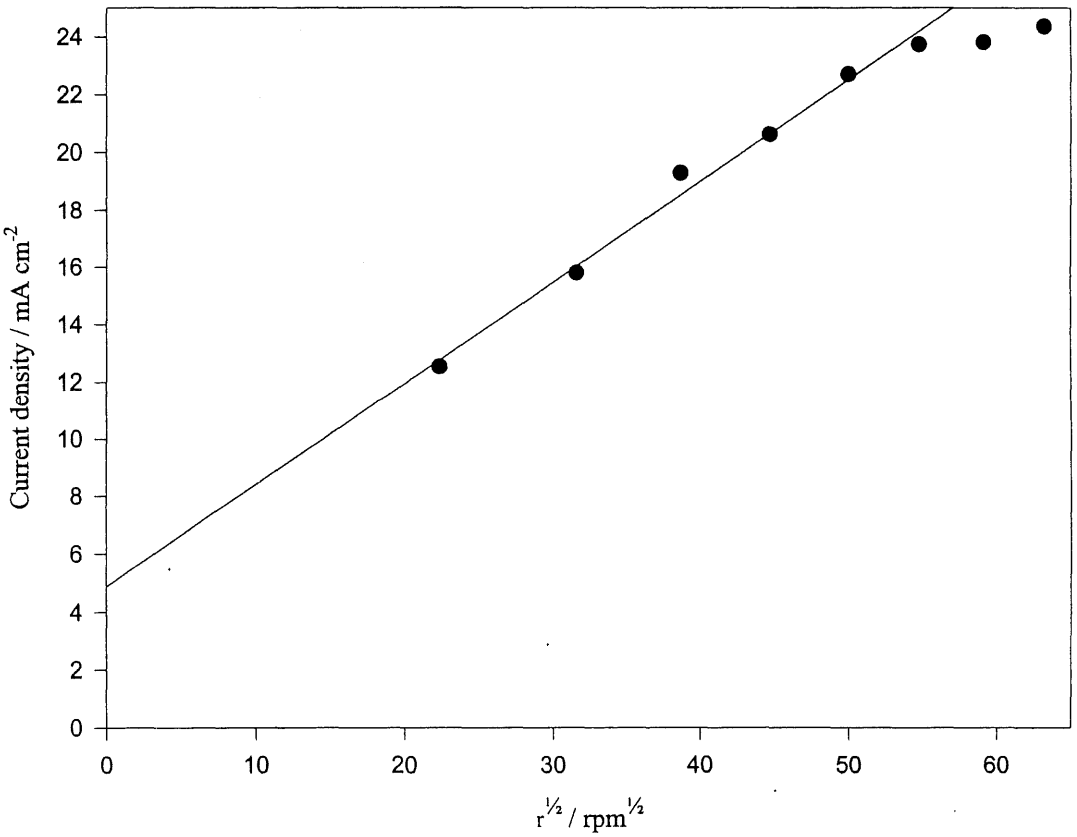

Figure 28. Effect of electrode rotation speed on the electrooxidation steady-state current density at -0.6 V for an iron electrode in an aqueous solution of 0.1M sulfate + 0.01M phosphate. Current density after 20 min at a constant applied potential of -0.6 V was used as the steady-state value.

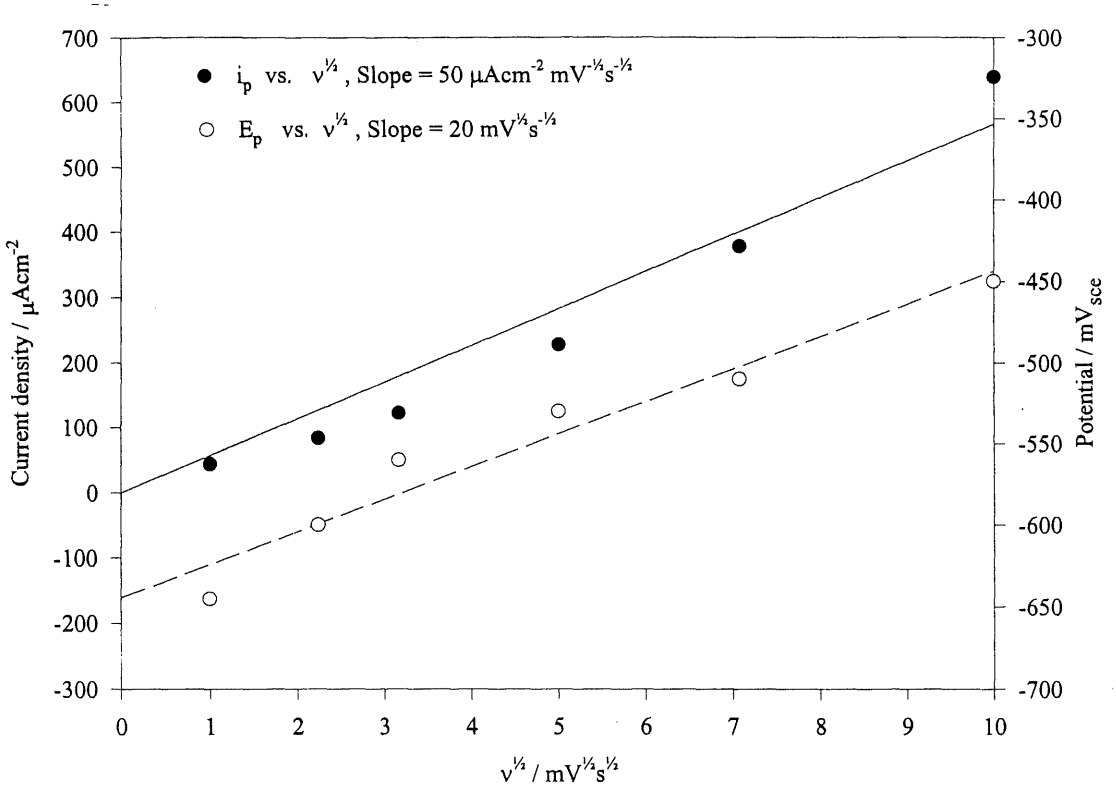

Figure 29. i_p and E_p plotted against the square root of the potential sweep rate for an iron electrode in an aqueous solution of 0.1M sulfate + 0.01M phosphate. rotation speed = 0 rpm, sweep rate ranges from 1 to 100 mVs^{-1}.

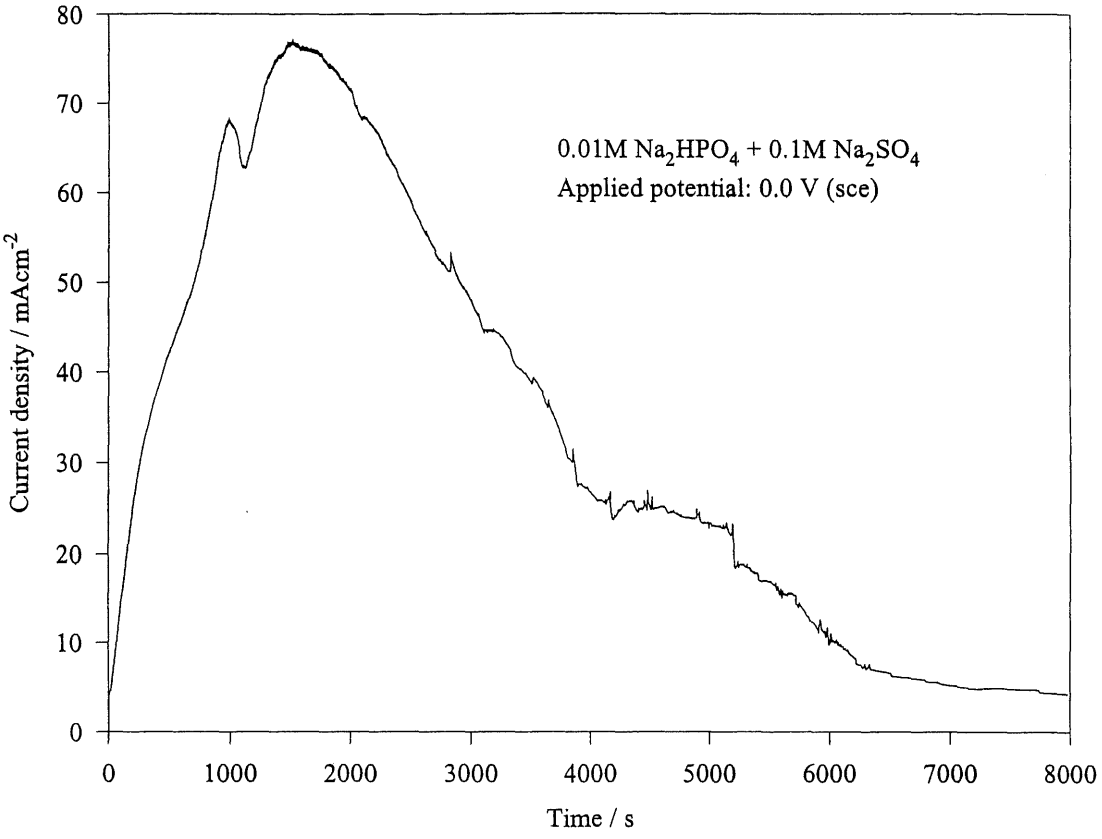

Figure 30. Chronoamperogram for an iron electrode in a 0.1M sulfate + 0.01M phosphate solution. rotation speed =1000 rpm. Applied potential: 0.0 V (SCE); Q_{ox}=250 C cm^{-2}.

TN-5 00 MON 28-OCT-96 12:52

Cursor: 0.000keV = 0 ROI (10) 0.000: 0.000

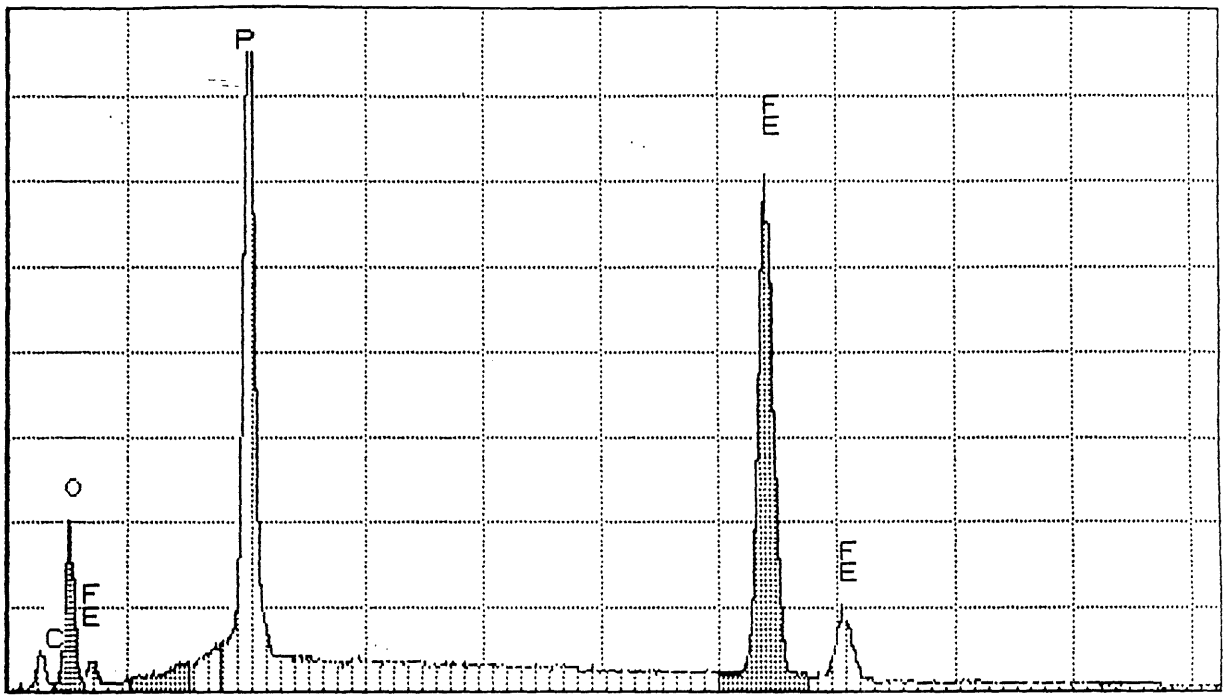

SQ: QUANTIFY

PRECIPITE DE FER
Standardless Analysis
15.0 kV 18.1 Degrees

Chi-sqd = 2.02

Element	Rel. K-ratio	Net Counts
Fe-K	0.78462 +/- 0.00913	25705 +/- 299
P -K	0.21538 +/- 0.00244	25099 +/- 284

ZAF Correction 15.00 kV 18.11 deg
No.of Iterations = 4

Element	K-ratio	Z	A	F	ZAF	Atom%	Wt%
Fe-K	0.688	1.030	1.011	1.000	1.041	58.31	71.60
P -K	0.189	0.948	1.588	0.999	1.504	41.69	28.40
						Total=	100.00%

Figure 31. Qualitative and quantitative X-ray fluorescence results of the precipitate after formation under the experimental conditions of Fig. 30.

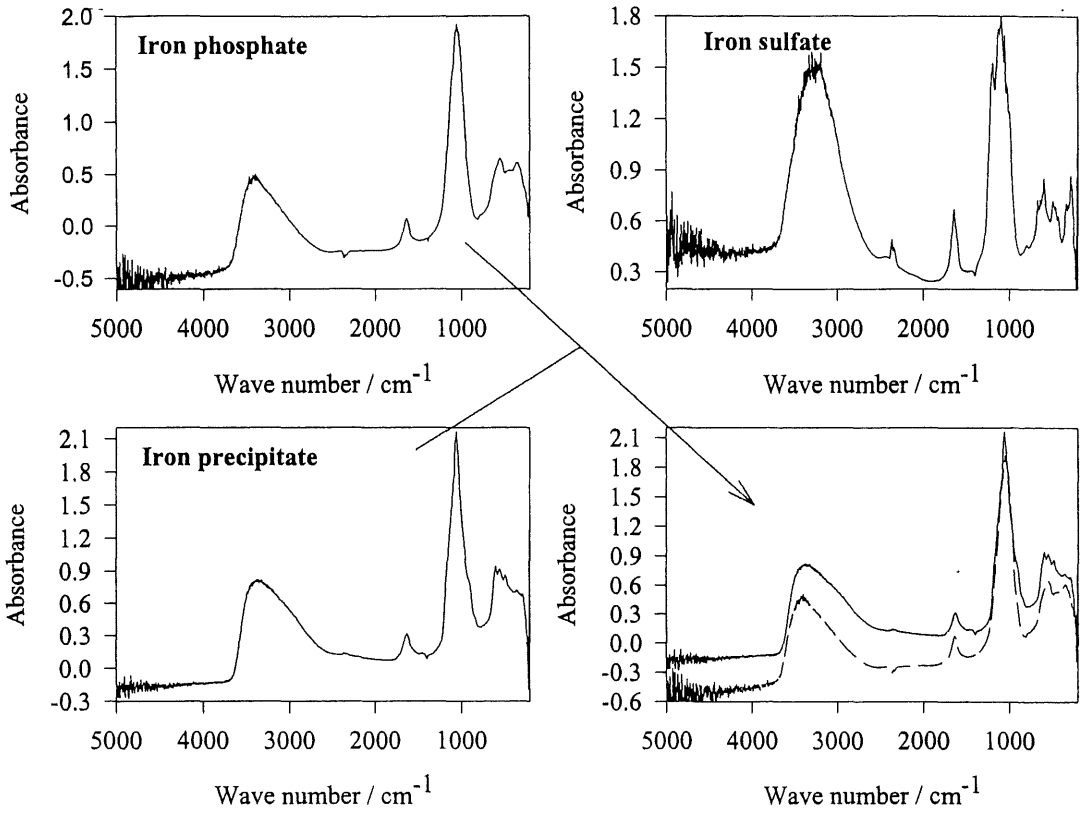

Figure 32. FTIR spectra of the precipitate after formation under the experimental conditions of Fig. 30. Spectra for iron phosphate and sulfate.

XPS measurement has been also carried out on the iron electrode in the same condition as previous part and results are more confirmation for the ratio we have already obtained. Distributions of phosphorus and sulfur on the electrode surface are shown by XPS chemical imaging in Fig. 33. As seen in Fig. 33, phosphate ions show a bigger distribution than sulfate ions. It shows that surface is covered mainly with phosphate and localized distribution of sulfate on the surface. It is in agreement of the adsorption of sulfate ions in acidic pH locally attained on the electrode surface.

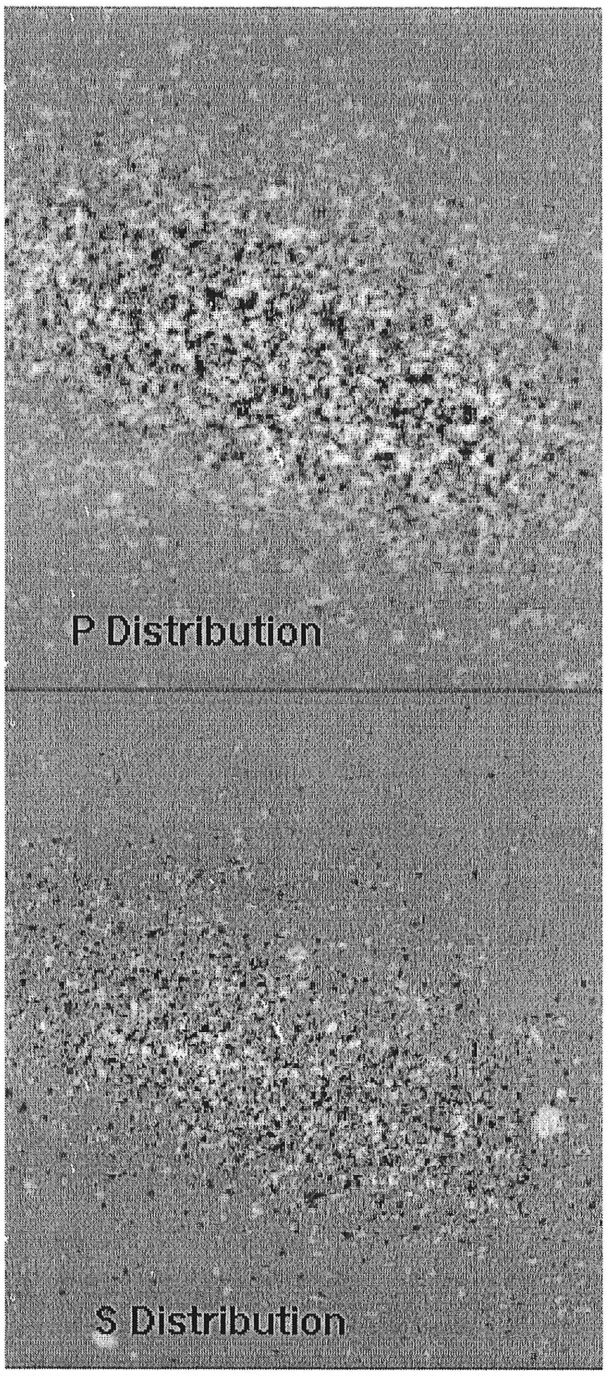

Figure 33. Chemical imaging by XPS for iron electrode in a solution of 0.1M sulfate + 0.01M phosphate ions. Applied potential: 0.0 V (SCE).

SEM pictures of the electrode surface after 1 min chronoamprometry at different applied potentials located in the peak II region were obtained (see Fig. 29 for an applied potential of 0.0 V). Shifting from E = -0.3 V to E = -0.2 V results in a larger localized attack. For 0.0 V (Q_{ox}=130 mCcm^{-2}), there is more pitting and more precipitate at the pit sites. The precipitate is amorphous. Stepping to more noble potentials, at E = 0.2 V (Q_{ox}=12 mCcm^{-2}) the pits decrease in number with less precipitate, and at E = 0.3 V (Q_{ox}=4 mCcm^{-2}) there is a further decrease in pits.

Figure 35 shows potential versus time curves recorded for different constant applied current densities ranging from 8 to 160 μAcm^{-2}. For applied current densities below 36 μAcm^{-2}, the potential quickly stabilizes in the region of peak I. For an applied current of 36 μAcm^{-2}, the potential is located in the peak I region up to 1500 s before its sudden increase in the transpassive region; this current is too low to initiate pitting under the experimental conditions of Fig. 35. For an applied current density larger than 36 μAcm^{-2}, the greater the current, the shorter the time during which the potential remains in the region of peak I. For 40 μA cm^{-2}, the potential jumps to -0.05 V after 800 s of polarization and pitting is initiated; a potential drop is further noted before potential stabilization at ~-0.3 V, i.e. in the region of peak II (Fig. 24); pit growth is observed. The picture is different for 48 μAcm^{-2}: after 500 s, the potential starts to shift in the positive potential direction and, at 0.1 V, the pitting process is noticed for a short time only before the potential shifts in the transpassive region. For an applied current density larger than 48 μAcm^{-2}, the greater the applied current density, the shorter the time to reach the transpassive region and no pits are formed.

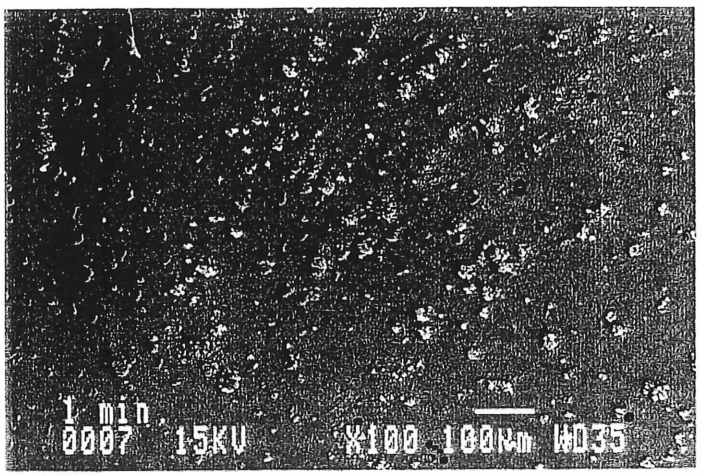

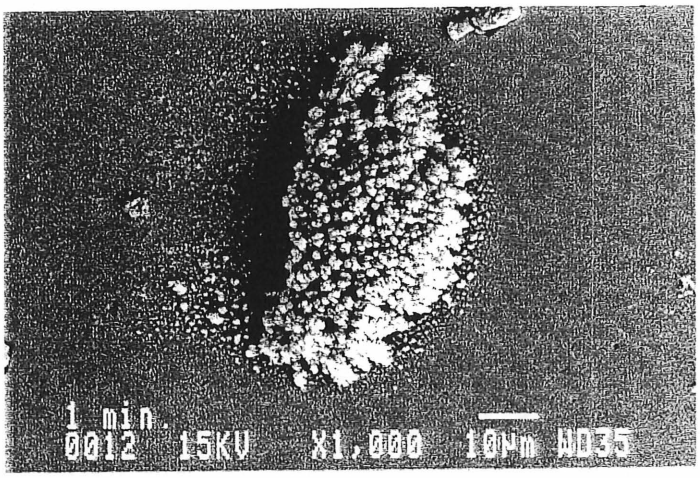

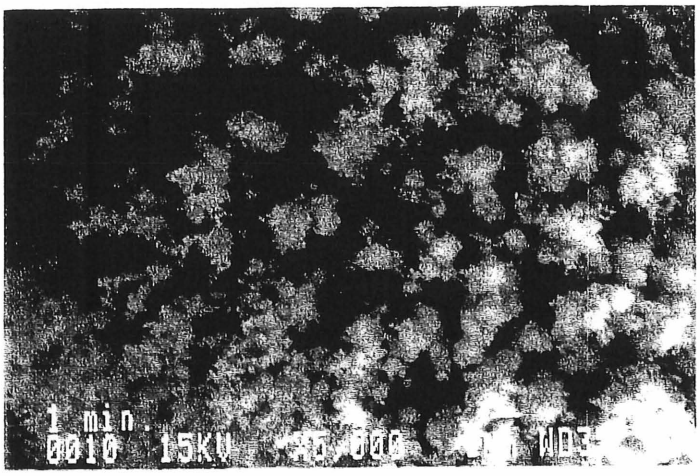

Figure 34. SEM pictures (magnifications: x100, x1000, and x5000) after iron electrode oxidation at 0.0V for 60 s in 0.1M sodium sulfate + 0.01M sodium phosphate solution; rotation speed =1000 rpm; Q_{ox}=130 mC cm^{-2}.

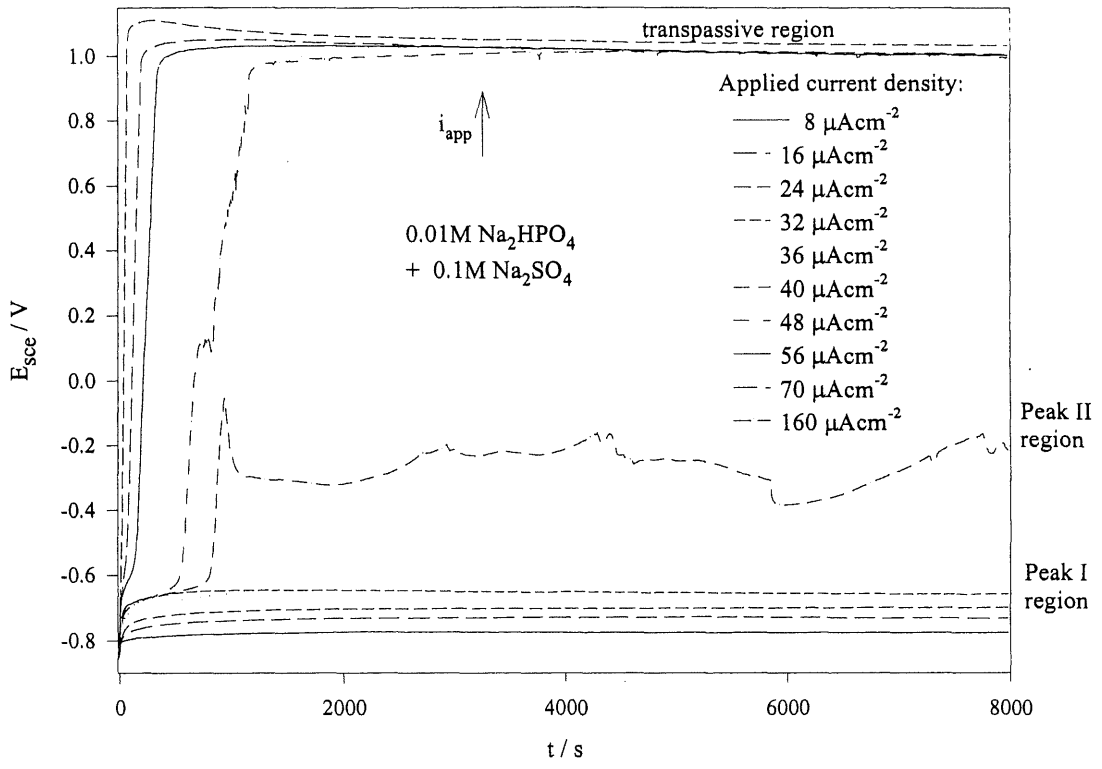

Figure 35. Chronopotentiograms for an iron electrode in a 0.1M sulfate + 0.01M phosphate solution. rotation speed =1000 rpm. Applied current density from 8 to 160 μAcm^{-2}.

Figure 36 shows the effect of the chloride ions on the potentiodynamic curve for iron electrodes in a solution containing 0.1M Na_2PO_4 + 0.01M and 0.02M NaCl. Iron electrodes were rotated at 1000 rpm and the potential scan rate was 0.005 Vs^{-1} from -0.84 V to 2.0 V. The anodic current for the iron electrode in both solutions starts to increase at -0.84 V to reach a maximum of 100 μAcm^{-2} at E=-0.7 V. This behavior is related to a dissolution-passivation mechanism. The peak current is followed by a large passive region ranging from -0.4 V to 0.9 V; for E > 0.9 V, the more anodic the applied potential, the greater the current density due to the onset of the oxygen evolution. No waves resulting from ferrate ion formation are observed in the transpassive region. Some pits are initiated in the transpassive region and further grow as the potential is swept in the negative direction; green corrosion products cover the pit sites during pit growth. The reminder of the electrode surface is untouched and looks shiny. The effect of the anodic potential reversal has been investigated for E_a of 1.0 and 1.5 V to demonstrate the absence of any pit initiation. Hence, it is at more anodic potentials located in the transpassive region that pits can initiate in the case of low chloride ion concentrations. Fig. 36 also shows that the higher the concentration in chloride ions, the greater the associated current density, the larger the amplitude and the higher the frequency of the current oscillations for the potentiodynamic curve in the anodic potential direction.

4.3 Discussion and conclusions

The electrochemical behavior of iron electrodes in sulfate aqueous solutions has been shown in previous chapter, it was established that the dissolution process is uniform in the presence of sulfate ions. As far as the potentiodynamic characteristics of iron electrode in phosphate solution are concerned (Fig. 23), passivation proceeds through a dissolution-precipitation mechanism as the potential is sufficiently anodic (30). In aqueous sulfate solutions (Fig. 24), a second anodic current peak on the potentiodynamic trace is characterized by current oscillations with a small amplitude, the current oscillations being linked to pitting corrosion.

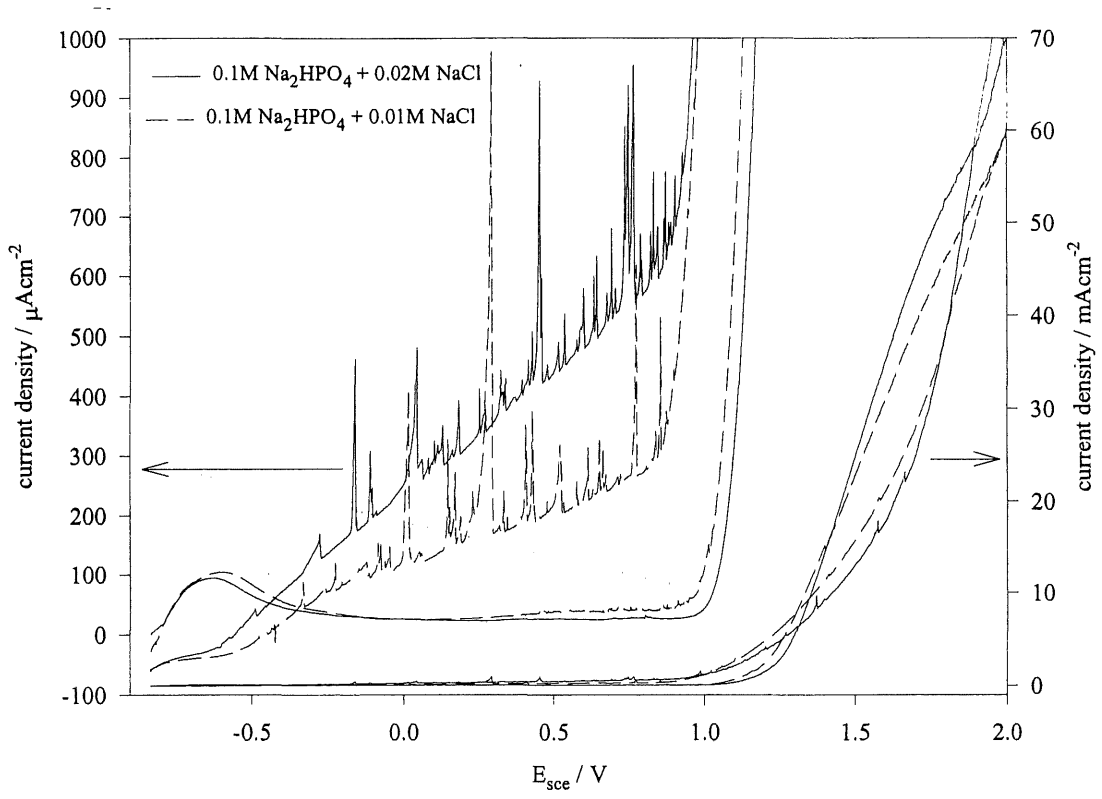

Figure 36. Voltammograms for an iron electrode in 0.01M phosphate + x M chloride, x= 0.01, and 0.02; dE/dt=5 mVs^{-1}; rotation speed =1000 rpm; starting potential: -0.84 V.

The potentiodynamic trace also displays a small wave in the transpassive region which is characteristic of ferrate ion formation. Since the formation of ferrate ions is noticed when both phosphate and sulfate ions are present together only, it is deduced that the formation of ferrate is possible through a synergetic effect of sulfate and phosphate ions. The addition of more phosphate to sulfate solutions (Figs. 25 and 26) resulted in an increase for peak current I and a decrease for peak current II. In solutions containing phosphate ions, it is relevant to consider the different species which can exist in the solution depending on the pH value (41). During iron dissolution in the presence of sulfate ions, surface pH can change by hydrolysis of iron species and, depending on the local pH attained in the vicinity of the electrode surface, stable species of phosphate can possibly affect the electrodissolution process. The anodic peak current I and II are most likely related to the formation of iron phosphate precipitates. For phosphate + sulfate solutions and as far as peak I region is concerned (Figs. 28 and 29), a dissolution-precipitation mechanism mainly controlled by diffusion of ionic species into the solution in the vicinity of the electrode surface is deduced, as reported for the dissolution of iron in aqueous phosphate solutions (30). It is deduced from FTIR spectra (Fig. 32) that the precipitate is iron phosphate. Chronoamperograms of iron electrodes at 0.0 V (Fig. 30) show how current density increases with the dissolution of iron during pit initiation and growth; then the pits cover up with precipitates (Fig. 32) and current density decreases with time.

Comparing the effect of chloride and sulfate ions on the electrooxidation behavior of iron surface in the presence of phosphate solutions, it was observed that chloride ions are very aggressive compared to the sulfate ions. However, for potentials that are negative with respect to the transpassive region, there is a critical chloride ion concentration with respect to phosphate ions below which limit the rate of electrodissolution process is small and the electrode surface remains untouched. It is also interesting to note that the presence of chloride ions results in the formation of green rust 1 as a corrosion product during the course of pitting corrosion, the precipitate being white in the presence of sulfate ions and phosphate ions. The iron dissolution with generations of ferrous ions within the pits combined with the presence of

phosphate ions induces the precipitation of ferrous phosphate (pK_{sp} = -32 compared to -26 for ferric phosphate) (81) (Figs. 30-34). The possible existence of any rust made from aqueous solutions of iron with both sulfate and phosphate ions by contrast to sulfate and carbonate ions remains open (82,83). Hence, it has been concluded that the mechanism of passivation by phosphate ions and bicarbonate ions is different, and chloride ions always produce green rust 1 for both solutions.

In summary, the following features are characteristics for iron electrodissolution in solutions containing phosphate ions in the presence of sulfate or chloride ions:
i) In phosphate solutions only, the passivation process proceeds through a dissolution-precipitation mechanism, ii) in solutions of phosphate + sulfate ions, the passivation process is unchanged compared to when in the presence of phosphate ions only; it is different from the one for sulfate solutions of bicarbonate, most likely because the low solubility of the phosphate precipitates affects their behavior, iii) in the presence of chloride ions, pitting corrosion goes through green rust 1 without any repassivation.

CHAPTER 5

Correlation between Aggressive and Inhibitive Ions on Breakdown Potential Using the Factorial Design

5.1 Introduction

Factorial designs are among popular class of experimental designs that are often used to investigate multifactor systems. One of the major advantages of factorial designs is that they can be used to reveal the existence of factor interaction when it is present in a system.

Historically, factorial designs were introduced by Fisher (62) to counter the prevalent idea that if one were to discover the effect of a factor, all other factors must be held constant and only the factor of interest should be varied. He showed that all other factors of interest could be varied simultaneously, and the individual factor effects and their interactions could be estimated by proper mathematical treatments. The Yates (84) algorithm and its variations are often used to obtain these estimates, but the use of least-squares fitting if the linear models gives essentially identical results (61).

Peng and Park (46) have investigated principal factors and interactions affecting microbiologically influenced corrosion. They considered chemical oxygen demand (COD), sulfate ion concentration, calcium precipitation, and bacteria inoculation as factors in their investigation. They found that $CaCO_3$ precipitation has a significant effect on biocorrosion of steel. In the supersaturated condition, sulfate ion concentration and bacterial inoculation had no appreciable effects on corrosion, but was affected by them in the undersatuarted condition.

Jordan et al. (47) have studied the effect of pH, oxygen, and red rust on the cathodic half-cell reaction on corroding electrogalvanized steel. They have found that the predominant cathodic reaction involves the reduction of atmospheric red rust (γ-FeOOH).

5.2 Experimental and calculation results

It has been already shown for iron electrodes in solutions containing bicarbonate + sulfate ions that there is no trace of pitting corrosion in the transpassive region (Chap. 3). Fig. 37 shows potentiodynamic curves for a rotating iron disk electrode in a solution of 0.005M NaCl + 0.3M $NaHCO_3$ for scan rates of 25, 50 and 100 mV s^{-1}. For the potential scan in the positive potential direction, the voltammogram shows an active-dissolution maximum current peak at -0.6 V and a wide passivation region ranging from -0.4 to 0.9 V without any localized attack. The transpassive region starts at about 0.9 V with a current plateau related to ferrate ion formation followed by the oxygen evolution reaction. Some small current oscillations are noticed at the plateau current, which are related to pit formation on the electrode surface. For the scan in the negative potential direction, current oscillations are larger in magnitude and more frequent; the current density starts to increase due to the growing of initiated pits in the forward scan. The high anodic current density remains over a wide potential range before decreasing to zero at the inhibition potential i.e. -0.1V, the current is cathodic for $E < -0.1V$. The hydrogen evolution is noticed at a sufficiently cathodic potential. The pitting process is under kinetic control because the potential corresponding to the pit initiation is more anodic, higher the potential scan rate.

Based on our knowledge and data from the literature (10), the behavior of an iron electrode in solutions containing bicarbonate ions as inhibitors and chloride or sulfate ions as aggressive ions is summarized in Fig. 38. Pitting is observed from a breakdown potential up to the oxygen evolution in the presence of chloride ions; by contrast, the pitting process stops in the presence of sulfate ions as the potential is sufficiently anodic. Concentrations of inhibitor and

aggressive ions have been selected based on a 2^2 full factorial design and breakdown potentials were measured. The potentiodynamic curves were recorded at different scan rates of 1, 2, 3, 4, and 5 mV s^{-1}. Polarization was stopped after pit initiation for a current of 60 μA (475 μAcm^{-2}) to minimize electrode surface damage. Table 5 shows the chloride and bicarbonate ion concentrations based on the factorial design. The bicarbonate ion concentration is 0.1 M for low and 0.5 M for high concentrations in the design and 0.05 M and 0.1 M, for chloride ions respectively.

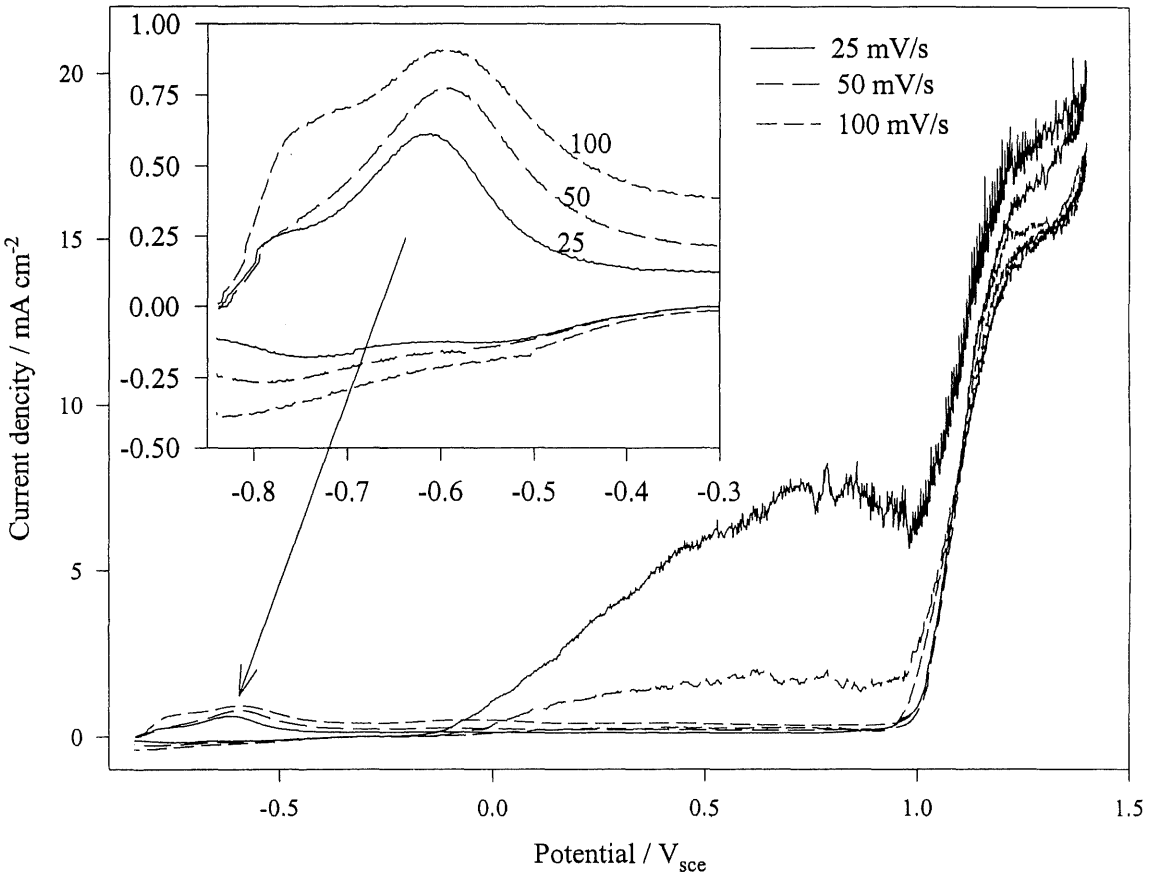

Figure 37. Linear sweep voltammograms of iron electrode rotated at 1000 rpm in solution containing 0.3 M bicarbonate + 0.005 M chloride ions at scan rates of 25, 50 and 100 mVs^{-1}. Potential being scanned from hydrogen evolution to oxygen evolution region.

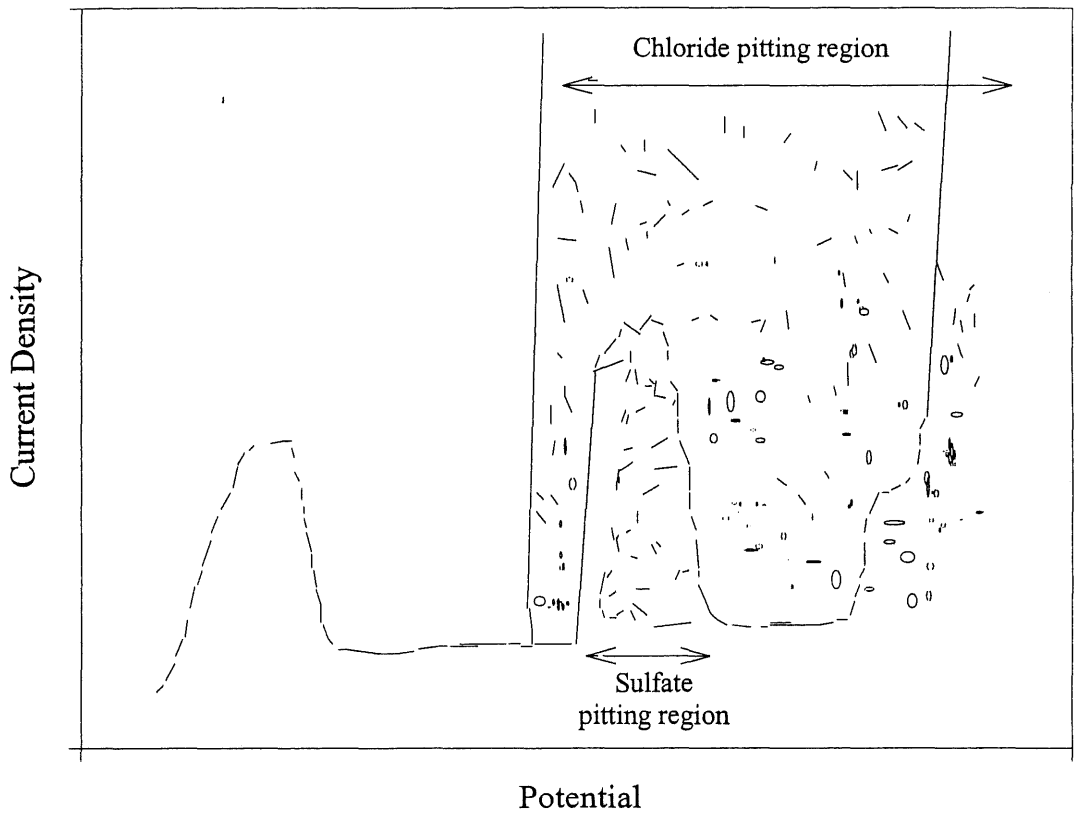

Figure 38. General schematic of the effect of the sulfate and chloride ions on the electrodissolution behavior of iron in bicarbonate solutions.

Voltammograms for the solution containing 0.1 M NaCl + 0.1 M $NaHCO_3$ with their regression line for obtaining pitting potentials at selected potential scan rates are shown in Fig. 39.

Table 5. Selected solutions containing chloride and bicarbonate ions for 2^2 full factorial design and corresponding pitting potentials

$C_{HCO_3^-}$ (M)	C_{Cl^-} (M)	$x_{HCO_3^-}$	x_{Cl^-}	E_b^0 (mV / sce)
0.1	**0.05**	**−1**	**−1**	**−113**
0.5	**0.05**	**+1**	**−1**	**+40**
0.1	**0.1**	**−1**	**+1**	**−123**
0.5	**0.1**	**+1**	**+1**	**−60**

Pooled S.D. for the center point in the design: 4.01

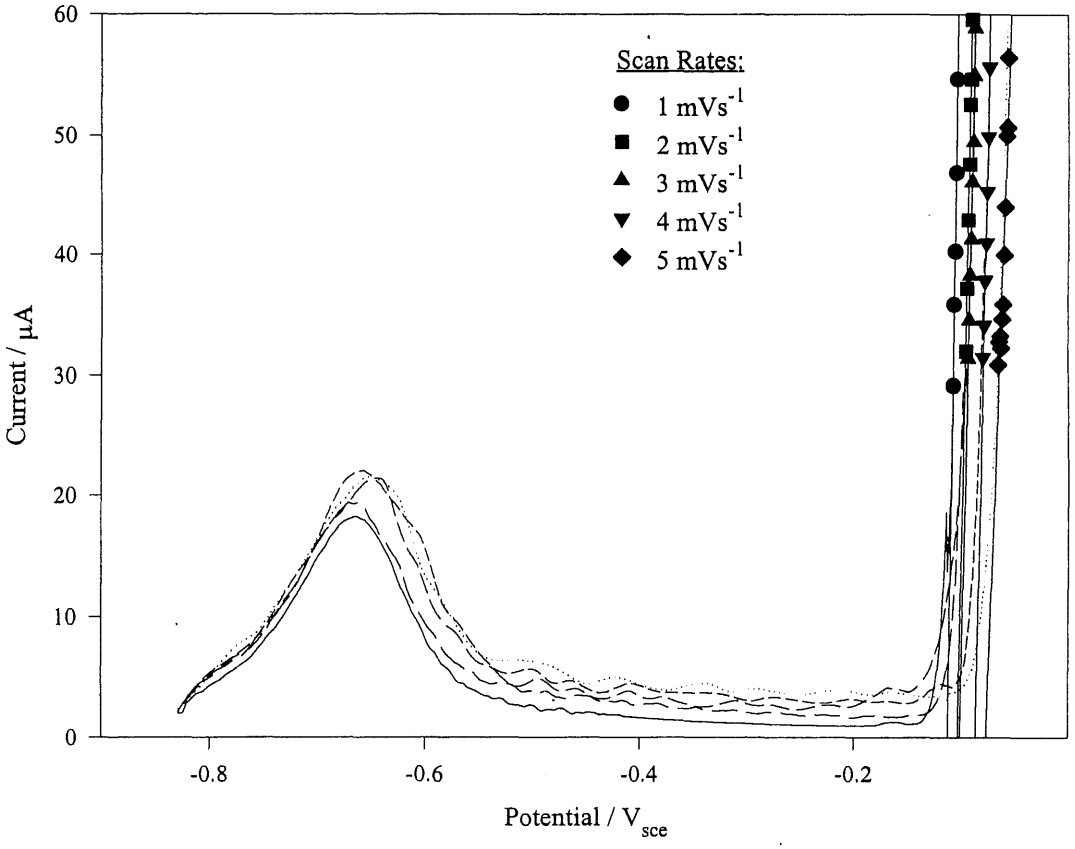

Figure 39. Linear sweep voltammograms of iron electrodes rotated at 1000 rpm in solution containing 0.1 M bicarbonate + 0.1 M chloride ions at scan rates of 1, 2, 3, 4, and 5 mVs^{-1}. Filled circle symbols correspond to the selected points used for linear regression and extrapolation for obtaining a pitting potential at zero current.

Since the pitting potential is dependent on the potential scan rate (85), i.e. a linear relationship of the pitting potential versus the potential scan rate using weighted linear regression (86) has been noticed, the pitting potential has been extrapolated up to a potential scan rate of 0 mV s^{-1} to determine the pitting potential at 0 mVs^{-1} (Fig. 40). The same approach was used for all the solutions in the design and final results with their standard deviations are tabulated in Table 5.

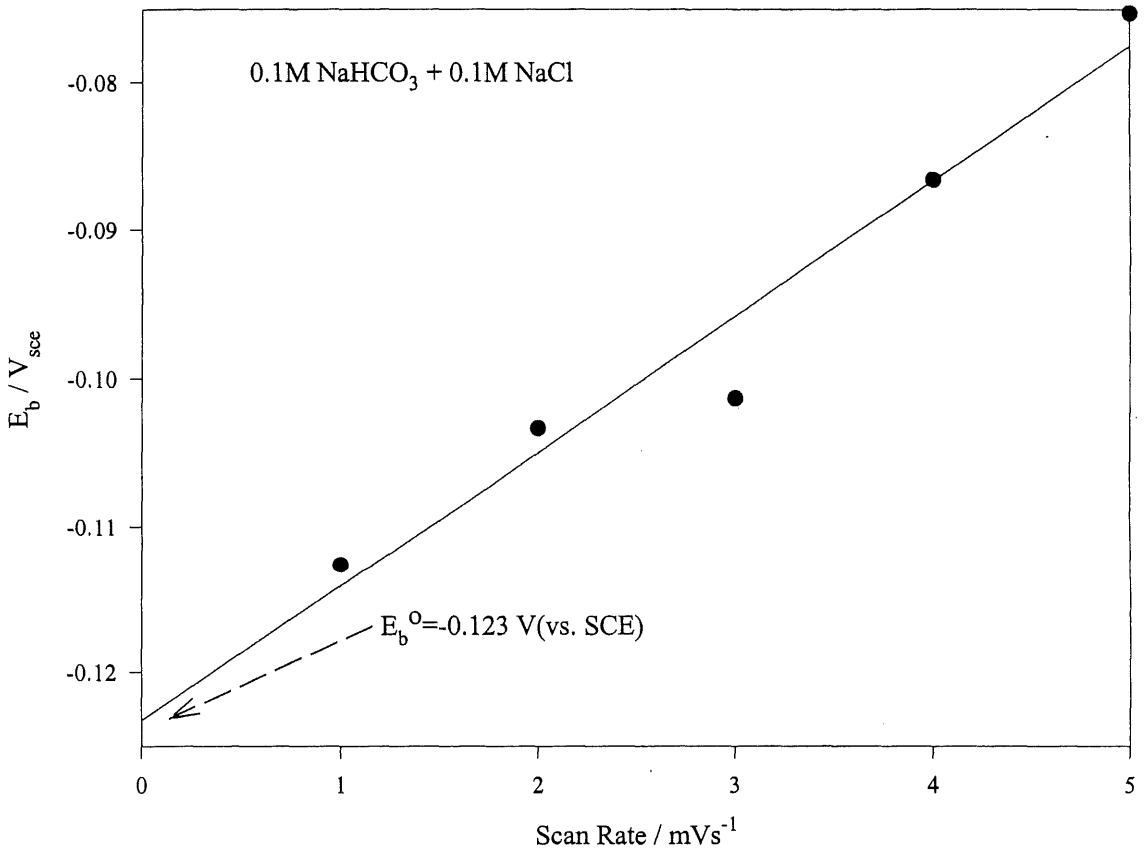

Figure 40. Linear plot of pitting potentials deduced from the curves of Fig. 39 against scan rate for the pitting potential determination at zero potential scan rate.

The following values have been obtained for the calculation of the coefficients in the design ($Y = X^T XB$):

$b_0 = -64$, $b_1 = 54$, $b_2 = -28$, $b_{12} = -23$

Considering the same standard deviation ($s_{b_j} = s_e / \sqrt{4} = 2.01$) for the coefficients calculated from the pitting potential measurements, the following t values are calculated for all the coefficients and compared with the tabulated value of 4.3 for the α=0.05 and 2 degrees of freedom (61):

$t_0 = |b_0|/s = 64/2.01 = 31.84$, $t_1 = 26.87$, $t_2 = 13.93$, and $t_{12} = 11.44$

Consequently, all the coefficients in the design are significant and the following relationship between the pitting potential at a zero scan rate (E_b^0) and scaled (dimensionless) concentrations of chloride and bicarbonate ions has been deduced:

$$E_b^0 = -64 + 54x_{HCO_3^-} - 28x_{Cl^-} - 23x_{HCO_3^-}x_{Cl^-} \qquad [5.1]$$

i.e. the higher the concentration in bicarbonate ions, the more anodic the pitting potential and the higher the chloride ion concentration, the less anodic the pitting potential. For example, a change in $x_{HCO_3^-}$ from -1 to +1 causes an effect of $108 - 46\,x_{Cl^-}$ mV in E_b^0. As is shown by the interactive term ($-23x_{HCO_3^-}x_{Cl^-}$) in Eq. 5.1, bicarbonate and chloride ions have a synergetic effect, i.e. interactive aggressive effect when both ions are present in the solution. This synergetic effect is an aggressive effect because of the negative coeffiecient (-23) and causes E_b^0 to become more anodic. Relation between E_b^0 and $x_{HCO_3^-}$ and x_{Cl^-} is shown in a 3D plot in

Fig. 41. Since all the coefficients are important, there is no degree of freedom for the goodness of fit test.

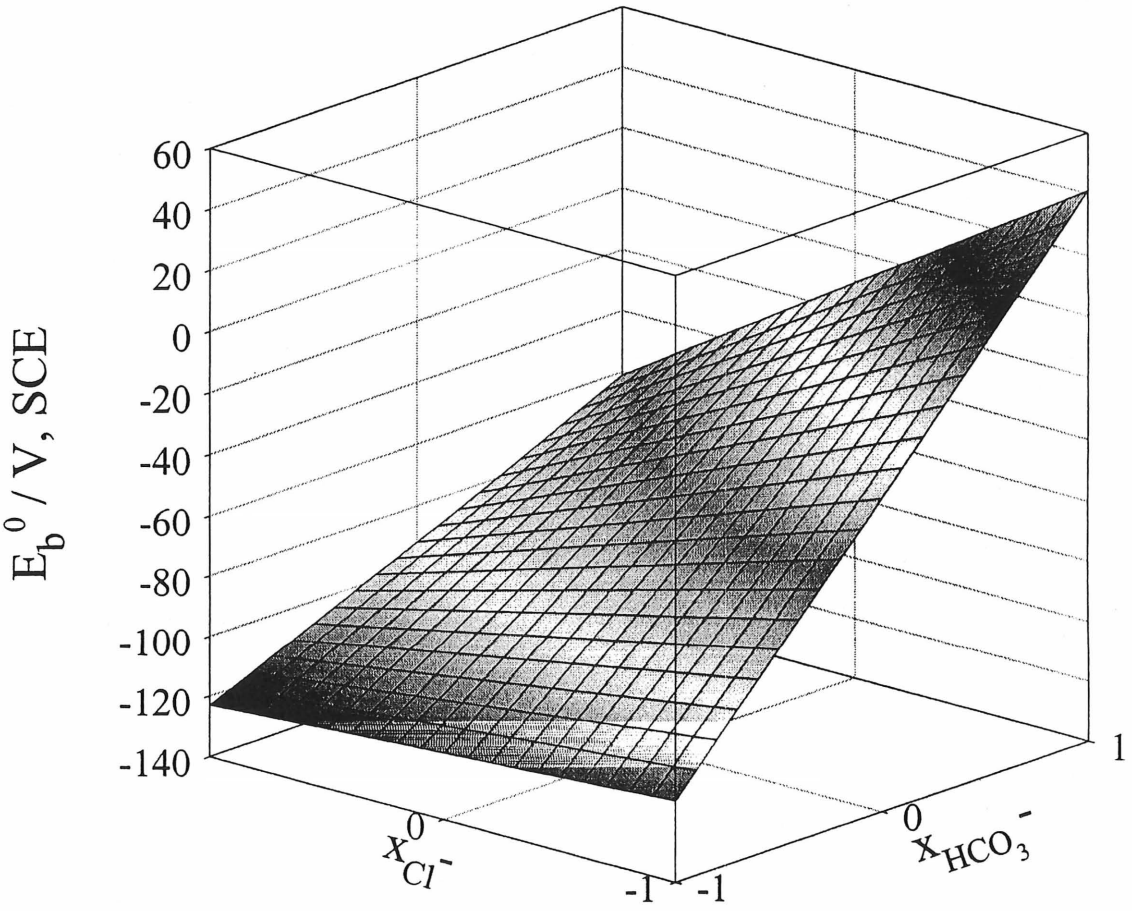

Figure 41. 3D plot of Relation between E_b^0 and $x_{HCO_3^-}$ and x_{Cl^-}.

Another set of experiments has been carried out for sulfate + bicarbonate ions in the solution. Table 6 shows their concentration and associated pitting potentials at 0 mVs^{-1} for iron electrodes. The concentration in bicarbonate ions is 0.1 M or 0.5 M compared to 0.3 M or 0.5 M for sulfate ions. Fig. 42 shows the potentiodynamic curves for an iron electrode in 0.1 M bicarbonate + 0.5 M sulfate solution, and the corresponding pitting potential values versus the potential scan rate are plotted in Fig. 43.

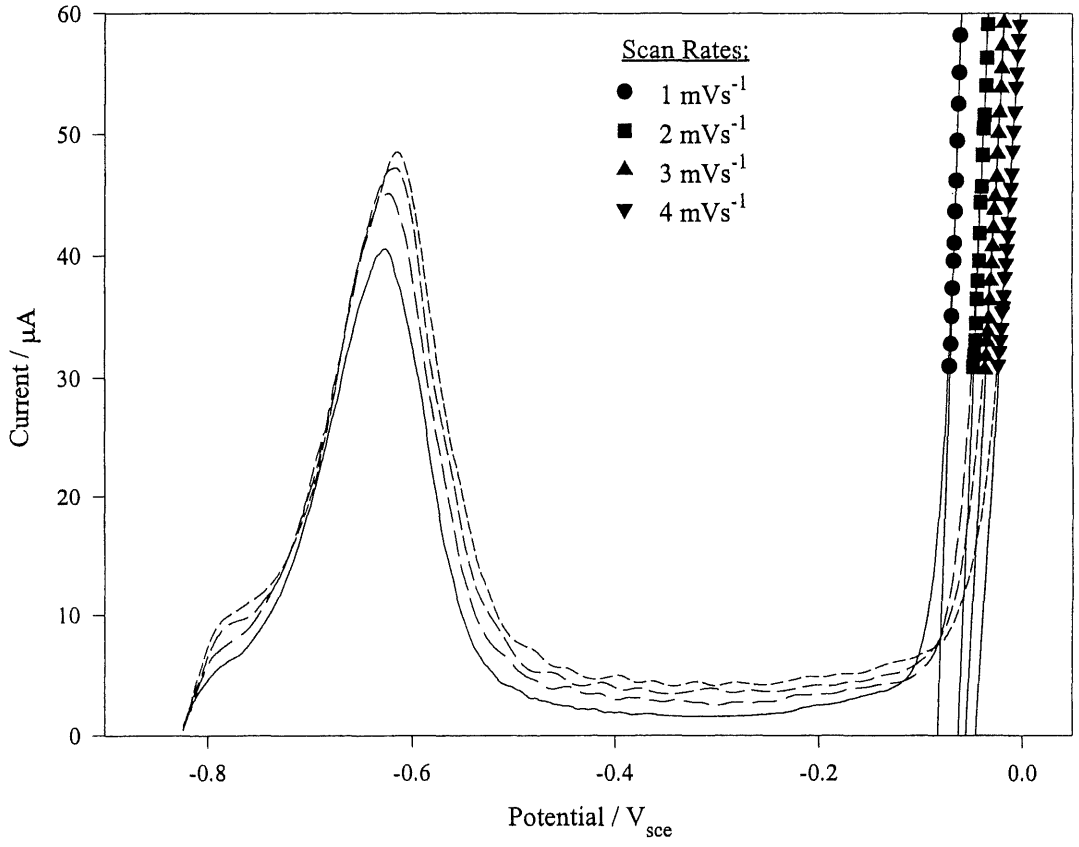

Figure 42. Linear sweep voltammograms of iron electrodes rotated at 1000 rpm in solutions containing 0.1 M bicarbonate + 0.5 M sulfate ions at scan rates of 1, 2, 3, 4 mVs^{-1}.

Table 6. 2^2 full factorial design for the effect of sulfate and bicarbonate ions

$C_{HCO_3^-}$ (M)	$C_{SO_4^=}$ (M)	$x_{HCO_3^-}$	$x_{SO_4^=}$	E_b^0 (mV / sce)
0.1	**0.3**	**–1**	**–1**	**–99**
0.5	**0.3**	**+1**	**–1**	**–38**
0.1	**0.5**	**–1**	**+1**	**–314**
0.5	**0.5**	**+1**	**+1**	**–93**

Pooled S.D. for the center point in the design: 4.50

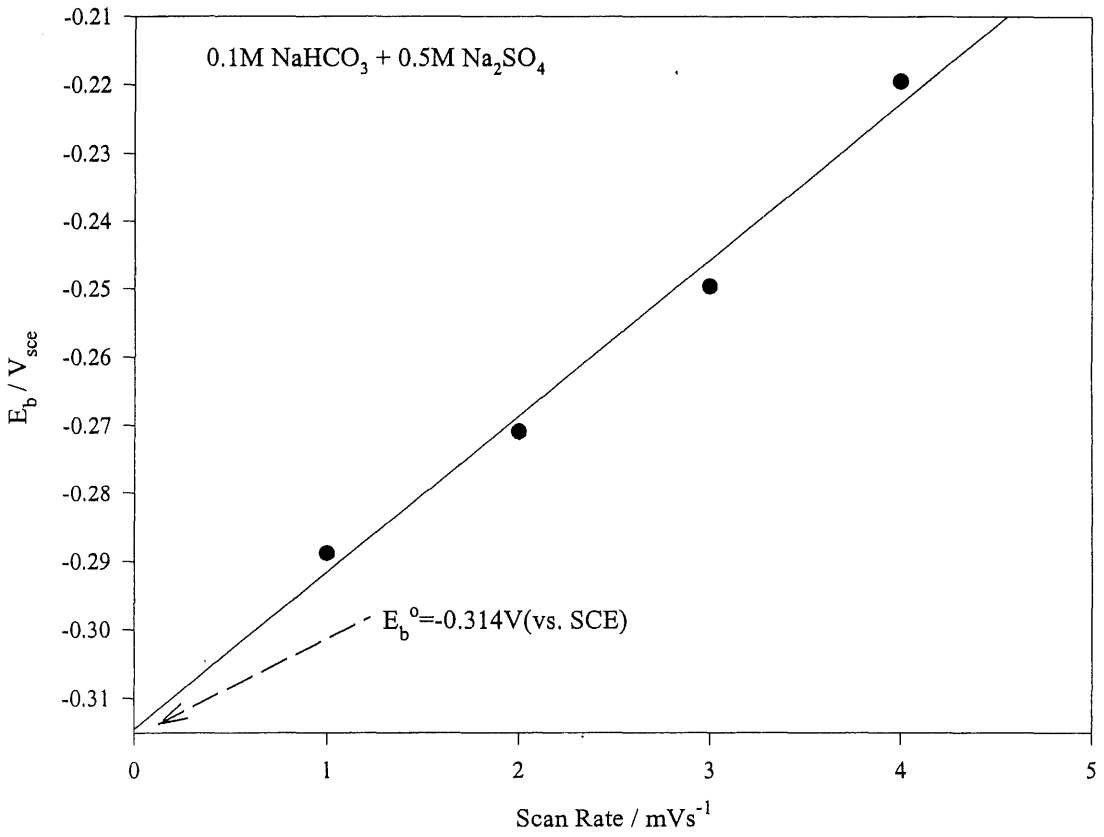

Figure 43. Linear plot of pitting potentials at zero current (deduced from the curves of Fig. 42) against the scan rate.

The significance t-test was done for the coefficients and the following relationship has been deduced:

$$E_b^0 = -136 + 71x_{HCO_3^-} - 68x_{SO_4^=} + 40x_{HCO_3^-}x_{SO_4^=} \qquad [5.2]$$

Here again, the direct effect of inhibitive and aggressive ions on the pitting potential is as anticipated, but the interactive term is related to a positive shift in pitting potential, i.e. interactive inhibitive effect. A change of -1 to +1 in $x_{HCO_3^-}$ causes a shift of $142+80\,x_{SO_4^=}$ mV in E_b^0.Again, no degree of freedom was left for the goodness of fit test. 3D plot of Relation between E_b^0 and $x_{HCO_3^-}$ and $x_{SO_4^=}$ is shown in Fig. 44.

In another set of experiments, a design for studying the effects of all three ions together was constructed (Table 7, Fig. 45) and after calculations and performing significance tests for coefficients and rejecting the insignificant coefficients, the following relationship was obtained:

$$E_b^0 = -115 + 25x_{HCO_3^-} - 32x_{Cl^-} + 11x_{HCO_3^-}x_{SO_4^=} \qquad [5.3]$$

The residual standard deviation has been calculated (S^2_R=17.78) and the F-test (F=0.68 < $F_{tab}(4,2, \alpha=0.05)$ =19.25) for the lack of fit test (61) was also determined. It shows that the above equation satisfies the observed results. The relationship shows that the interaction between bicarbonate and sulfate ion is important to be considered. The main effects have been shown through the inhibitive effect of bicarbonate ions, the aggressive effect of chloride ions, and the inhibitive synergetic effect of bicarbonate and sulfate ions together on the breakdown potential.

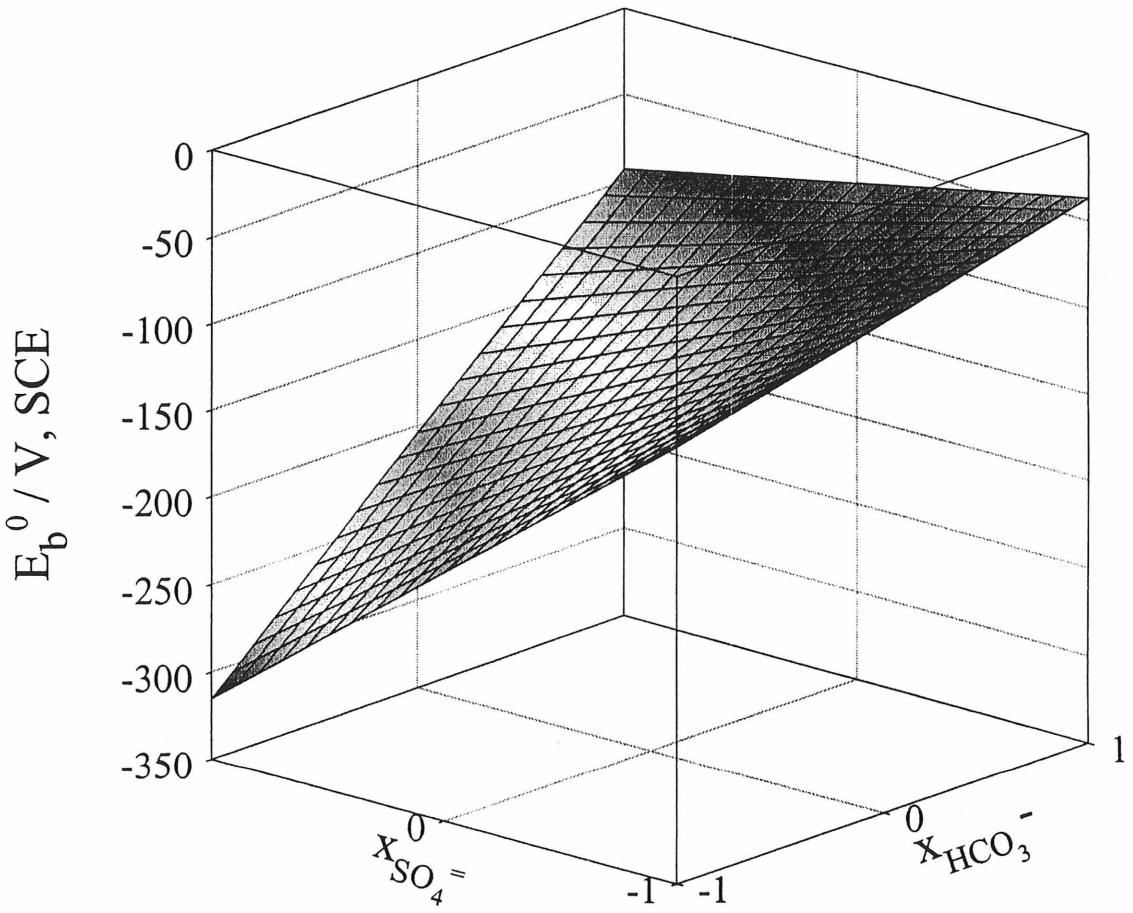

Figure 44. 3D plot of Relation between E_b^0 and $x_{HCO_3^-}$ and $x_{SO_4^=}$.

Measuring the breakdown potential for low concentrations of sulfate ions is questionable because the very weak signal results in an ill-defined value. In the presence of chloride ions, it is possible to investigate the effect of sulfate ions on low concentrations. As it is seen in solutions of all three ions together, bicarbonate ions have an inhibitive effect and chloride ions an aggressive effect. The aggressivity of sulfate ions in this range of concentration is marginal when chloride ions are present, but its inhibitive effect in the presence of bicarbonate ions is shown by positive interactive the above equation.

Table 7. 2^3 Full factorial design for the effects of bicarbonate, chloride, and sulfate ions on pitting potential

$C_{HCO_3^-}$ (M)	C_{Cl^-} (M)	$C_{SO_4^{=}}$ (M)	$x_{HCO_3^-}$	x_{Cl^-}	$x_{SO_4^{=}}$	E_b^0 (mV / sce)
0.1	**0.05**	**0.05**	**–1**	**–1**	**–1**	**–93.5**
0.2	**0.05**	**0.05**	**+1**	**–1**	**–1**	**–75**
0.1	**0.15**	**0.05**	**–1**	**+1**	**–1**	**–174**
0.2	**0.15**	**0.05**	**+1**	**+1**	**–1**	**–140**
0.1	**0.05**	**0.1**	**–1**	**–1**	**+1**	**–113**
0.2	**0.05**	**0.1**	**+1**	**–1**	**+1**	**–50**
0.1	**0.15**	**0.1**	**–1**	**+1**	**+1**	**–180**
0.2	**0.15**	**0.1**	**+1**	**+1**	**+1**	**–95**

Pooled S.D. for the center point in the design: 5.13

5.3 Discussion and Conclusion

Two aspects were noted from the electrochemical behavior of iron in chloride and sulfate solutions in the presence of bicarbonate ions: i) in the case of sulfate ions, pitting corrosion ceases as the potential becomes sufficiently anodic, ii) for chloride ions, pitting corrosion is noted up to the oxygen evolution in the transpassive region. Based on the relationships between the concentration of aggressive and inhibitive ions and the pitting potential (Equations 5.1 and 5.2), a direct relationship between the concentration of aggressive ions and the pitting potential and a reverse relationship for inhibitive ions are observed.

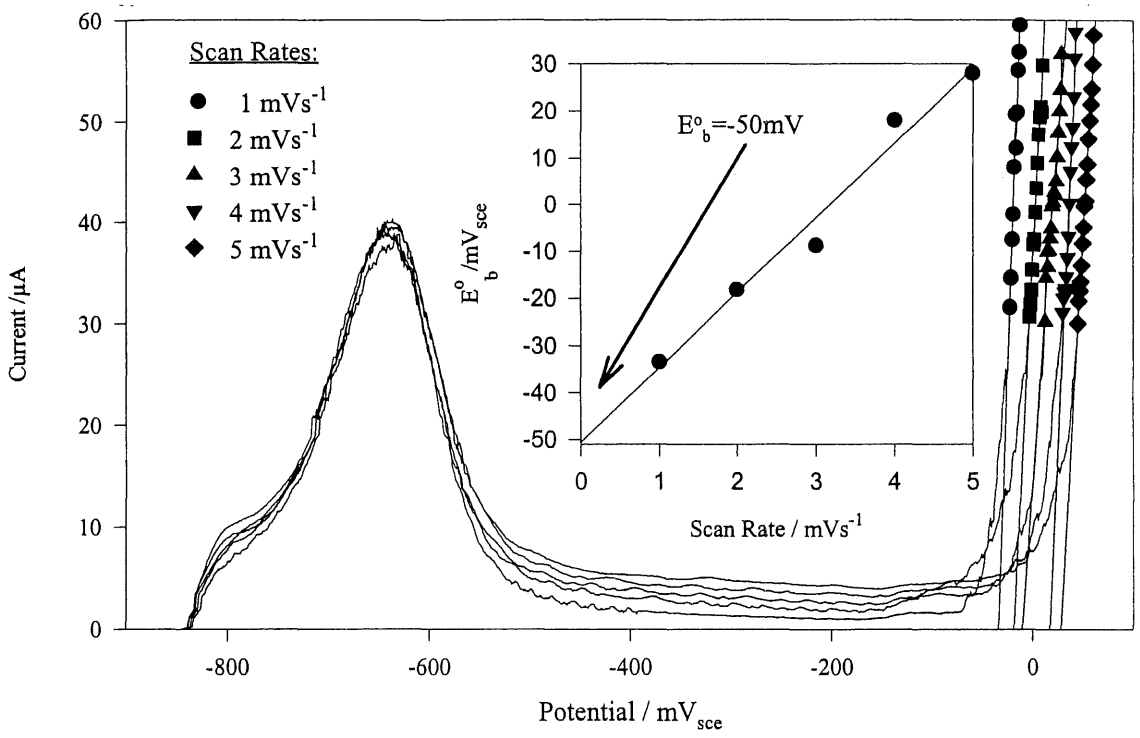

Figure 45. Linear sweep voltammograms of iron electrodes rotated at 1000 rpm in solution containing 0.2 M bicarbonate + 0.05 M chloride + 0.1 M sulfate ions at scan rates of 1, 2, 3, 4 mVs^{-1}.

It is interesting to look at the interactive terms in Equations 5.1 and 5.2. In the case of chloride ions, it shows that their interactions with bicarbonate ions is also aggressive (negative coefficient) and promotes pitting corrosion. It is in agreement with the fact that there is no passivation with chloride ions after film breakdown for the given experimental conditions. On the other hand, the interactive term for sulfate and bicarbonate ions has an inhibitive effect (positive coefficient) which is again in agreement with the experimental observations. The above observations are explainable by referring to recent publications on E-pH diagrams of green rust 1 and 2 for iron in solutions of chloride and sulfate ions (21-27). In the active dissolution region for iron in slightly alkaline solutions, in the presence of chloride ions + bicarbonate ions or sulfate ions + bicarbonate ions, the adsorption of bicarbonate ions on the electrode surface is more important compared with the one for other ions. The effect of bicarbonate ions at this stage leads to the initiation of surface passivation. At more positive potentials, localized acidification in the vicinity of the electrode surface (87) promotes a better adsorption of aggressive ions as chloride and sulfate ions. The result is an easier passive film breakdown and generation of green rust 1 ($3Fe(OH)_2$. $Fe(OH)_2Cl$. nH_2O) and green rust 2 ($4Fe(OH)_2$. $2FeOOH$. $FeSO_4$. nH_2O) for chloride and sulfate ions respectively. The latter two compounds have a different selectivity towards anion migration in the order of $CO_3^{=}$ > $SO_4^{=}$ > Cl^- (21). In the case of sulfate + bicarbonate ions (for the given experimental conditions), adsorption of carbonate species after saturation of pit sites with corrosion products is predominant and leads to repassivation. For chloride + bicarbonate ions, repassivation is more difficult most likely because of the smaller size of chloride ions compared to sulfate ions (1:8 ionic radius ratio), i.e. the saturation necessary for precipitation in pit sites may not be obtained in the presence of chloride ions. This is why the interactive term in equation 1 is positive and has an aggressive interactive effect. This is also understandable by comparing oxidation numbers of green rusts: +2.33($GR1(CO_3^{=})$) > +2.29($GR2(SO_4^{=})$) > +2.25($GR1(Cl^-)$). One can conclude that $GR1(Cl^-)$ is more soluble and shows more dissolution in the pit sites. The combined effect of all three ions on the pitting potential (Equation 5.3) shows that chloride ions are always aggressive and sulfate ions, depending on the concentration range,

could be aggressive or inhibitive. An interesting point in Equation 5.3 is that the interactive term of chloride and bicarbonate is not present. This may be explainable by the transformation of GR1(Cl^-) to GR2($SO_4^{=}$) (22):

$$7[3Fe(OH)_2 .Fe(OH)_2Cl.nH_2O] + 4SO_4^{=} \rightarrow 4[4Fe(OH)_2 .2FeOOH .FeSO_4 .nH_2O] + 8H_2O + 7Cl^- + e^- \quad [5.4]$$

Hence, by producing GR2 from the above reaction, the interactive term is once again represented by sulfate and bicarbonate ions. The transformation of corrosion products may possibly be considered as an important parameter in the investigation of iron localized attacks in natural media. Localized attacks can be induced by chloride ions and the accumulated corrosion products may react with the environment to incorporate anions present in such an environment.

In summary, using the pitting potential as an object function in factorial design makes it possible to investigate the behavior of an electrode with a minimum set of experiments. Using the factorial design, it is possible to see both the direct and interactive effects of parameters on the system under study. In this study, it has been shown that chloride and sulfate ions have a direct effect on pit formation but their interactive effects with bicarbonate are different. For chloride ions, this term shows aggressivity while for sulfate, the effect is inhibitive. It has been observed that in solutions containing all three anions together, comparing the interactive terms between sulfate and bicarbonate plus chloride and bicarbonate ions, the greater effect for sulfate is ascribed to the fact that GR1(Cl^-) is transformable to GR2($SO_4^{=}$). Finally, by using this method one can get ideas not only descriptive about the processes involved in the system under study but also obtain primary ideas for further mechanistic studies.

CONCLUSIONS

A different electrochemical behavior for iron in sulfate and chloride solutions containing bicarbonate ions has been observed. The main difference is that for iron in a chloride solution, the current increases sharply after breakdown of passive film and does not show any repassivation, indicating that the pitting corrosion products are not protective because of their high solubility and formation of iron complexes with chloride ions. In accordance with the existence of green rusts as intermediate corrosion compounds, depending on the ratio of Fe^{2+}/OH^- during the dissolution reactions and changes in the surface pH, different transient compounds can be formed. However, for the case of bicarbonate and sulfate ions, there is a competition between sulfate and carbonate species. The anodic peak currents I and II in solutions of bicarbonate and sulfate ions (Fig. 15) are related to the formation of soluble $FeHCO_3^+$ complex and green rust 2 (GR2: $4Fe(OH)_2.2FeOOH.FeSO_4.nH_2O$), respectively. It has been found that green rusts have a different selectivity toward sulfate and carbonate ions and their selectivity is more pronounced for carbonate ions than sulfate ions. Hence, as the transient green rusts form, carbonate species accumulate on the electrode surface, the current starts to decrease and passivation begins. In the mixture of bicarbonate + chloride ions, green rust I (Cl^-) is produced which is more soluble than GR2 ($SO_4^=$) and repassivation is not attained because of easy leaving of corrosion products from pit sites.

The case of phosphate as inhibitor in aggressive media is different from that of bicarbonate and it is linked to the solubility of phosphate products. The results of the analysis have shown that the precipitate is mainly iron phosphate even in solutions containing the molar ratio of 10 for $SO_4^=/PO_4^{\equiv}$ in the solution. It is due to the low solubility of iron phosphate which leads to the accumulation of phosphate ions on the electrode surface as iron (II) phosphate. This was shown by analyzing the precipitate by FTIR spectroscopy, and ICP analytical measurement.

In the transpassive region, the stabilization of ferrate species by the presence of HCO_3^- or $SO_4^{=}$ + $PO_4^{\equiv}$ ions have been observed. This has been clearly observed as a wave in transpassive region accompanied by oxygen avulsion reaction on the electrode surface.

Applying Factorial Design as a correlation technique for investigation the relationship between breakdown potential and concentration of aggressive and inhibitive ions in aqueous solutions has been shown. It was found that by these calculations, it is possible to interpret the observed behavior of iron in such environments by looking at the coefficients in the obtained equations. It has been shown that negative coefficients in the equation is related to aggressivity of the ion and positive one related to passivity. It has been also shown that difference between the behavior of sulfate and chloride ions is explainable from the interactive coefficients in the equations and their sign. It showed that sulfate ions in the presence of bicarbonate ions shows aggressivity by negative coefficients for sulfate ions and inhibition by positive coefficient in the interactive term of sulfate and bicarbonate ions in the equation. These facts are explained by the possibility of transient compounds like green rusts and other chemical properties like solubility of the products. The results are promising and show the usefulness of this technique to evaluate effect of different ions on pitting corrosion of iron electrodes. Moreover, by equations obtained from this method, is it possible to calculate pitting potential for the ions present in the solution in the concentration range used in the design. One can also obtain ideas about mechanisms about the processes involved in the corrosion of the metal under investigation and use it for later mechanistic studies.

With using electrochemical techniques, surface analytical methods, and correlation techniques like factorial design, it has been possible to explain some interactions of iron surface with ions present in the aqueous solutions. This results help to better understanding of corrosion phenomena in media containing such ions.

REFERENCES

1. R. GILBERT, Institut de Recherche d'Hydro-Québec, Internal Report IREQ-4150B (1988); G. LAROCHELLE, L. BRROSSARD and P. COURCHESNE. Internal Report IREQ-4529 (1989).
2. N. SATO, Corros. Sci., 37, 1947 (1995).
3. M. YAMAGUCHI, H. NISHIHARA and K. ARAMAKI, Corros. Sci., 37, 571 (1995).
4. YT. CHIN and B.D. CAHAN, J. Electrochem. Soc., 139, 2432 (1992).
5. R.D. GRIMM, A.C. WEST and D. LANDOLT, J. Electrochem. Soc., 139, (1992), 1622.
6. K. CHO and H.W. PICKERING, J. Electrochem. Soc., 138, L56 (1991).
7. J.A. BARDWELL and B. MACDOUGALL, J. Electrochem. Soc., 135, 2157 (1988).
8. V. JOVANCICEVIC, J.OÆM. BOCKRIS and J.L. CARBAJAL, J. Electrochem. Soc., 133, 2219 (1986).
9. T. ZAKROCZYMSKI, CJ. FAN and Z. SZKLARSKA-SMIALOWSKA, J. Electrochem. Soc., 132, 2868 (1985).
10. Z. SZKLARSKA-SMIALOWSKA, in Pitting Corrosion of Metals, published by NACE 1986.
11. P. MARCUS and J. OUDAR , Corrosion Mechanisms in Theory and Practice, published by Marcel Dekker, Inc. NY 1995.
12. Z. SZKLARSKA-SMIALOWSKA, Corros. Sci., 18, 97 (1978).
13. J.F. MARCO, J.R. GANCEDO, N. MEISEL, P. GRIESBACH and P. GÜTLICH, Corrosion (NACE) 47, 498 (1991).
14. H.E.H. BIRD, B.R. PEARSON and P.A. BROOK, Corros. Sci., 28, 81 (1988).
15. T. KODAMA, Boshoka Gijutso, 23, 5 (1974).
16. B. MACDOUGALL and J.A. BARDWELL, J. Electrochem. Soc., 135, 2437 (1988).
17. J. GUI and T.M. DEVINE, Corros. Sci. 36, 441 (1994).
18. C.A. ACOSTA, R.C. SALVAREZZA, H.A. VIDELA and A.J. ARVIA, Corros. Sci. 25,

291 (1985).

19. B.G. POUND, G.A. WRIGHT and R.M. SHARP, Corrosion (NACE) 45, 386 (1989).
20. M. ABDELMOULA, PH. REFAIT, S.H. DRISSI, J.P MIHE and J.M. GÉNIN, Corros. Sci., 38, 623 (1996).
21. S.H. DRISSI, PH. REFAIT, M. ABDELMOULA and J.M.R. GÉNIN, Corros. Sci., 37, 2025 (1995).
22. PH. REFAIT, M. ABDELMOULA and J.M.R. GÉNIN, Corros. Sci., 36, 55 (1994).
23. A.A. OLOWE and J.M.R. GÉNIN, Corros. Sci., 32, 965 (1991).
24. A.A. OLOWE, B. PAURON and J.M.R. GÉNIN, Corros. Sci., 32, 985 (1991).
25. A.A. OLOWE, PH. REFAIT and J.M.R. GÉNIN, Corros. Sci., 32, 1003 (1991).
26. A.A. OLOWE and J.M.R. GÉNIN, Corros. Sci., 32, 1021 (1991).
27. A.A. OLOWE and J.M.R. GÉNIN, in Proceedings of the Internatinal Symposium on Corrosion Science and Engineering CEBELCOR RT297, 363 (1989).
28. M. J. PRYOR and M. COHEN, J. Electrochem. Soc. 98, 263 (1951).
29. M. J. PRYOR and M.COHEN, J. Electrochem. Soc. 99, 542 (1951).
30. J. BENZAKOUR and A. DERJA, Electrochimica Acta 38, 2547 (1993).
31. R.D. ARMSTRONG, L. PEGGS and A. WALSH, J. Appl. Electrochemistry 24, 1244 (1994).
32. M. COHEN , J. Electrochem. Soc. 32, 461 (1976).
33. GÖSTA WRANGLÉN, An Introduction to Corrosion and Protection of Metals, Chapman and Hall, London, 1985.
34. G. GÓRECKI, Corrosion 48, 613 (1992).
35. G. VATANKHAH, M. DROGOWSKA, L. BROSSARD and H. MENARD, J. Appl. Electrochemistry, 28, 173 (1998).
36. G. T. Burstein and D. H.Davies, Corrosion Sci., 20 , 1143 (1980).
37. J.E.O. MAYNE and J.W. MENTER, J. of The Chem. Soc., 103 (1954).
38. K. TOKUNAGA, Japanese J. of Applied Physics, 21, 1693 (1982).

39. C.A. MELENDRES, N. CAMILLONE III and T. TIPTON Electrocimica Acta, 34, 281 (1989).
40. K. AZUMI, T. OHTSUKA and N. SATO, J. Electrochem. Soc., 134, 1352 (1987).
41. J.B. LUMSDEN and Z. SZKLARSKA-SMIALOWSKA, Corrosion, 34, 169 (1978).
42. D.L. MASSART, B.G.M. VANDEGINSTE, S.N. DEMING, Y. MICHOTTE and L. KAUFMAN, Chemometrics: A Textbook, Elsevier, Amsterdam 1988.
43. G.A. CRAGNOLINO and N. SRIDHAR, Corrosion, 47, 464 (1991).
44. F. MANSFELD, S.H. LIN and L. KWIATKOWSKI, Corrosion, 50, 838 (1994).
45. F. MANSFEL , S.H. LIN and L. KWIATKOWSKI, Corrosion Sci, 34, 2045 (1993).
46. C.G. PENG and J.K. PARK, Corrosion, 50, 669 (1994).
47. D.L. JORDAN, L.L. FRANKS and J.S. KALLEND, Corrosion, 52, 187 (1996).
48. M.G. FONTANA AND N.D. GREENE, Corrosion Engineering 2nd ed., McGraw-Hill. New York, 1978.
49. T.P. HOAR, D.C. MEARS and G.P. ROTHWELL, Corros.Sci., 5, 279 (1965).
50. K.J. VETTER and H.H. STREHBLOW, Ber. Bunsenges. Phys. Chem., 74, 1024 (1970).
51. N. SATO, Electrochim. Acta 16, 1683 (1971))(N. SATO, K. KUDO and T. NODA, Electrochim. Acta 16, 1909 (1971).
52. YA.J. KOLOTYRKIN, Corrosion, 19, 261t (1964).
53. T.P. HOAR and W.R. JACOB, Nature, 216, 1299 (1967).
54. J. MANKOWSKI and Z. SZKLARSKA-SMIALOWSKA, Corrosion Sci., 15, 493 (1975).
55. T. SUZUKI, M. YAMABE and Y. KITAMURA, Corrosion, 29, 18 (1973).
56 A.J. SEDRIKS, Corrosion of Stainless Steels 2nd ed., John Wiley & Sons, New York, 1996.
57. J.M. KLOTYRKIN, Corrosion 19, 261 (1963).
58. W.SCHWENK, Corrosion Sci., 5, 245 (1965).
59. J. HORVATH and H.H. UHLIG, J. Electrochem. Soc., 115, 791 (1968).
60. A.J. BARD and L.R. FAULKNER, Electrochemical Methods, Wiley, NY, 1980, p. 283.

61. S. AKHNAZAROVA and V. KAFAROV, Experiment Optimization in Chemistry and Chemical Engineering, Mir Pub., Moscow, 1982.
62. R.A. FISHER, The Design of Experiments, Oliver and Boyds, 1935.
63. W.J. LORENZ and K.E. HEUSLER, "Corrosion Mechanisms", edited by F. MANSFELD, Marcel Dekker, 1987.
64. F. BECK, R. KAUSS and OBERST, Electrochim. Acta, 30, 173 (1985).
65. C.M. RANGEL, R.A. LAITÃO and I.T. FONSECA, Electrochim. Acta, 34, 255 (1989).
66. C.M. RANGEL, I.T. FONSECA and R.A. LAIT O, Electrochim. Acta, 31, 1659(1986).
67. J.G.N. THOMAS, A.D. MERCER AND J.D. DAVIES, Proceedings of the Internatinal Conference on Corrosion Inhibition, edited by R.H. Heusler, 1983, p. 89.
68. D.B. GIBBS and M. COHEN, J. Electrochem. Soc., 119, 416 (1972).
69. M. POURBAIX, Atlas of Electrochemical Equilibria in Aqueous Solutions, published by NACE, 1974.
70. L.D. BURKE and M.G. LYONS, J. Electroanal. Chem., 198, 347 (1986).
71. K. OGURA AND K. SATO, Passivity of Metals, edited by R.P. Frankental and J. Kruger, Published by The Electrochemical Soc. Inc., 1978, p. 443.
72. E.B. CASTRO, J.R. VILCHE and A.J. ARVIA, Corros. Sci. 32, 37 (1991).
73. CRC Handbook of Chemistry and Physics, 71st Ed. (1990-1991).
74. J. GUI and T.M. DEVINE, Corros. Sci., 37, 1177 (1995).
75. S. SIMARD, M. DROWGOSKA, L. BROSSARD and H. MENARD, J. Applied Electrochem., 27, 317 (1997).
76. YA.M. KOLOTYRKIN, R.M. LAZORENKO-MANEVICH and L.A. SOKOLVA, J. Electroanal. Chem., 228, 301 (1987).
77. H.W. PICKERING, Corros. Sci., 29, 325 (1989).
78. A. MENDIBOURE and R. SCHÖLLHORN, Revue de Chimie Minérale, 23, 819(1986).
79. L. SIMON, J.M.R. GÉNIN and PH. REFAIT, Corrosion Sci., 39, 1673 (1997).
80. R.P. FRANKENTHAL and J. KRUGER, Passivity of Metals;

The Electrochemical Society: Princeton, NJ, 1978.

81. W. STUMM and J.J. MORGAN, Aquatic Chemistry, John Wiley and Sons, NY, 1996.
82. J.M.R. GÉNIN, A.A. OLOWE, PH. REFAIT AND L. SIMON, Corrosion Sci., 38, 1751 (1996).
83. E. ALMEIDA, D. PEREIRA, M. O. FIGUEIREDO, V.M. LOBO and M. MORCILLO, Corros. Sci., 39, 1561 (1997).
84. YATES, F. The Design and Analysis of Factorial Experiments: Bulletin 35; Imperial Bureau of Soil Science, Harpenden, Herts, Macmillan: Hafner, England 1937
85. P. LECKIE, J. Electrochem. Soc., 117, 1152 (1970).
86. H.W. PRESS, Numerical recipes in FORTRAN: the art of scientific computing; Cambridge University Press New York 1992.
87. H.E.H. BIRD, B.R. PEARSON and P.A. BROOK, Corros. Sci., 28, 81 (1988).